University of Padova

Department of Physics "Galileo Galilei"

XXI cycle – Ph. D. thesis

Di-cluster description of ^{7}Li and ^{7}Be

School director:
Ch.mo Prof Attilio Stella

Supervisor:
Ch.mo Prof. Andrea Vitturi

Author:
Antonio Mason

Contents

List of Figures

List of Tables

Sommario

Scopo di questa tesi è lo studio dei nuclei ^{7}Li e ^{7}Be in un modello a due cluster. L'idea fondamentale consiste nel considerare ^{7}Li e ^{7}Be come un sistema a due corpi, nel quale le eccitazioni vanno ascritte al moto relativo; i singoli cluster sono considerati inerti. Vengono discusse alcune significative proprietà statiche, come i raggi quadratici medi di massa e di materia, i momenti di quadrupolo elettrico e di dipolo magnetico, le energie degli stati legati e delle risonanze. Si considerano poi proprietà dinamiche come la risposta elettromagnetica agli stati del continuo e le transizioni di quadrupolo elettrico e di dipolo magnetico tra i due stati legati. Queste risposte vengono poi utilizzate per il calcolo delle sezioni d'urto per i processi di foto-dissociazione e di cattura radiativa, di particolare importanza nel campo dell'astrofisica. Si confrontano i risultati ottenuti con i dati sperimentali riguardanti il fattore astrofisico, attraverso il quale viene abitualmente riparametrizzata la sezione d'urto di cattura radiativa. L'accordo trovato è soddisfacente.

Si motiva l'importanza di utilizzare una descrizione a cluster utilizzando le regole di somma per le interazioni di dipolo e quadrupolo elettrico. Si nota come la struttura a cluster influenzi pesantemante la risposta elettromagnetica. Questo fatto è lampante nel caso dell'interazione di dipolo elettrico: la regola di somma TRK (Thomas-Reiche-Kuhn) infatti sovrastima di un ordine di grandezza le risposte elettromagnetiche effettivamente trovate, mentre la regola di somma molecolare, che sottrae i contributi intrinseci dei due cluster, si accorda ottimamente con i calcoli.

Si deriva infine una nuova regola di somma per l'interazione di dipolo magnetico che incorpora fin dall'inizio la struttura a cluster di questi nuclei, utilizzando la decom-

posizione in cluster del momento di dipolo magnetico e trovando un buon accordo tra il valore dato da questa regola di somma e il valore ottenuto sommando i contributi calcolati numericamente per ciascuna transizione.

Si è cercato di scrivere un lavoro completo, autoconsistente e nello stesso tempo non prolisso. Di conseguenza le formule più importanti vengono dimostrate in dettaglio, in modo da averne chiara l'origine e in modo da fissarne i limiti di validità. In quest'approccio va intesa la trattazione del momento di dipolo magnetico, a partire dalla formulazione nel modello a shell, o delle cariche efficaci, argomenti di per se stessi ben noti.

Vengono infine illustrati nelle conclusioni i risultati di un'analisi tuttora in corso, volta al calcolo della sezione d'urto di break-up di un fascio di ^{7}Be su un target di ^{208}Pb, in vista di un possibile futuro esperimento ai Laboratori Nazionali di Legnaro.

Introduction

How many bodies are required before we have a problem? G.E. Brown points out that this can be answered by a look at history. In eighteenth century Newtonian mechanics the three body problem was insoluble. With the birth of relativity around 1910 and quantum mechanics in 1930 the two- and one-body problems became insoluble. And within modern quantum field theory the problem of zero bodies (vacuum) is insoluble. So, if we are out after exact solution no bodies at all is already too many.

Richard Mattuck

A common feature of physics is the importance of choosing the most suitable variables in order to extract the properties of a system. The large number of models commonly employed in nuclear physics is an outstanding example of this aspect. Indeed, dealing with nucleons, we have to face the lack of a simple potential able to describe the nucleon-nucleon interaction, because of the non fundamental nature of this force. As a result we are concerned with effective theories, in which all the exchanges of particles due to the strong interaction are contained in a phenomenological potential. We pay for the simplicity of this description with the lack of a theory that could simultaneously work for most nuclei: one is indeed forced to fix the parameters of this potential almost for each nucleus.

Similarly the notion of elementary particle is not an absolute one: it heavily relies on our ability in reaching energies so high as to fragment it in its constituents. Usually

the energies used in nuclear physics are such that we can consider protons and neutrons as our building blocks. But the non vanishing magnetic moment of the neutron and the anomalous gyromagnetic factors of protons and neutrons remind us that nucleons are not really elementary particles, but we can consider them in this way because of the energies involved in the low part of the nuclear spectra.

In spite of these difficulties people have been able to describe a large number of nuclei using simple and well-established theories. These models work very well for stable nuclei along the valley of stability making possible the understanding of many properties of these nuclei. A noticeable example is the explanation of the magic numbers by the introduction of a spin-orbit potential in addition to the mean central potential in 1949.

But, when we move towards the drip-lines there are not theories able to describe all the phenomenology and different theories predict different positions also for the drip-lines. These nuclei, often very unstable, deserve a special treatment.

Moreover there are stable nuclei, like ^{7}Li, that cannot be properly described in a shell model picture, but ask for different ideas. Now it is well-known that it can be essential to employ an intermediate level between the single nucleons and the nucleus as a whole. Many examples exist, both in the field of halo nuclei and in cluster nuclei. In this work we will focus on di-cluster nuclei ^{7}Li and ^{7}Be, by considering ^{7}Li as formed by two inert subsystems, α-particle and ^{3}H and ^{7}Be as formed by α-particle and ^{3}He. We will emphasize the necessity of this intermediate level description, by pointing out the drawbacks of the shell model picture in describing these odd-A nuclei, both dealing with static properties, like the dipole magnetic moment, than dealing with the electromagnetic response, by discussing the energy weighted sum rules.

In detail the work is divided in three parts. In the first chapter we will give a brief overview of standard models in nuclear physics, by using the semi-empirical mass formula as a mean to introduce the liquid drop model, the Fermi gas model and the nuclear shell model. We will also discuss the spin-orbit correction and we will give some hint on other models, such as the collective model and the Interacting Boson Model (IBM), usually employed for medium-heavy nuclei. This chapter is only aimed at establishing the basic

nuclear models and at discussing the limits and drawbacks of these models.

In the second chapter we will deal with halo nuclei. This chapter does not claim absolute completeness, but the selection of the topics serves two purposes, namely to show the connection between the field of halo nuclei with the field of cluster physics and to prove some formulas, regarding matter and charge square mean radii or effective charges, that are often found in literature without any comment.

In the third chapter we will give a complete description of ^{7}Li and ^{7}Be in a di-cluster model. We will discuss the ideas and the limits of the di-cluster description and we will focus on the electric and magnetic response. We will point out the need of a cluster description by means of energy weighted molecular sum rule for electric transitions, and by deriving a proper energy weighted molecular sum rule for magnetic dipole interaction. We will compare our calculation with experimental S-factors finding a satisfactory agreement and we will show the importance of the inclusion of the nuclear potential in dealing with continuum states. Finally in the last chapter we will present our conclusions and a work in progress concerning the break-up of ^{7}Be into α+^{3}He in the electrostatic field generated by a ^{208}Pb target.

Thanks

This thesis has been written during the last months of life of my father and the first ones after his death. It was not easy because my thoughts were absorbed by these grave problems, therefore the conclusion of my Ph. D. was in background. But, if I have managed to do this task, the merits have to be divided among many people. First of all I have to thank my father for his wisdom: he never obstructed my turns and he tried, with all his human strengths, not to lie heavy on me and on my family. So, because of him, I could study what I really like without worrying about other things.

My mother, Margherita, deserves a special mention for her care in taking my father until his last breathe. She has lived for him and he rewarded her by living much beyond the doctors' predictions and by dying peacefully and without loss of blood. My mother

has showed a power and a self-denial during the illness of my father that has been astonishing me day after day. The last member of my family is my younger brother Filippo. He has grown a lot during my father's illness and he has helped me, maybe without being fully aware of this: his simple happiness is a joy, his speeches against school and teachers are very amusing and his lessons of music and cinema are touching and professional at the same time.

Without my girlfriend Alessandra all things would have been much worse. She is able to cheer me up in a way that cannot be learned. There are not wasted words but only a warm hug and a pleasant shoulder. She manages to make me smile just with her appearance. My father liked her and for my mother she is a member of the family.

Many other people helped me and my family about looking after my father and I'm not able to thank all these ones in the way they deserve. I only mention the relatives of my mother and in particular her bigger brother Giuseppe, commonly named "Pepé". A big man with a bigger heart. He and his wife have done much for me, my brother, my mother and my father and I cannot forget these things. For my mother he is her big brother, for me and my brother is our big uncle. Other people deserve a special attention although they didn't help directly my father, but with their kindness and sympathy they allowed me to give all I could to my mother and my father. These are my supervisor, prof. Andrea Vitturi , and my colleague Lorenzo Fortunato. "Fortunato" in Italian means "lucky" but I was lucky in meeting them. Also the people who work in the room 344 at the Department of physics were important for me: that room full of amusing and clever people has helped me to break off my woeful thoughts with the results of preserve my mind from depression or madness. Probably there are many other people who merit a thank for their help in these days and I can't remember all these ones in the way it meant to be. All these people, without name in these pages, are well known in my mind and I will be always grateful to them.

Maybe it is strange, but I feel that in the future these few pages thesis will be the most important for me. They will remember me the strong feelings of this period and the importance of many people in my life.

Chapter 1

Nuclear models

In this chapter the basic standard nuclear models will be briefly discussed. This chapter is aimed to illustrate the successes, the limits and the drawbacks of these models. There are anyhow a number of cases that are not easily described within these basic models and call for a different theoretical explanation. These phenomena will be the subject of the next chapter.

1.1 The liquid drop model

If we consider the behavior of the binding energy (B.E.) of stable nuclei, see figure (1.1) we can extract some important features: from medium-high mass number nuclei we can extract a few informations about the nuclear force. From the figure it is clear that the nuclear B.E. is roughly constant. This information allows us to conclude that the nuclear force between nucleons is a short range one, compared with the size of the nucleus (11; 24).

Indeed, if the nuclear force were a long range one, like the electromagnetic force, the nuclear B.E. would be proportional to the number of couples of nucleons, i.e. $A(A-1)/2 \sim A^2/2$ if $A \gg 1$. In detail, the couples of nucleons that interact via the nuclear force are only those ones inside the interaction volume $v_{\text{int}} \ll V_{\text{nucleus}}$ yielding an integrated

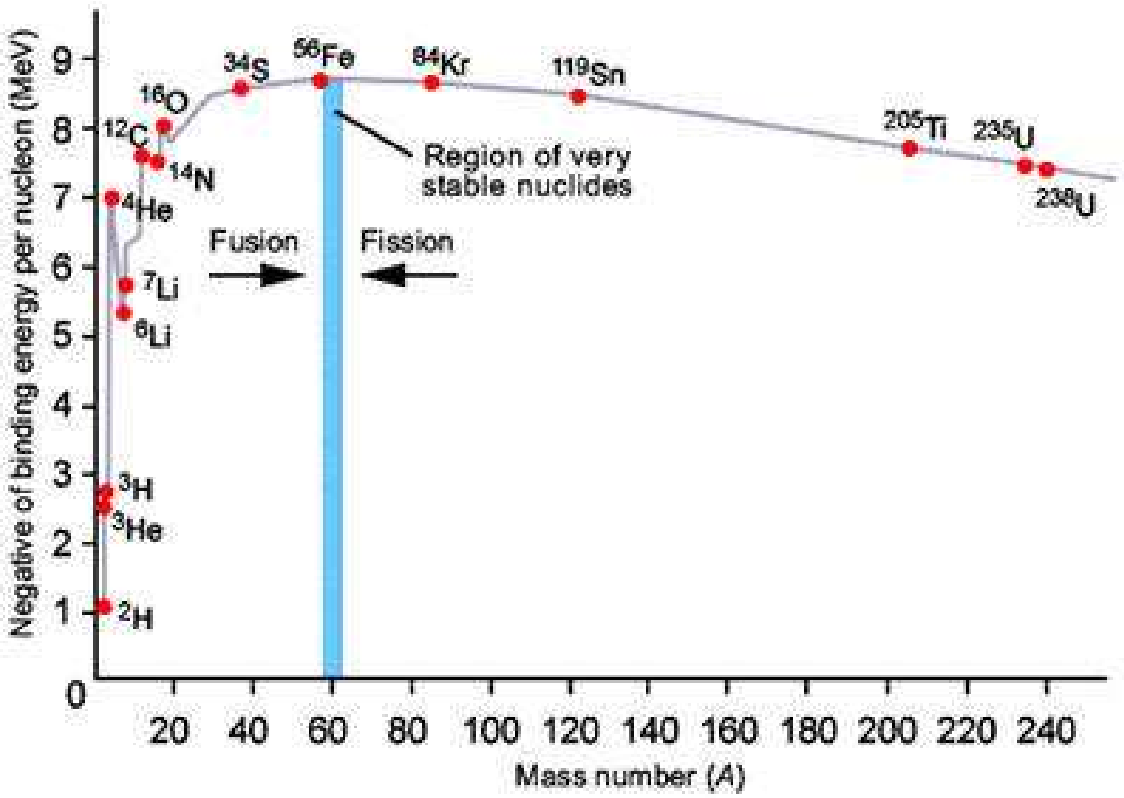

Figure 1.1: Negative binding energy per nucleon in MeV, as a function of mass number A. Some remarkable nuclei are indicated.

energy of approximately

$$E \simeq -\frac{1}{2}A(A-1)\overline{U}\frac{v_{\text{int}}}{V_{\text{nucleus}}}\ , \tag{1.1}$$

where $\overline{U}$ in the mean interaction energy between two nucleons. The product $\overline{U}v_{\text{int}}$ does not depend on A but it is a characteristic of the nuclear force. Hence if we force in equation (1.1) $E \propto A$ we have the condition $V_{\text{nucleus}} \simeq A$. Hence, by assuming a short range nuclear force we can explain two typical features of nuclear systems:

- $E \simeq A$, according to spectrometry data.
- $V_{\text{nucleus}} \simeq A$, according to other "liquid" systems.

We can refine this model by introducing correction to the gross formula $E \simeq A$, by including surface effects and the Coulomb repulsion between protons. If we consider the nucleus as a sphere of radius R, that is a good approximation for most nuclei, we have

$$R = r_0 A^{1/3} \quad S = 4\pi r_0^2 A^{2/3} \quad V = \frac{4\pi}{3} r_0^3 A \ , \tag{1.2}$$

where S in the surface of the nucleus. Because of the smallness of A, also in the biggest nuclei ($A \leq 250$) surface effect are not negligible and we expect a positive correction to the binding energy proportional to $A^{2/3}$, i.e. $b_1 A^{2/3}$. Moreover we include the Coulomb repulsion between protons, proportional to the number of couples of protons and inversely proportional to the mean distance between them:

$$E_{Cou} = \frac{1}{2} Z(Z-1) e^2 \langle \frac{1}{r} \rangle = b_2 \frac{Z(Z-1)}{A^{1/3}}$$

because $\langle 1/r \rangle \propto A^{-1/3}$. Summarizing, by considering the nucleus as a liquid drop we can explain its basic features and we have a formula for its binding energy:

$$E(A,Z) = -b_0 A + b_1 A^{2/3} + b_2 \frac{Z(Z-1)}{A^{1/3}} \ , \tag{1.3}$$

where b_0, b_1, b_2 are parameters to be fitted from by an interpolation between experimental data. At this point the agreement between theory and experiment is not good and we cannot explain a common feature of nuclei at small A, i.e. the trend to have $N = Z$. In fact, a nucleus made up of only neutrons should be more bound because of the lack of Coulomb repulsion, but we know that stable nuclei made of only neutrons do not exist. This feature can be naturally explained by considering the fermionic nature of protons and neutrons, as showed in the next section.

1.2 The Fermi-gas model

If we consider the figure (1.2) we note that light stable nuclei are along the $N = Z$ line, while for medium heavy nuclei there is a neutron excess. The reason for this behavior relies of the fermionic nature of nucleons, in other words they have to follow the Pauli

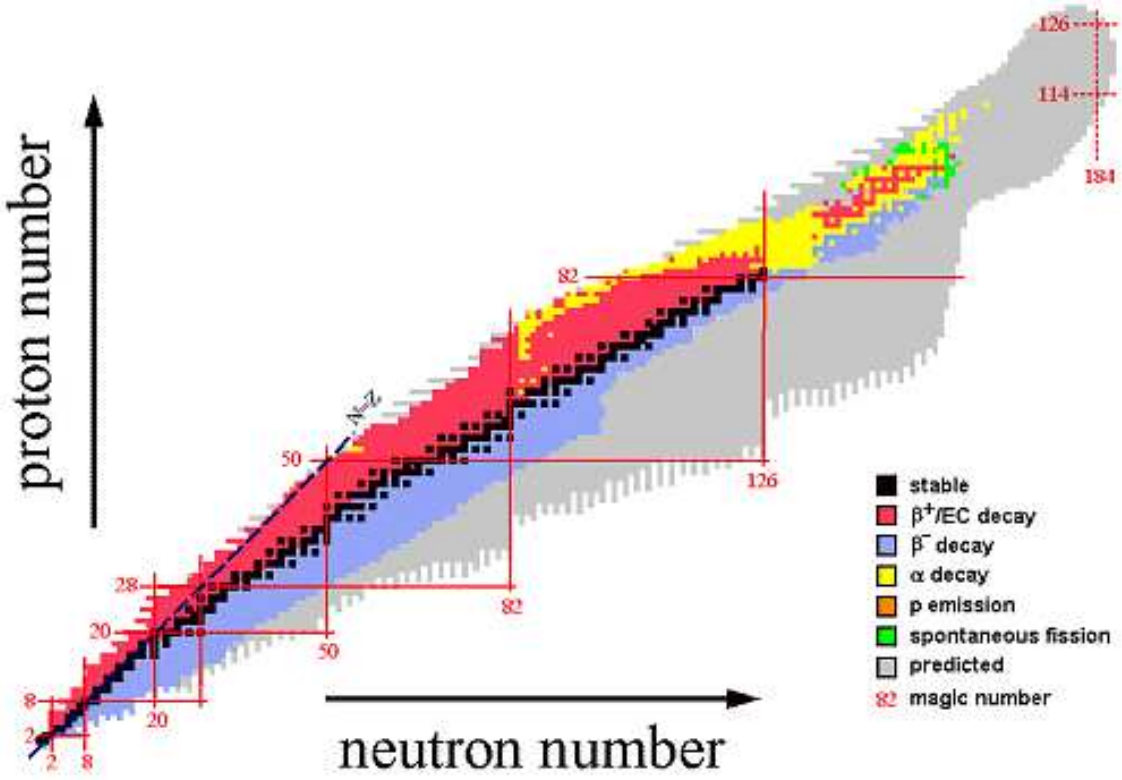

Figure 1.2: The nuclides chart. See the legend of the chart for a detailed explanation

exclusion principle (11; 24). We indicate with $n(p)$ the density of states as a function of the particle momentum, therefore $n(p)dp$ is the number of nucleons bound states, with modulus of linear momentum between p and $p + dp$. In the ground state of a certain nucleus, all states are filled up to maximal momentum (Fermi momentum)p_{F_n} and p_{F_p} for neutrons and protons,

$$\int_0^{p_{F_n}} n(p)dp = N \qquad \int_0^{p_{F_p}} n(p)dp = Z \ , \tag{1.4}$$

and, in the same way, for the kinetic energies of nucleons

$$E_{\text{kin}} = \int_0^{p_{F_n}} \frac{p^2}{2M} n(p)dp + \int_0^{p_{F_p}} \frac{p^2}{2M} n(p)dp \ , \tag{1.5}$$

where we have neglected the small difference between the proton and neutron masses ($M_p \sim M_m \equiv M$). In order to evaluate the distribution function $n(p)$ we consider a simple model, namely the square well model. In this model we consider the nucleons as free particles moving in a potential well of volume $V = 4\pi/3R^3$, that is the volume of the nucleus, and depth U_0. This simple model is a good starting point since nucleons are quite free in the nucleus, because of their high mean kinetic energy and their fermionic nature. In this model

$$n(p) = 2V\frac{4\pi p^2}{(2\pi\hbar)^2}\ , \tag{1.6}$$

where V is the volume of the nucleus, $\hbar$ is the reduced Planck constant and 2 is a spin factor. By substituting this equation in (1.6) in order to calculate the Fermi momenta p_{F_n} and p_{F_p} and by computing eq. (1.5) we obtain:

$$E_{\text{kin}} = \underbrace{\frac{3}{40}\left(\frac{9}{4\pi^2}\right)^{2/3}\frac{h^2}{Mr_0^2}}_{C} A\left\{\left(\frac{N}{A}\right)^{5/3} + \left(\frac{Z}{A}\right)^{5/3}\right\}\ , \tag{1.7}$$

where we have used $V = (4\pi/3)r_0^3 A$. By expanding in power of $(N-Z)/A$ eq. (1.7) we obtain the approximate relation

$$E_{\text{kin}} \simeq \frac{1}{2^{2/3}}C\left\{A + \frac{5}{9}\frac{(N-Z)^2}{A}\right\}\ . \tag{1.8}$$

This term, named asymmetry term, has two components: one linear in A, showing that the b_0 term in (1.3) is not the depth of the potential well, but it is decreased by the mean kinetic energy due to the Pauli principle, while the other term explains the trend $N = Z$ for light nuclei. Now we can refine eq. (1.3) adding this new term obtaining:

$$E(A,Z) = -b_0 A + b_1 A2/3 + b_2\frac{Z(Z-1)}{A^{1/3}} + b_3\frac{(N-Z)^2}{A} \tag{1.9}$$

where we have the following relations:

$$b_3 = \frac{5}{9}\frac{1}{2^{2/3}}C \qquad U_0 \simeq b_0 + \frac{9}{5}b_3\ , \tag{1.10}$$

and C is the constant defined in eq. (1.7).

The last equation is still incomplete: experimentally we observe that nuclei with Z and N even are the more stable, those ones with Z and N odd are the less stable and those ones with A odd are intermediate between these two cases. If we consider nuclei with the same A from eq. (1.9) the quadratic dependence of the binding energy on Z, because of the Columbian and asymmetry terms becomes clear. We can therefore arrange isobaric nuclei along a parabola. When A is odd formula (1.9) reproduces experimental data quite well, while when A is even we have two parabolas, according to Z,N both even or both odd. With respect to eq. (1.9) even-even nuclei are more bound while odd-odd nuclei are less bound.

From a phenomenological point of view we can add another term to eq. (1.9) in the following way:

$$\begin{aligned} \delta(A) &= 0 && \text{A odd} \\ &= -\frac{b_4}{A^{1/2}} && \text{Z even, N even} \\ &= \frac{b_4}{A^{1/2}} && \text{Z odd, N odd .} \end{aligned} \tag{1.11}$$

In the Fermi-gas model we cannot give a physical explanation for this term because it relies on the intrinsic spin of the nucleons and in the explicit dependence of the nuclear force on the spin. Hence, in order to give an explanation of eq. (1.11) in the next section we will introduce the Nuclear Shell Model, a milestone among nuclear models.

1.3 The nuclear shell model

A large number of experimental data has lead people to consider the filling of nuclear levels in analogy to the atomic shell model (11; 24; 23; 14): when a nucleus has certain given numbers of N or Z it exhibits a strong stability, not fully predicted by eq. (1.9). Even by including the pairing term, eq. (1.11), this fact cannot be account for. There is a strong evidence for very stable configurations is Z or N are equal to $2, 8, 20, 28, 50, 82, 126$. These numbers are different with respect to the atomic case and

were named "magic numbers". In figure (1.3) the deviation between the experimental binding energy and the prediction of semi-empirical mass formula in shown. Clearly the biggest deviations are around the magic numbers.

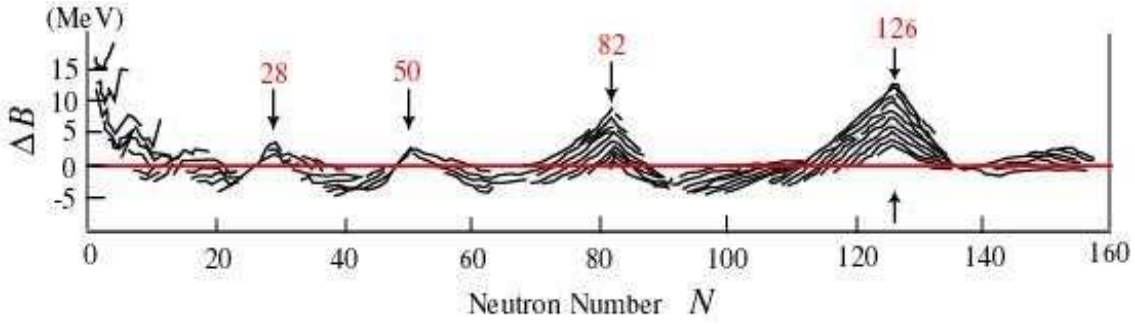

Figure 1.3: Deviations between experimental binding energies and predictions of semi-empirical mass formula, as a function of the neutron number.

Another feature, well understandable in a shell model, is the large excitation energy of the first excited state first for a neutron in a magic nucleus, as shown in figure (1.4). Indeed, when a nucleus has its last shell totally filled, the first excited level is on the next shell that is typically few MeV above.

Other experimental evidences confirm the nuclear shell model, as the isotopic abundances, i.e. when Z is magic the number of stable isotopes is bigger with respect to Z not magic or the vanishing of the quadrupole moment for magic nuclei.

In order to reproduce the magic numbers we have to choose a phenomenological nuclear potential. We suppose that each nucleon moves in a spherical well given by the other nucleons, but without any correlations between the motions of the nucleons. A common central potential is the Wood-Saxon one:

$$V(r) = -\frac{V_0}{1 + e^{\frac{r-R}{a}}} \ , \tag{1.12}$$

where $V_0 \simeq 50 - 60$ MeV for most nuclei, is the strength of the potential, $R \simeq 1.3 \cdot 10^{-13} A^{1/3}$ cm is the radius of the nucleus and $a \simeq 0.5 \cdot 10^{-13}$ cm is the diffusiveness.

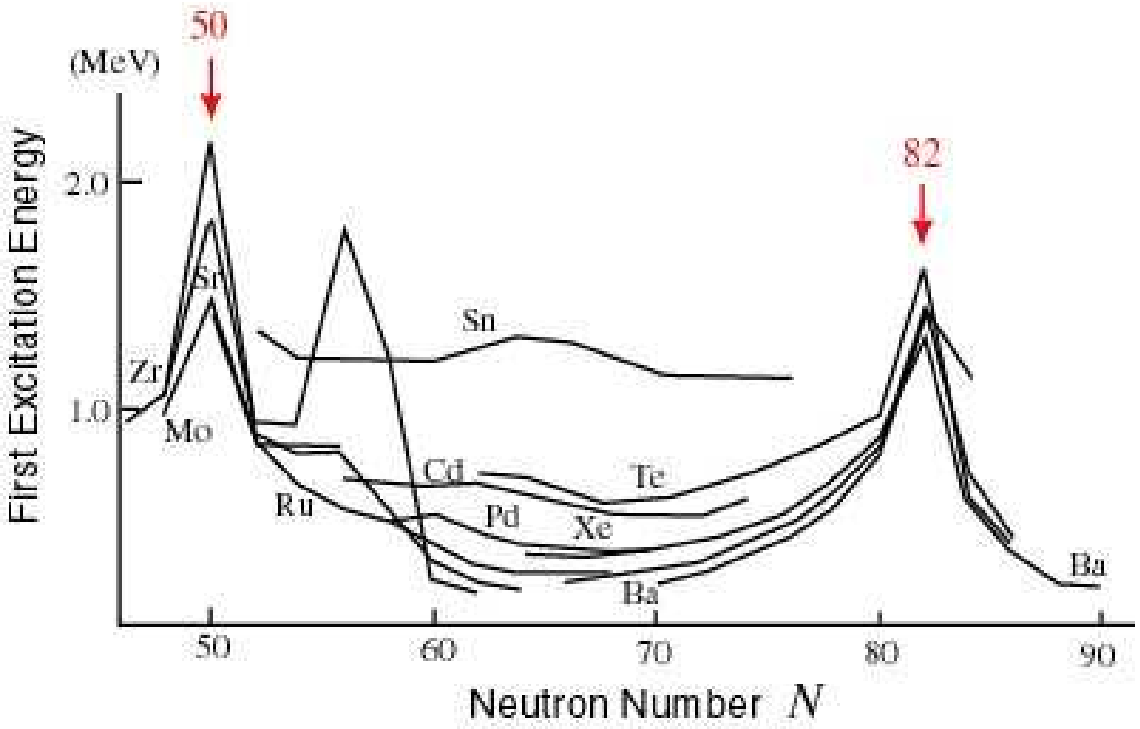

Figure 1.4: First excitation energy for a neutron as function of neutrons number for some isotopes. Magic numbers 50 and 82 are indicated with arrows.

Note that for $a \to 0$ the Wood-Saxon potential reduces to a finite spherical well of radius R and strength V_0 and its shape is connected with the Fermi-Dirac distribution.

The Woods-Saxon potential is central so we can label the eigenstates according to the orbital angular momentum l. Moreover the eigenvalues of the Hamiltonian cannot depend on the direction of l. By taking into account also the spin s of the nucleon a given level of angular momentum l has a degeneration $2(2l+1)$. In this way, by supposing that the first level is an s one, and the next is a p one we reproduce the magic numbers 2 and 8, but there is no simple and natural way to reproduce higher magic numbers. The shape of the potential is essential in order to reproduce large magic numbers, while the first two seem related to the angular momentum. Indeed also other potentials are able to reproduce the magic numbers 2 and 8, such as the spherical well and the harmonic

oscillator potential

$$V(r)\frac{1}{2}M\omega^2 r^2 \ , \tag{1.13}$$

where M is the nucleon mass ($M_p \simeq M_n \equiv M$) and ω is the only free parameter of the potential. This potential is not realistic but it is expected to be a good approximation for very deep states, near the bottom of the well. The eigenvalues are those of a 3-dimensional harmonic oscillator, namely

$$E = \left(n_1 + n_2 + n_3 + \frac{3}{2}\right)\hbar\omega \ . \tag{1.14}$$

The energy depends only on $n = n_1+n_2+n_3$ and the level degeneration is straightforward. As an example $n = 0$ can be obtained only in one way, $n = 1$ in three ways and $n = 2$ in six ways giving the degeneration (by including the spin) $2, 6, 12$ that explain the first three magic number $2, 8, 20$. The harmonic oscillator potential of eq. (1.13) doesn't work for larger magic numbers so we are forced to introduce more refined potential. In the next sub-section we will introduce the spin-orbit potential that is able to reproduce all magic numbers.

1.4 The spin-orbit interaction

In the last section we have briefly discussed the nuclear shell-model. The ability to account for phenomenological observations is, at this point, quite unsatisfactory: it reproduces only the first three magic numbers. By using only central forces, we are not able to infer the spin J of nuclei: consider ^{17}O, where we have a single neutron out of two closed shells. The spin of this nucleus depends only on the quantum numbers of this unpaired nucleon, but the shell model does not give a value for this spin. Experimentally the value is $J = 5/2$, namely the biggest one following the order of shells. If we consider ^{15}N, all nucleons are paired expect one proton and, also in this case, we cannot choose between the values $3/2$ and $1/2$. Experimentally the value is $J = 3/2$, the biggest one. This behavior is quite common and can be stated in the following way: given an

orbital momentum l for the unpaired nucleon, the spin is the highest, according to Pauli principle.

The simplest interpretation of this phenomenon was given by Mayer, Haxel, Jensen and Suess in 1949 (11; 14; 24; 23). It is based on the introduction of a spin-orbit interaction, similar to the atomic case, but much stronger:

$$V_{nuc} = V_{WS}(r) + V_{so}(r)\vec{l}\cdot\vec{s}\,. \tag{1.15}$$

Because of this interaction $\vec{l}$ and $\vec{s}$ are not conserved but the total spin $\vec{J} = \vec{l} + \vec{s}$ is a constant of motion, hence we can classify the energy levels according to this good quantum numbers. Given an eigenstate $|Jls\rangle$ from the usual equations

$$\begin{aligned} \langle jls|\vec{l}\cdot\vec{l}|jls\rangle &= l(l+1) \\ \langle jls|\vec{s}\cdot\vec{s}|jls\rangle &= 3/4 \\ \langle jls|\vec{J}\cdot\vec{J}|jls\rangle &= J(J+1)\,, \end{aligned}$$

we obtain the following degeneration breaking:

$$\begin{aligned} \text{if} \quad J = l + \frac{1}{2} \qquad\qquad & \vec{l}\cdot\vec{s} \to \frac{l}{2} \\ \text{if} \quad J = l - \frac{1}{2} \quad (l \geq 1) \quad & \vec{l}\cdot\vec{s} \to -\frac{l+1}{2} \\ \text{if} \quad l = 0, \quad J = \frac{1}{2} \qquad\qquad & \vec{l}\cdot\vec{s} \to 0\,. \end{aligned} \tag{1.16}$$

By supposing that in eq. (1.15) $V_{so}(r) < 0$, levels with $J = l + 1/2$ are lower than levels with $J = l - 1/2$. In this way we can explain why ^{17}O has $J = 5/2$ and ^{15}N has $J = 3/2$. Obviously levels with a given J have the same degeneration: if $J = l+1/2$ then $2J+1 = 2l+2$, if $J = l-1/2$ then $2J+1 = 2l$ and the sum of this degeneration is $2(2l+1)$, namely the original degeneration. In figure (1.5) we show the energy level obtained by using a Wood-Saxon interaction with a spin-orbit correction. Now levels are no longer roughly equidistant among each-other, but the spin-orbit interaction, raising some levels and lowering others, reproduces the big gaps corresponding to magic numbers.

With respect to a shell model with only central forces the power of this model is greatly increased because one can explain the ground state spin of odd A nuclei. There

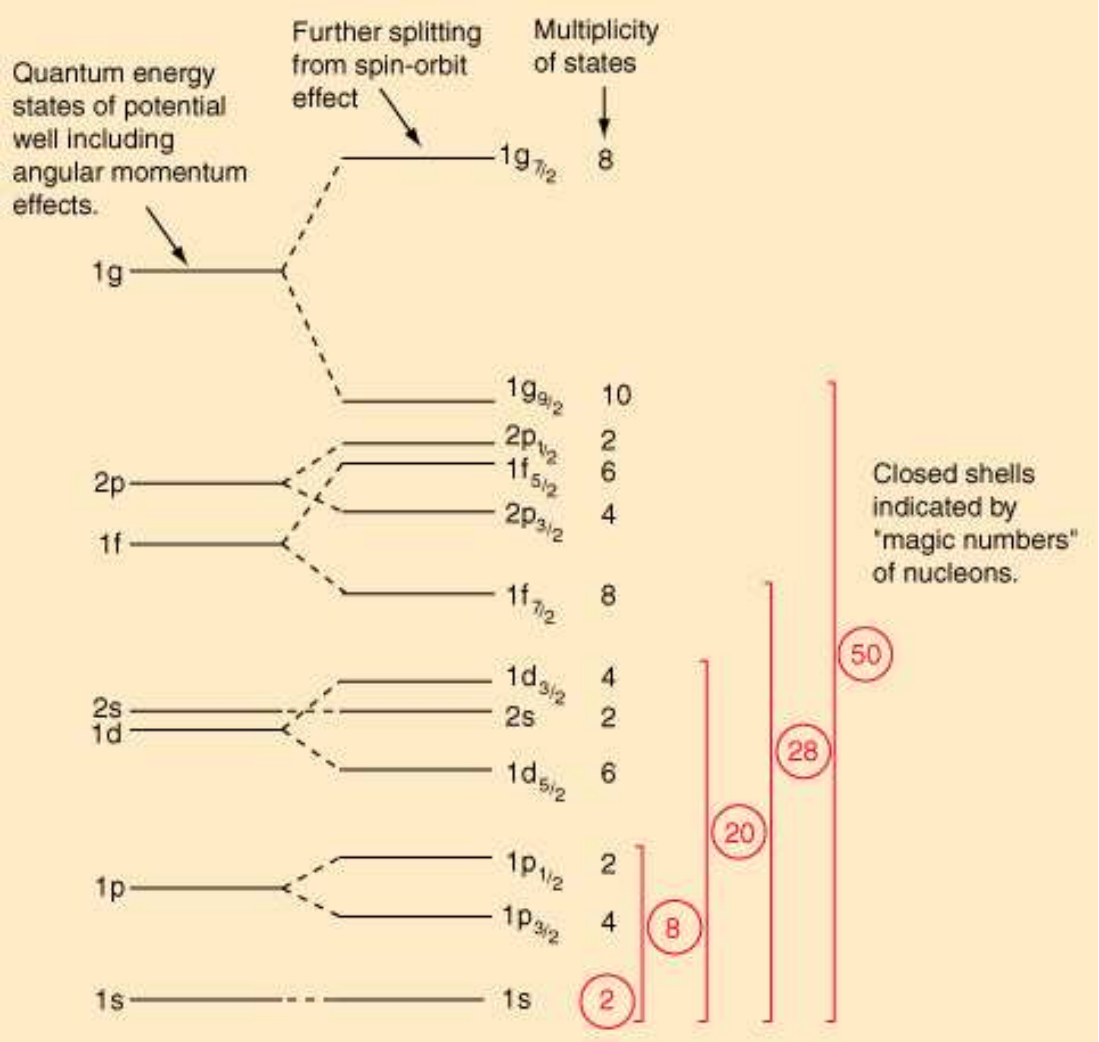

Figure 1.5: Magic numbers obtained by adding a spin-orbit interaction to a Woods-Saxon one.

are however some exceptions, explained by introducing an *adhoc* interaction that makes couples between nucleons with high angular momenta more bound. From this treatment nuclei with N and Z odd are excluded because in this model deals with independent particles moving in a mean field, therefore we cannot properly consider the interaction between two particle out of closed shells.

1.5 Other Models

The phenomenology of nuclei is very large and exhibits many peculiar features. As a consequence many different models have been developed to describe the variety of nuclear systems. For sake of completeness, we only mention two well-established model, suited for the description of medium and heavy nuclei, namely the collective Bohr-Mottelson model (14) and the Interacting Boson Model (IBM) (33). The Bohr-Mottelson model refines the liquid-drop model by describing the excited states of high-mass nuclei in terms of the dynamics of the nuclear surface. In this way we can describe excitations that are not of a single particle nature but are shared among many, and sometimes all, the nucleons. This model can be used in order to described nuclear fission and many features of the energy levels of high-mass nuclei, from the vibrational behaviour near the shell closure to the motion of deformed shapes in open shell nuclei.

In the original IBM, suited for even-even nuclei, the protons and neutrons (treated as a unique species of nucleons) of a nucleus are paired in couples, that are assumed to behave like bosons with angular momentum equal to 0 or 2 (s and d bosons) and interacting via a boson Hamiltonian. This approach has its basis on the behavior of valence nucleons: due to the residual short-range interaction they prefer to couple in states with angular momentum equal to 0 or 2, explaining why the ground state of even-even nuclei is 0^+ and the first excited states is (almost always) 2^+. There are also many extension of IBM, aimed to a better description of medium-heavy nuclei. Among these we mention the interacting boson-fermion model (IBFM), that can describe odd-even nuclei, by considering an unpaired nucleon as a fermion moving in single-particle orbital.

1.6 Summary

In this brief chapter we have given an account of the fundamental observations that have led to the development of simple models in nuclear physics. This chapter deals with well known topics. In the next chapter we will give a phenomenological overview of many

nuclear systems that cannot be thoroughly treated in a naive shell model, especially in light systems, as in particular those displaying halo behaviour. We will concentrate on topics that can be well related to the physics of di-cluster nuclei, by deriving few formulas usually employed for di-cluster nuclei.

Chapter 2

Beyond shell model: halo nuclei

2.1 Motivation

In this chapter we want to discuss the drawbacks and the limits of shell model plus spin-orbit interaction. There is a large phenomenology, both in light nuclei and in medium-heavy nuclei, of nuclides that cannot be described in a standard shell model picture (4; 5; 30; 35; 36; 55; 56; 57; 74). Also other common features, like the relation between the mass number and the radius of the nucleus, i.e. $R \propto A^{1/3}$, fail and the quite common idea of a nucleus with spherical shape in its ground state, is not always correct. Many of these unusual features lie among the nuclei far from the valley of stability, like halo nuclei, but there are also stable nuclei, like ^{7}Li, or near the valley of stability, as ^{7}Be, that exhibit very peculiar behaviors (17; 27; 37; 71).

The main goal of this thesis is to set up a quite comprehensive treatment of di-cluster nuclei, in particular ^{7}Li and ^{7}Be, therefore it can be useful a long digression on similar systems like halo nuclei: halo and cluster nuclei share many features, first of all the possibility of being described in a intermediary level between the single nucleons and the whole nucleus. We can think of these nuclei as two- or three-body systems with frozen subsystems. Many of the ideas and of the formalism developed for a two-body halo nucleus can be applied in a two-cluster nucleus. The difference between these two

kind of systems is in the relative sizes of the two clusters: in a halo nucleus we have a relatively heavy core plus a valence particle, i.e. a neutron or a proton, while in a cluster nucleus we have two clusters of comparable sizes and the distinction between core and valence becomes irrelevant. Finally, for sake of completeness, we will also briefly discuss three-body halos like ^{11}Li (4; 25; 35).

2.2 Halos: meaning and examples

The term *halo* refers to the peculiar structure of some light nuclei, where the last one or two nucleons are spatially decoupled from an inner core (4; 5; 35; 36; 55; 56; 57; 63; 64; 65; 68; 74). The most famous examples are the three-body halo-nuclei ^{11}Li=^{9}Li +n +n and ^{6}He=^{4}He+n+n and the two-body halo-nucleus ^{11}Be=^{10}Be+n. One common feature of these nuclei is the weak-binding energy of the last one or two particles, therefore the halo is a threshold effect: the combination of weak binding and short-range nuclear force allows for a not negligible probability of finding the valence particle(s) outside the nuclear potential well, in the classically forbidden region. Strictly speaking, an accepted definition of a halo is the fulfillment of this condition: the halo particle has to be found in the classically forbidden region with a probability p_h larger than 50% (56; 68). The border between halo and non-halo nuclei is not well defined, but we can say that the larger is p_h the clearer are the halo features. It is important to point out that in order to have a halo nucleus, the condition of weak binding energy is necessary, but is not sufficient. Otherwise we could find halo states, among the excited states of nuclei (4). The most impressive halos are neutron halos because of the lack of the confining Coulomb barrier and, for similar reasons, we can find halos if the valence particle is in a low relative angular momentum, i.e. s or p wave, in order to prevent the confining effect of the centrifugal barrier (55).

In figure (2.1) a section of the Segre chart showing halo nuclei and other peculiar aspects of light nuclei is presented. According to the legend, black squares indicate stable nuclei, grey square one-proton halo nuclei, such as ^{8}B, ^{13}N and the first excited

state of ^{17}F. Yellow squares refer to the large phenomenology of nuclei towards the neutron drip-line: two-neutrons halo nuclei, also named "Borromean" nuclei, like ^{6}He, ^{11}Li, ^{14}Be and ^{17}B. The label "Borromean" refers to the coat-of-arms of the Borromeo family: three circles bounded in such a way that every pair of circles is unbound. Finally one-neutron halo nuclei as ^{11}Be, ^{15}C and ^{19}C and systems at the boundaries between halo nuclei and neutron skin, a situation in which a nucleus is surrounded by a thick neutron skin, like ^{8}He, ^{19}B and ^{22}C are also shown.

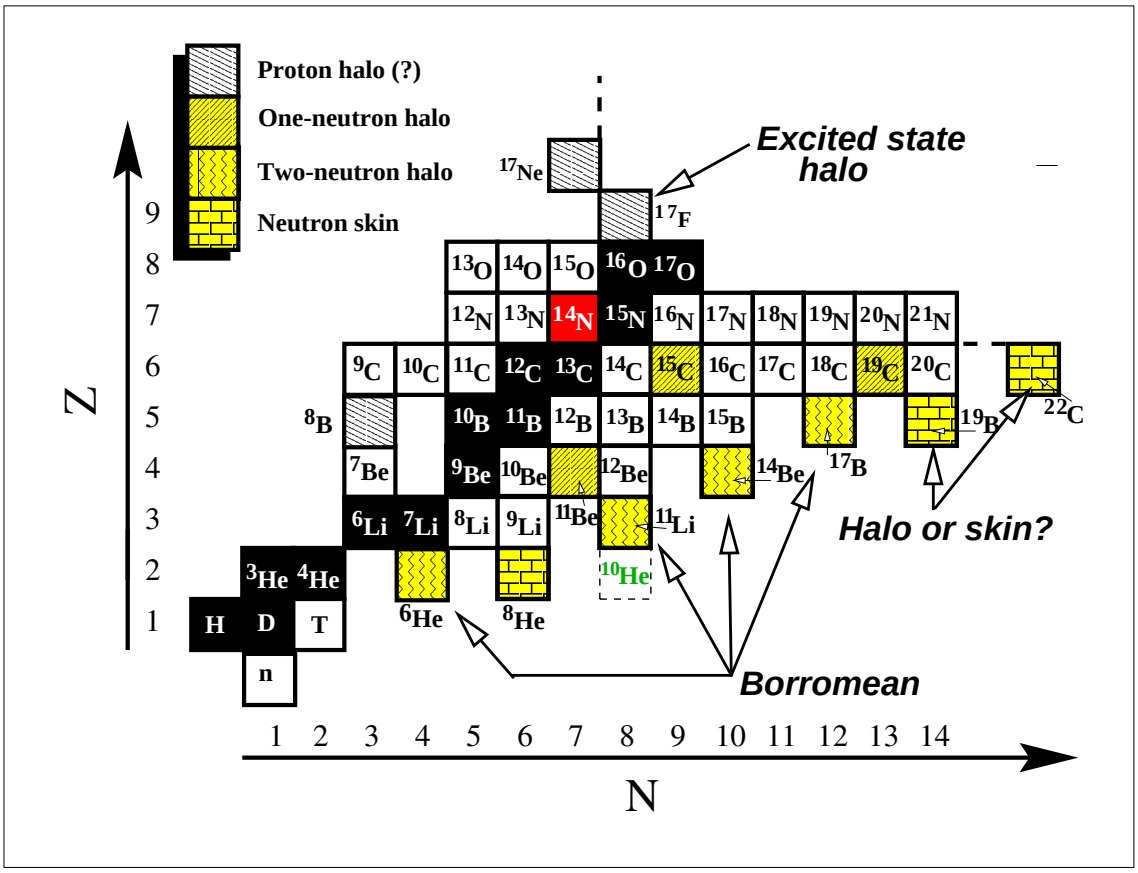

Figure 2.1: The light nuclei of the Segre chart. See the text for a complete explanation.

2.3 Scaling functions

Nuclei with pronounced halo features can be described in a unified picture by the introduction of certain scaling parameters (55; 56; 68). In order to give a simple, but accurate description we will consider in this section one neutron halo nuclei for the following reasons:

- they are two-body systems, so they can be compared with di-cluster nuclei.
- the Coulomb barrier is absent because there is no Coulomb repulsion, therefore the only repulsive contribution to the radial potential originates in the centrifugal barrier, if that is present.
- in the limits where the (positive) nucleon separation energy S_n approaches zero, the probability of finding the valence neutron in the potential well goes to zero, hence we can neglect the contribution of the inner part of wave function, i.e. for $0 \leq r \leq R$, with R the radius of the potential well, allowing for analytical calculations.

The neutron separation energy is $S_h = \hbar^2\chi^2/(2\mu)$ where χ, named "inverse decay length" is related to the extension of the halo neutron and μ is the core-neutron reduced mass. If R is the radius of the potential well we can define the dimensionless parameter $\gamma = \chi R$. A halo nucleus has $\gamma \ll 1$, in other words its wave-function has an extension much larger than the potential well radius. In detail $R(r)$ is the solution of the outer radial Schrödinger equation for the relative motion of a core plus neutron system:

$$\left(\frac{d^2}{dr^2} + \frac{2}{r}\frac{d}{dr} - \chi^2 - \frac{l(l+1))}{r^2}\right)^2 R(r) = 0 \,, \tag{2.1}$$

where r is the relative coordinate and l is the angular momentum quantum number. The solution of equation (2.1) can be expressed by means of the spherical modified Bessel function $k_l(\chi r)$. These functions explicitly are (56):

$$\begin{aligned} k_0(x) &= \frac{e^{-x}}{x} \\ k_1(x) &= \frac{e^{-x}}{x}\left(1+\frac{1}{x}\right) \\ k_{l+1}(x) &= \frac{2l+1}{x}k_l(x) + k_{l-1}(x) \ , \end{aligned} \tag{2.2}$$

from which we can easily calculate the mean square radius $\langle r^2 \rangle$:

$$\langle r^2 \rangle = \frac{\int_0^\infty r^2 R^2(r) r^2 dr}{\int_0^\infty R^2(r) r^2 dr} \ . \tag{2.3}$$

In particular for a s-wave relative motion, eq.(2.3) yields (4):

$$\langle r^2 \rangle = \frac{\hbar^2}{4\mu S_n} \ , \tag{2.4}$$

showing an explicit dependence from the scaling parameter S_n. In particular the mean square radius diverges for s- and p-waves when S_n goes towards zero as can be calculated by inserting $k_l(\chi r)$ in eq. (2.3) with $l = 0, 1$. When $l \geq 2$ the mean square radius remains finite, even if S_n approaches zero, due to the centrifugal barrier.

The calculations that have led to eq. (2.3) and (2.4) are approximated expressions. In general one has to consider both the outer wave-function and the inner wave-function, where, due to the absence of the nuclear potential an analytical solution is not possible. It can be useful however to find an expression for matter (and charge) mean square radius that includes from the beginning the few-body structure. Because of the usefulness of this approach for di-cluster nuclei, that will be examined in the next chapter, we will derive the formula of charge and matter mean square radii for general di-cluster nuclei with mass number $A + B$ and charge Z composed by two clusters of mass and charge numbers A, Z_A and B, Z_B, respectively. The result to be proved for the matter square radius of a di-cluster nucleus is the following (4; 71):

$$\langle r^2 \rangle_{A+B} = \frac{A}{A+B}\langle r^2 \rangle_A + \frac{B}{B+A}\langle r^2 \rangle_B + \frac{AB}{(A+B)^2}\langle R^2 \rangle \ , \tag{2.5}$$

where we have these identifications:

- $\langle r^2 \rangle_A$ and $\langle r^2 \rangle_B$ are the intrinsic mean square radii of the two clusters.
- $\langle R^2 \rangle$ is the mean separation between the centers of mass of the two clusters.

In figure (2.2) a sketch of a di-cluster nucleus is shown, pointing out the vectors used in order to prove eq. (2.5)

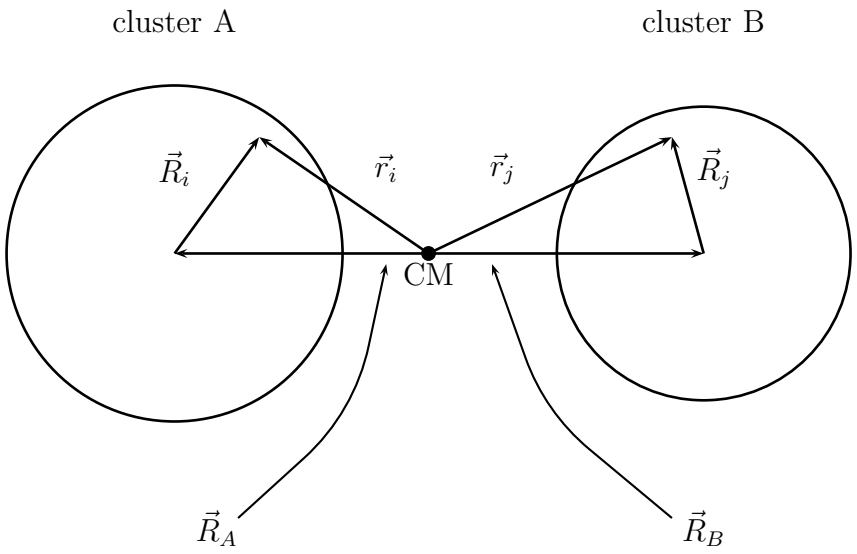

Figure 2.2: A sketch of a di-cluster nucleus coordinate system: $\vec{r}_i$ and $\vec{r}_j$ refer to the vector position of nucleons with respect to the whole nucleus center of mass, while $\vec{R}_i$ and $\vec{R}_j$ refers to the vector position with respect to the single cluster center of mass. $\vec{R}_A$ and $\vec{R}_B$ are vectors connecting the whole center of mass with the single cluster c.m.

We label the whole nucleus center of mass vector with $\vec{R}_{cm}$, and the clusters' center of mass with $\vec{R}_A$ and $\vec{R}_B$. In the center of mass frame we have the relations

$$\begin{aligned} \vec{R}_A &= -\frac{B}{A+B}\vec{R} \\ \vec{R}_B &= \frac{A}{A+B}\vec{R}\,. \end{aligned} \tag{2.6}$$

We label with $\vec{R}_i$ the nucleon coordinates of cluster A with respect to its center of mass and with $\vec{R}_j$ is the same for cluster B.

By definition we have to calculate

$$\begin{aligned} \langle r^2\rangle_{A+B} &= \frac{\sum_{i=1}^{A}\vec{r}_i^{\,2}+\sum_{j=1}^{B}\vec{r}_j^{\,2}}{A+B} \\ &= \frac{\sum_{i=1}^{A}(\vec{R}_A+\vec{R}_i^2)+\sum_{j=1}^{B}(\vec{R}_B+\vec{R}_j)^2}{A+B}\,. \end{aligned} \tag{2.7}$$

We note that

$$\sum_{i=1}^{A}(\vec{R}_A+\vec{R}_i)^2 = AR_A^2 + A\langle r^2\rangle_A + 2\cdot\underbrace{\sum_{i=1}^{A}\vec{R}_A\cdot\vec{R}_i}_{0}\,, \tag{2.8}$$

where we have used

$$\langle r^2\rangle_A = 1/A\cdot\sum_{i=1}^{A}R_i^2 \quad\text{and}\quad \sum_{i=1}^{A}\vec{R}_A\cdot\vec{R}_i = \vec{R}_A\cdot\sum_{i=1}^{A}\vec{R}_i\,,$$

and $\sum_{i=1}^{A}\vec{R}_i = 0$ because of cluster spherical symmetry. Obviously the same arguments are applied to cluster B. So, by substituting in (2.7) and using (2.6) for R_A and R_B we find (2.5). In a halo nucleus, where the cluster A in the core and the cluster B is a proton of a neutron one usually can neglect the intrinsic valence contribution to the matter radius in eq. (2.5) since it is proportional to $\simeq A\cdot A^{1/3}\propto A^{4/3}$ times smaller obtaining the standard result ($\langle r^2\rangle_{A+B}\to\langle r^2\rangle_{tot}\,,\langle r^2\rangle_A\to\langle r^2\rangle_{core}\,,A\to m_c\,,B\to m_h$):

$$\langle r^2\rangle_{tot} = \frac{m_c}{m_c+m_h}\left(\langle r^2\rangle_{core} + \frac{m_h}{m_c+m_h}\langle R^2\rangle\right) , \tag{2.9}$$

where m_c and m_h are the core and halo masses, respectively. Following the same steps we can easily obtain the formula for the charge mean square radius of a di-cluster nucleus:

$$\langle r^2\rangle^{ch}_{A+B} = \frac{Z_A}{Z}\langle r^2\rangle^{ch}_{A} + \frac{Z_B}{Z}\langle r^2\rangle^{ch}_{B} + \frac{\langle R^2\rangle}{Z}\left(\frac{Z_A B^2 + Z_B A^2}{(A+B)^2}\right) , \tag{2.10}$$

where we have similar identifications with respect to the preceding proof:

- $\langle r^2\rangle^{ch}_{A}$ and $\langle r^2\rangle^{ch}_{B}$ are the intrinsic charge mean square radii of the two clusters.
- A,B are the mass numbers of the two clusters with atomic numbers Z_A and Z_B.
- $\langle R^2\rangle$ is the mean square separation between the centers of mass of the two clusters.

We label with $\vec{R}_i$ the proton coordinates of cluster A respect to its center of mass and with $\vec{R}_j$ is the same about cluster B.

Starting from the definition

$$\langle r^2\rangle^{ch}_{A+B} = \frac{\sum_{i=1}^{Z_A}(\vec{R}_A+\vec{R}_i)^2 + \sum_{i=1}^{Z_B}(\vec{R}_B+\vec{R}_i)^2}{Z_A+Z_B} . \tag{2.11}$$

We have, with $Z = Z_A + Z_B$,

$$\langle r^2\rangle^{ch}_{A+B} = \frac{1}{Z}\left(\sum_{i=1}^{Z_A}(R_A^2 + R_i^2 + 2\vec{R}_A\cdot\vec{R}_i) + \sum_{j=1}^{Z_B}(R_B^2 + R_j^2 + 2\vec{R}_B\cdot\vec{R}_j)\right) . \tag{2.12}$$

We note that

$$\sum_{i=1}^{Z_A}\vec{R}_A^2\cdot\vec{R}_i = \sum_{j=1}^{Z_B}\vec{R}_B^2\cdot\vec{R}_j = 0 , \tag{2.13}$$

because of proton cluster spherical symmetry. Therefore by using the definition of intrinsic mean square charge radius of the two clusters, equation (2.11) becomes

$$\langle r^2\rangle^{ch}_{A+B} = \frac{Z_A}{Z}\langle r^2\rangle^{ch}_{A} + \frac{Z_B}{Z}\langle r^2\rangle^{ch}_{B} + \frac{1}{Z}\left(Z_A R_A^2 + Z_B R_B^2\right) \ . \tag{2.14}$$

Inserting (2.6) in (2.14) we find (2.10).

We can perform a similar approximation, as done from eq. (2.5) to eq. (2.9), with the advantage that, for neutron halo nuclei the contribution of the valence neutron to the charge radius is actually zero, hence the two formulas coincide.

2.3.1 Three-body systems

In order to consider the matter radius of a three-body system an extension of formula (2.9) is required. The standard treatment of Borromean nuclei consists of introducing Jacobi coordinates $(\vec{r}_1, \vec{r}_2)$ as shown in figure (2.3) and the related hyper-radius $\rho^2 = r_1^2 + r_2^2$ (25; 74).

Following this formalism the overall matter radius of a three-body halo nucleus is defined as

$$\langle r^2\rangle = \frac{1}{A}\left((A-2)\langle r^2\rangle_{core} + \langle \rho^2\rangle\right) \ , \tag{2.15}$$

where $\langle r^2\rangle_{core}$ is the mean square radius of the core. It is worthwhile noticing that there are many ways of defining the matter radius of a three-body nucleus (4). In example the matter radius of ^{11}Li, as defined in eq. (2.15) is 3.5 fm, similar to the radius of ^{48}Ca. If one follows the approach of atomic physics, the radius of ^{11}Li is given by the extension of its valence nucleons, giving a matter radius of 9 fm, as the isotopes of lead. In any case the radius obtained by reaction cross section measurements is quite different with respect to the standard law $r \sim A^{1/3}$, as shown in figure (2.4).

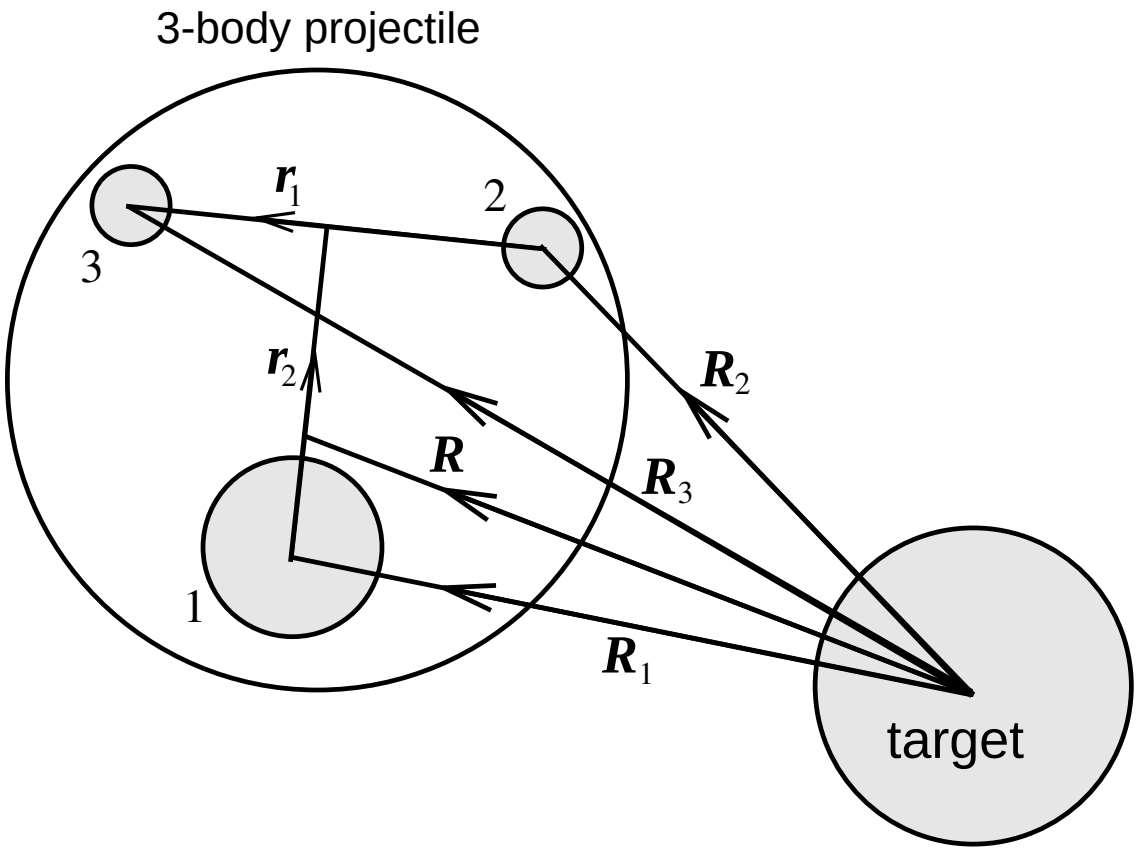

Figure 2.3: Jacobi coordinates $\mathbf{r_1}$ and $\mathbf{r_2}$ for a three-body projectile. Figure taken from (5), with permission of the authors.

2.4 Effective charges

In our calculation we often use the effective charge number of multi-polarity λ for a dicluster nucleus (A,B are the mass numbers of the clusters, with Z_A and Z_B as charge numbers)

$$Z_{eff}^{\lambda} = Z_B \left(\frac{A}{A+B}\right)^{\lambda} + Z_A \left(-\frac{B}{A+B}\right)^{\lambda} . \tag{2.16}$$

For instance it appears when we evaluate the matrix element between two states, by

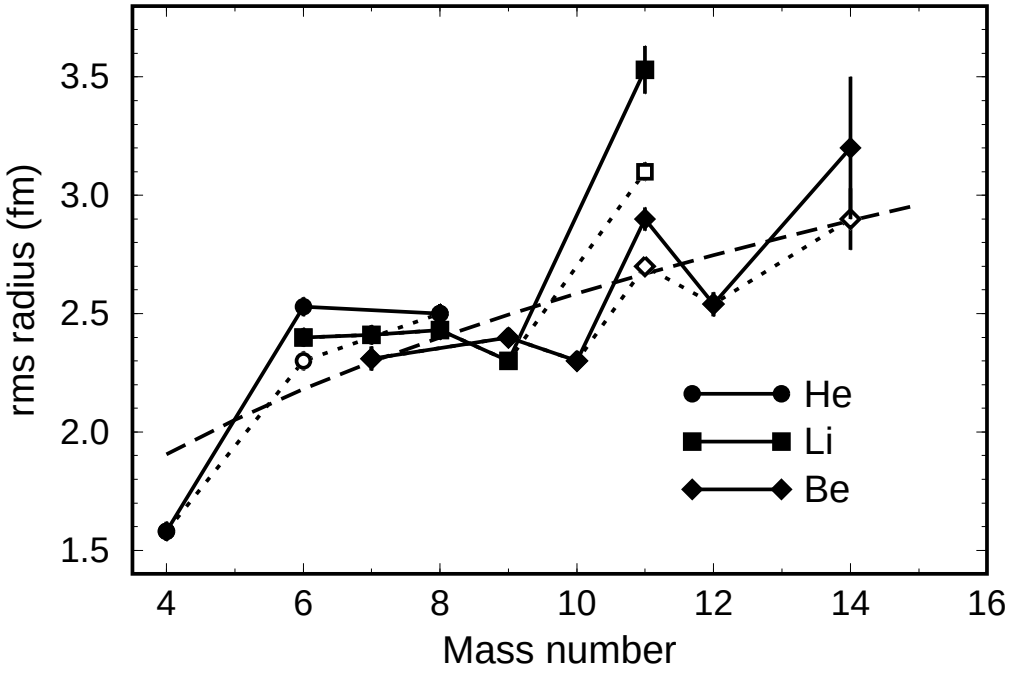

Figure 2.4: Matter radii of He, Li and Be isotopes, compared with the prediction of $r \sim A^{1/3}$. Figure taken from (5), with permission of the authors.

inserting the operator for an Eλ transition (56):

$$\mathcal{M}(E\lambda\mu) = Z_{eff}^{(\lambda)} e r^{\lambda} Y_{\lambda\mu}(\hat{r}) \; . \tag{2.17}$$

For sake of completeness it is useful to give a derivation of formula (2.16) starting from the concept of effective charge (14; 24; 56; 68). Consider a nucleus with A nucleons and Z protons. The electric dipole operator is defined as:

$$\vec{D} = \frac{e}{2} \sum_{i=1}^{A} (1 + \tau_3(i)) \, \vec{\xi}_i \; , \tag{2.18}$$

where e is the proton charge, τ_3 is the third component of the isospin, $\tau_3 = 1$ for protons and $\tau_3 = -1$ for neutrons. The coordinates $\vec{\xi}_i$ are measured in the center of mass

frame. This is essential in order to delete spurious degrees of freedom due to center of mass motion: if we expand $\vec{\xi_i} = \vec{R}_i - \vec{R}_{cm}$ in (2.18) and insert also $\vec{R}_{cm} = 1/A \cdot \sum_{i=1}^{A} \vec{R}_i$ we obtain

$$\vec{D} = e\frac{N}{A}\sum_{i=1}^{Z}\vec{r}_i - e\frac{Z}{A}\sum_{i=1}^{A-Z}\vec{r}_i \,, \tag{2.19}$$

giving the well known result for the effective charges of protons and neutrons.

Now let's consider a di-cluster nucleus and decompose the dipole operator given in (2.18) in three parts:

$$\vec{D} = \vec{D}_A + \vec{D}_B + \vec{D}_M \,, \tag{2.20}$$

where $\vec{D}_A$ and $\vec{D}_B$ are the single-cluster dipole operators with respect to their own center of mass, and $\vec{D}_M$ is the "molecular" operator associated with the relative motion of the two fragments, namely the dipole operator of two point charges, set in $\vec{R}_A$ and $\vec{R}_B$, with charges Z_A and Z_B with respect to the whole center of mass. Labeled $\vec{R}$ the vector connecting cluster A with cluster B, we have by definition:

$$\vec{D}_M = e\left(Z_A(\vec{R}_A - \vec{R}_{cm}) + Z_B(\vec{R}_B - \vec{R}_{cm})\right) \,, \tag{2.21}$$

and after inserting

$$\vec{R}_A = -\frac{B}{A+B}\vec{R} \qquad \vec{R}_B = \frac{A}{A+B}\vec{R} \,, \tag{2.22}$$

we finally obtain

$$\vec{D}_M = e\left(-Z_A\left(\frac{B}{A+B}\right) + Z_B\left(\frac{A}{A+B}\right)\right)\vec{R} \,, \tag{2.23}$$

where we recognize the effective charge number of equation (2.16) with $\lambda = 1$. In order to conclude the proof of equation (2.16) we consider the general operator Q_λ for a set of discrete charges:

$$Q_\lambda = e\sum_{i=1}^{Z} R_i^\lambda Y_{\lambda 0} \,. \tag{2.24}$$

When we decompose the operator, as in eq. (2.20), and we consider the molecular contribution we in a straightforward manner obtain eq. (2.16) just by inserting eq. (2.22) in the decomposition.

The electromagnetic response can be a very useful tool in order to study a halo structure (56; 68): operators like eq. (2.17) enhance the effect of the tail of the wave-functions and historically the unexpected large E1 transition probability between the two bound state of ^{11}Be has been a clear indication of a halo structure. In the next chapter we will deal extensively with magnetic interactions, in this section we only point out the structure of the magnetic dipole operator in order to focus on its main features (23; 24). In a general formalism in which the two clusters have mass and charge numbers A, Z_A and B, Z_B, respectively, one has

$$\mathcal{M}(M1,\mu) = \mu_N \sqrt{\frac{3}{4\pi}} \left[g_s s_\mu + l_\mu \frac{Z_B A^2 + Z_A B^2}{AB(A+B)} \right] , \tag{2.25}$$

where μ is the z-component of the magnetic dipole operator, μ_N is the nuclear magneton and s_μ and l_μ are the components of the valence particle spin and of the relative angular momentum and g_s is the gyromagnetic factor of the valence particle. As in the di-cluster picture, developed in the next chapter, the core is considered inert and structureless, therefore there is no contribution from core intrinsic degree of freedom. Two important points are to be discussed: magnetic interactions $M\lambda$ depends on $r^{\lambda-1}$ hence there is less enhancement of the tail of the wave-functions with respect to the electric interactions of the same multi-polarity. In particular, for $M1$ interaction the radial contribution is just the overlap of initial and final states, therefore, if the quantum numbers of initial and final states are the same, the $M1$ interaction between these states vanishes, because of orthogonality of different states of the same Hamiltonian, as explained in details later in this thesis.

2.5 Reaction models

Various models are able to describe the reactions involving halo nuclei to various degrees of accuracy. Some of them are suited to the high-energy regime, like the Glauber model, a semi-classical reaction model that requires the reliability of the eikonal approximation, stating that the projectile moves along a straight line trajectory through the field of the target nucleus (4; 5; 28). This model allows for a simple derivation of many reaction cross section expressions. An improvement of this model consists on including a few-body generalization in order to yield realistic calculations of the scattering processes involving halo nuclei. As said above this semi-classical model can be applied to high-energy beams, also including corrections to the straight-line trajectory of the eikonal approximation. The range of energy considered in this model is well above the typical energies of astrophysical interest. Because of these reasons we address to the large literature on this field and we will focus for the rest of this chapter on reaction models suited for weakly bound nuclei as halo nuclei or dicluster nuclei. In details we will introduce the coupled-channel approach (5; 6; 9) and then we will discuss two approximations necessary in order to perform calculations, i.e. the coupled discretised continuum channels (CDCC) and the adiabatic or sudden model.

2.5.1 Coupled Channels

Consider a generic reaction in which a projectile a, with energy E moves towards a target A (26). Before the collision the wave-function of the system is the product of the plane-wave for the projectile motion and of the intrinsic wave-functions of projectile and of target, namely:

$$\Psi = N e^{i\vec{k}_\alpha \cdot \vec{r}_\alpha} \psi_a \psi_A \ , \tag{2.26}$$

where N is a normalization constant, $\vec{k}_\alpha$ is the relative wave number of the system and $\vec{r}_\alpha$ is the relative coordinate. After the collision we have in addition to eq. (2.26)

a certain number of scattering wave-functions, one for each channel β corresponding to residual nuclei b, B:

$$\Psi = ne^{i\vec{k}_\alpha \cdot \vec{r}_\alpha}\psi_a\psi_A + \sum_\beta \Psi_{scatt,\beta} \ , \tag{2.27}$$

where n is the corresponding normalization constant in the final state wave-function. We can set the scattering wave-function $\Psi_{scatt,\beta}$ at large distance from the target as a spherical wave modulated by a function $f_\beta(\theta, \phi)$, multiplied by the intrinsic wave functions of projectile and target in the state β:

$$\Psi_{scatt,\beta}(r, \theta, \phi) \rightarrow A f_\beta(\theta, \phi)\frac{e^{ik_\beta r_\beta}}{r_\beta}\psi_\beta\psi_B \ . \tag{2.28}$$

The function $Af_\beta(\theta, \phi)$ is called scattering amplitude and it is straightly related to the cross section. In order to solve the scattering problem we consider the Schrödinger equation of the system $H\Psi = E\Psi$, where E is the total energy and H is the total Hamiltonian:

$$H = H_a + H_A - \frac{\hbar^2}{2\mu_\alpha}\nabla^2_\alpha + V_\alpha \ . \tag{2.29}$$

In the last equation H_a and H_A are the intrinsic Hamiltonians of the projectile and target and they satisfy $H_a\psi_a = \epsilon_a\psi_a$ and $H_A\psi_A = \epsilon_A\psi_A$ respectively, being $\epsilon_{a(A)}$ the binding energy of the projectile (target). The reduced mass of the system is μ_α and $\vec{r}_\alpha = \vec{r}_a - \vec{r}_A$ is the relative coordinate. The functions ψ_a and ψ_A form a complete set, therefore we can expand Ψ in this basis:

$$\Psi = \sum_{a',A'} \xi_{a'A'}(r_\alpha)\psi_{a'}\psi_{A'} \ . \tag{2.30}$$

By inserting this equation in $H\Psi = E\Psi$, with H given in eq. (2.29) we obtain

$$\sum_{a',A'} \left(H_a + H_A - E - \frac{\hbar^2}{2\mu_\alpha}\nabla^2_\alpha + V_\alpha \right) \xi_{a'A'}(r_\alpha)\psi_{a'}\psi_{A'} = 0 \ . \tag{2.31}$$

By multiplying on the left by $\psi_a^*\psi_A^*$, by integrating on the inner coordinates of projectile and target, and by remembering the orthogonality properties of ψ_a and ψ_A

$$\int \psi_a^*\psi_A^*\psi_{a'}\psi_{A'}dr_{a'}dr_{A'} = \delta_{aa'} \ , \tag{2.32}$$

eq. (2.31) becomes:

$$\left[\nabla_\alpha^2 - U_{aA,aA}(r_\alpha) + k_{aA}^2\right]\xi_{aA}(r_\alpha) = \sum_{\substack{a' \neq a \\ A' \neq A}} \xi_{a',A'}(r_\alpha)U_{aA,a'A'}(r_\alpha) \ , \tag{2.33}$$

where we have the following identifications:

$$\begin{aligned} k_{aA}^2 &= \frac{2\mu_\alpha}{\hbar^2}(E - \epsilon_a - \epsilon_A) \\ U_{aA,a'A'}(r_\alpha) &= \frac{2\mu_\alpha}{\hbar^2}\int \psi_a^*(x_\alpha)\psi_A^*(x_A)V_\alpha\psi_{a'}(x_\alpha)\psi_{A'}(x_A)dx_a dx_A \end{aligned} \tag{2.34}$$

The left side of the equation (2.34) describes the elastic scattering of a particle by the potential $U_{aA,aA}(r_\alpha)$. The right side instead describes the coupling with all the other states. In principle the number of coupled equation is infinite, therefore the mere knowledge of $U_{aA,aA}(r_\alpha)$ is not enough to solve the system. A truncation of the number of equation is necessary and it can be accomplished by selecting only the strongly coupled channels. Following this procedure an approximated solution can be found (an example is the distorted wave Born approximation (DWBA) approach). In our specific context, dealing with weakly bound system, the coupling with the continuum is vital, hence in the remaining of this chapter we will discuss two common methods in order to solve the coupled equations (2.33), where continuum is included.

2.5.2 Coupled discretised continuum channels

The coupled discretised continuum channels (CDCC) is a theoretical technique used for reactions involving a two-cluster projectile (5; 6; 9). The idea underlying this method

is the discretisation of the continuum: relative motion continuum states of the two projectile clusters, in principle infinite, are discretised in a discrete number N of square integrable states ϕ_α up to a maximal energy value. Therefore, given the projection operator

$$P = \sum_{\alpha=0}^{N} |\phi_\alpha\rangle\langle\phi_\alpha| \ , \tag{2.35}$$

where $|\phi_\alpha\rangle$ is an eigenstate of the intrinsic projectile Hamiltonian, namely $H_\alpha\phi_\alpha = \epsilon_\alpha\phi_\alpha$, the Hamiltonian of $CDCC$ is $H^{CDCC} = PHP$. The CDCC approximation of the scattering wave-function (2.27) is

$$\Psi^{CDCC}(\vec{R},\vec{r}) = \sum_{\alpha=0}^{N} \phi_\alpha(\vec{r})\chi_\alpha(\vec{R}) \ , \tag{2.36}$$

where $\alpha = 0$ refers to the projectile ground state, $\vec{R}$ is the vector from the target to the projectile center of mass and $\vec{r}$ is the relative vector between the two projectile clusters. By labeling with T_R the projectile center of mass kinetic energy operator, with $V_{\alpha\beta}(\vec{R}) = \langle\phi_\alpha|U(\vec{R}_1,\vec{R}_2)|\phi_\beta\rangle$ the coupling interaction and with $E_\alpha = E - \epsilon_\alpha$ (E is the total energy of the projectile), the set of coupled equations (2.33) becomes:

$$\Big[T_R + V_{\alpha\alpha}(\vec{R}) - E_\alpha\Big]\,\chi_\alpha(\vec{R}) = -\sum_{\beta\neq\alpha} V_{\alpha\beta}(\vec{R})\chi_\beta(\vec{R}) \ . \tag{2.37}$$

There is a certain number of features that have to be briefly discussed: practical calculations of coupling potentials have to be additionally truncated both in the maximum order used in the multipole expansion of the interaction U and in the maximum relative distance r. The number of energy bins in the continuum and their upper limit depend on the states involved in the calculations. In is important to choose carefully the parameters in order to include properly any essential features of the projectile continuum, like narrow resonant states. In general the projectile treated with CDCC calculations have few bound states, quite commonly bound exited states are absent, therefore this method

can be applied to weakly bound nuclei, as well as halo nuclei that usually have only one or two bound states.

2.5.3 Sudden or adiabatic model

For the sake of completeness we discuss also a useful simplification of the CDCC method, suited for incident projectile energies above a few tens of MeV per nucleon (4; 5). The idea is reducing the three-body problem, two-body projectile plus target, in a two-body problem, projectile as a whole plus target, in which the internal coordinate $\vec{r}$ is regarded as a parameter. This approximation is reliable if the projectile has enough energy: the relative coordinate between the target and the projectile center of mass $\vec{R}$ changes much faster than $\vec{r}$, therefore we can consider $\vec{r}$ as a fixed parameter to be evaluated later. Starting from the general Schrödinger equation for a n-body projectile

$$\left[T_R + U(\vec{R}_1, \ldots, \vec{R}_n) + H_p - E\right] \Psi(\vec{r}_1, \ldots \vec{r}_{n-1}, \vec{R}) = 0 \ , \tag{2.38}$$

where T_R is the kinetic energy operator for the center of mass of the projectile, $U(\vec{R}_1, \ldots, \vec{R}_n)$ is the sum of the interaction potential of the projectile clusters with the target, and H_p is the projectile internal Hamiltonian and $\vec{r}_{n-1}$ are the internal projectile coordinates (see figure (2.3)). The adiabatic approximation consists is replacing H_p with the ground-state energy ϵ_0. By labeling with $\Phi(\vec{R}, \vec{r})$ the wave-functions in the adiabatic approximation eq. (2.38) becomes, for a two-body projectile:

$$\left[T_R + U(\vec{R}, \vec{r}) - E + \epsilon_0\right] \Phi(\vec{R}, \vec{r}) = 0 \ . \tag{2.39}$$

In this equation the only dependence from the intrinsic coordinate $\vec{r}$ is in the potential $U(\vec{R}, \vec{r})$ and can be considered as a parameter, hence the original three-body problem is reduced in a two-body one. The crucial step of this approach, namely replacing H_p with ϵ_0 must be further commented: it means that all the eigenstates of the projectile are considered degenerate with the ground-states. This approximation is good if the total energy of the projectile E is much higher than ϵ_0. For the consistency of this model

another condition has to be fulfilled: the continuum energies where the projectile breaks up have to satisfy the same condition $E \gg \epsilon_0$. It has been shown that the adiabatic approximation works well also for incident energies of about 10 MeV/nucleon (61). This is because the first-order non-adiabatic corrections affects the scattering close to the target, where the dominant process is not scattering but absorption. Therefore, if the projectile core-target optical potential has a strong imaginary part, the adiabatic model can be used reliably also for quite low scattering energies. For two body nuclei, CDCC calculations are more accurate than adiabatic ones, especially at low energies, but in this last method both tricky convergence issues or computational limitations are absent.

2.6 Conclusion

In this chapter we have summarized a few well-known aspects of the field of halo nuclei, including reactions models. Several review works exist on this subject. Arguments have been selected with the aim of showing the links between these kind of nuclei with the two-cluster nuclei, that will be the subject of the next chapter. Following this approach, most of this chapter has been devoted in deriving standard formulas as those about charge and mass mean square radii or about the effective charges in electric transitions, that are often found in literature without any comment.

In the next chapter we will discuss in great detail di-cluster nuclei, by focusing on static properties of ^{7}Li and ^{7}Be and on their response to electromagnetic interactions. In particular we will give a quite complete treatment of magnetic dipole interaction from a theoretical point of view.

Chapter 3

Di-cluster Nuclei

3.1 Introduction

It is well known that the properties of $A = 7$ mass nuclei may be effectively described in terms of a dicluster model: two (inert) clusters in interaction with each other (7; 17; 38; 39; 40; 44; 71; 73). A long-standing description of these nuclei with such a dicluster picture has achieved excellent results and a continued interest because it catches the essential physics within a very simple, yet powerful, model. Such a simple nuclear structure scheme may then be used in reaction calculations (27). The need to go beyond this level of description may be justified only with the aim of taking into account more refined considerations on the role of the Pauli principle or on the occurrence of complex phenomena like polarization of the clusters, and not because the model itself does not reproduce static and dynamic properties of $A = 7$ nuclei to a good degree of accuracy. For example *ab initio* shell model calculations using a computationally heavy Monte Carlo method have successfully reproduced many properties of these and other light nuclei starting from a nucleon-nucleon interaction (50). By computing ground state overlap functions, these calculations have shown that ^{7}Be has a spectroscopic factor of almost 1 in the $\alpha + {}^3$He configuration and, similarly, ^{7}Li has a large spectroscopic factor in the $\alpha + t$ channel. A number of other approaches, that we will not discuss here, such as

Resonating Group Methods or Generator Coordinates Methods, are available to various degrees of complication and success. In addition we must mention a very recent study by Canton and Levchuk on the low-energy capture reactions (18) using the Multichannel Algebraic Scattering approach that has been applied to the ^{3}He$(\alpha,\gamma)^7$Be reaction at astrophysical energies achieving a good agreement with S-factors data. The dicluster model can be used in order to calculate a number of static and dynamic properties of ^{7}Li and ^{7}Be (54), especially in connection with excitations to the continuum in break-up processes. Indeed a peculiar feature of these nuclei is the concentration of multipole strength just above the continuum threshold, namely for the break-up of ^{7}Li in α + ^{3}H and of ^{7}Be in α + ^{3}He (47). In addition we investigate the magnetic excitations to the continuum. It is in fact important to give proper estimates of their contributions to reaction cross-sections, especially at energies of astrophysical interest. These two isospin mirrors not only display very similar ground state properties, but also manifest a similar behavior as long as their response to the continuum is considered. Nowadays it is becoming more and more evident that to properly describe structure and reactions of loosely bound systems, e.g. nuclei along the drip lines, it is essential to take into account the coupling to the continuum and the break up channel. This is relatively simple in the case of one-particle halo nuclei. In the case of more complex weakly-bound nuclei such as ^{7}Li or ^{7}Be, the cluster picture offers the possibility of describing the ground and a few excited states in terms formally analogous to that of a single-particle picture, with the *caveat* that the single particle is not just a neutron or a proton, but a composite one, like for instance a triton.

3.2 Dicluster description of ^{7}Li and ^{7}Be

Di-cluster nuclei ^{7}Li and ^{7}Be share many properties: their ground state is a $3/2^-$ one, and they have only another excited bound state with spin-parity equal to $1/2^-$. Both can be seen as made of two well separated clusters, α and ^{3}H for ^{7}Li and α and ^{3}He for ^{7}Be. The B(E2) transitions between their bound states are of comparable magnitude. They

show the same qualitative behavior about the response to the continuum, i.e. both ones have a peaked resonance with quantum numbers equal to $7/2^-$ and a smooth resonance with quantum numbers equal to $5/2^-$. See tables (3.2) and (3.3) for a summery of their electric static properties and figure (3.4, 3.5, 3.6, 3.7) for a summary of their electric response to the continuum.

Also for magnetic properties they share the same behavior, as discussed later in this chapter.

All these similarity make possible to use a unique framework to calculate all their physical properties. Of course, as in any theory driven by phenomenological considerations, a certain degree of approximation comes into play, and one needs to consider the pros and cons of the approach. We mention therefore that considering the clusters as spherical and elementary, but not point-like, has some implications: i) one neglects possible polarization effect, which may come into play because of the proximity of the two clusters and ii) one neglects nucleon-exchange effects between the two clusters. We shall prove that these limitations are not severe (see also (27)) and the model works rather well for the $A = 7$ nuclei.

Our inter-cluster potential is assumed to be the sum of a nuclear Woods-Saxon potential, a Coulomb potential and a spin-orbit interaction. A simple picture of the potential used and of bound and resonant states for ^{7}Li and ^{7}Be is sketched in figure (3.1).

In detail the procedure we use is to solve the radial Schrödinger equation for the inter-cluster reduced radial wave-function ψ, namely

$$\frac{d^2\psi}{dr^2} = \left(\frac{2\mu}{\hbar^2}(V_{WS} + V_{\vec{l}\cdot\vec{s}} + V_{coul}) + k^2 + \frac{l(l+1)}{r^2}\right)\psi \,, \tag{3.1}$$

where μ is the reduced mass of the two clusters, k is the wave-number of the bound states and the potentials used are a nuclear Wood-Saxon potential, a spin-orbit potential and an electrostatic potential of the form:

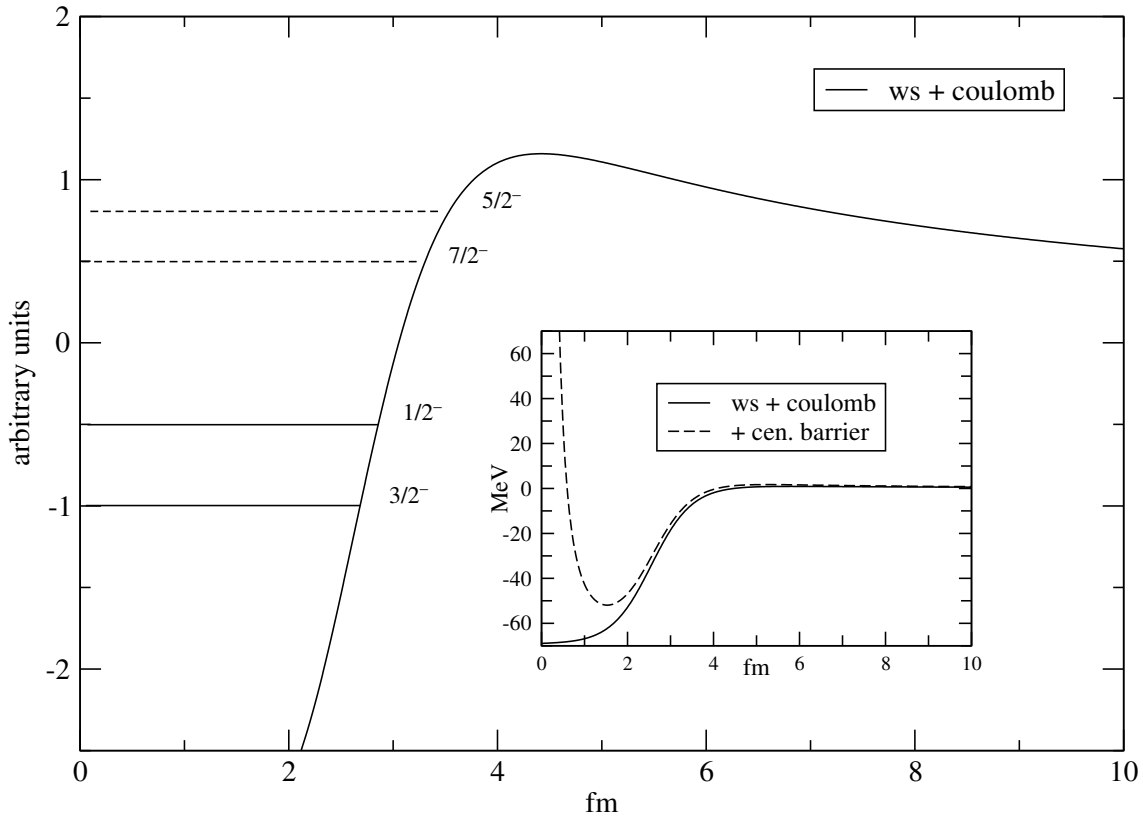

Figure 3.1: A sketch of the inter-cluster potential is shown. The outer plot shows the qualitative level structure of ^{7}Li and ^{7}Be, while in the inner plot we show the potential in a quantitative fashion. Indeed, by inspecting values of table (3.1), in is outstanding that optical potentials of ^{7}Li and ^{7}Be are quantitatively very similar.

$$
\begin{aligned}
V_{WS}(r) &= -\frac{V_0}{1+e^{\frac{r_0 A^{1/3}-r}{a}}} \\
V_{\vec{l}\cdot\vec{s}}(r) &= V_{so}\,\vec{l}\cdot\vec{s}\,\frac{r_0^2}{r}\,\frac{dV_{WS}(r)}{dr} \\
V_{coul}(r) &= \begin{cases} \frac{Z_A Z_B e^2}{r} & \text{if} \quad r > r_p \equiv r_0(A^{1/3}+B^{1/3}) \\ \frac{Z_A Z_B e^2}{2r_p}\left(3-\frac{r^2}{r_p^2}\right) & \text{if} \quad r > r_p \end{cases}
\end{aligned}
\tag{3.2}
$$

The Coulomb potential has the standard $1/r$ behavior at distances larger than r_p, but at small distances we use the Coulomb potential generated by a uniform spherical charge distribution. Note that it is not possible to identify one of the two clusters as a core and the other as a valence particle, since the two fragments have comparable masses and charges. In the spin-orbit interaction, r_0 is the radius of the Woods-Saxon potential, $\vec{l}$ refers to the relative angular momentum, and $\vec{s}$ refers to the spin of the triton (^{3}He) which can be seen as a "heavy" single-particle for ^{7}Li (^{7}Be).

For the actual values used see the table (3.1).

Quantity	^{7}Li(bound)	^{7}Li(resonances)	^{7}Be(bound)	^{7}Be(resonances)
V_0 (MeV)	-74.923	-68.255	-73.851	-64.68
V_{so} (MeV)	1.934	3.115	1.275	1.94
r_0 (fm)	1.506		1.60	
a (fm)	0.68		0.48	

Table 3.1: The optical parameters for ^{7}Li and ^{7}Be are shown. In detail V_0, r_0 and a are the depth, the radius and the diffusivity of the Woods-Saxon potential and V_{so} is the depth of the spin-orbit potential. Column "bound" refers to the parameter used for bound states and continuum non-resonant states. Finally column "resonances" refers to parameter used in order to reproduce the two f-resonances. As one can see only the depths of the two potentials differ in dealing with resonant and non-resonant states, radius and diffusivity of Wood-Saxon potential are the same for all the states considered.

The Schrödinger equation (3.1) is solved numerically with the proper boundary conditions: for bound states, outside the nuclear potential, the asymptotic wave-function is proportional to a Whittaker function, $W_{\eta,\, l_i+1/2}(2kr)$ (68), where η is the Sommerfeld parameter, while for $r \to 0$ the wave-functions is $\propto r^l$. The correct shape is obtained by matching the internal and the external solutions. Dealing with continuum wave functions the method is the same, just one has to use a combination of regular and irregular Coulomb wave-functions for the outer wave-function, $\psi(E_c, r) \propto$

$\cos(\delta)F_l(\eta;kr)+\sin(\delta)F_l(\eta;kr)$ (1; 68). The correct phase-shift δ is obtained by matching this outer solution with the internal one. In figure (3.2) we show a continuum radial wave-function of the system $\alpha+{}^3$He evaluated for $E=50$ keV. A comparison between the used wave-function, which includes the Coulomb and the nuclear potential, and the asymptotic one, i.e. keeping only the Coulomb potential (see chapter 14 of (1)) is presented: these two wave-functions are identical far outside the nuclear well, whilst they differ in the interior region. This difference, although spatially very confined, it is essential in evaluating the matrix element because of the shape of the bound wave-function (see figure (3.10 and 3.11) later in this chapter).

In figure (3.3) the integrand $\psi_b(r)r\psi_c(E_c,r)$, which serves in the evaluation of the matrix elements, is shown. It is clear that the difference between the inclusion or not of the nuclear potential in the calculation is not negligible.

3.3 Electric properties

In the cluster model we can calculate many static and dynamic properties of ^{7}Li and ^{7}Be. In tables (3.2) and (3.3) some of these are computed. Matter and charge mean square radii have been theoretically discussed in the previous chapter, whilst the reduced matrix element between the ground state and the first excited state $B(E2,3/2^-\rightarrow 1/2^-)$ and the response to the continuum will be discussed later in this chapter. For sake of completeness we give a derivation of the formulas used to evaluate the charge quadrupole moment.

Matter and charge quadrupole operators moments are defined as

$$\begin{aligned} Q^{matter} &= \sum_{i=1}^{A+B} r_i^2 Y_{20}(\theta_i,\phi_i) \\ Q^{charge} &= \sum_{i=1}^{A+B} e_i r_i^2 Y_{20}(\theta_i,\phi_i)\ , \end{aligned} \tag{3.3}$$

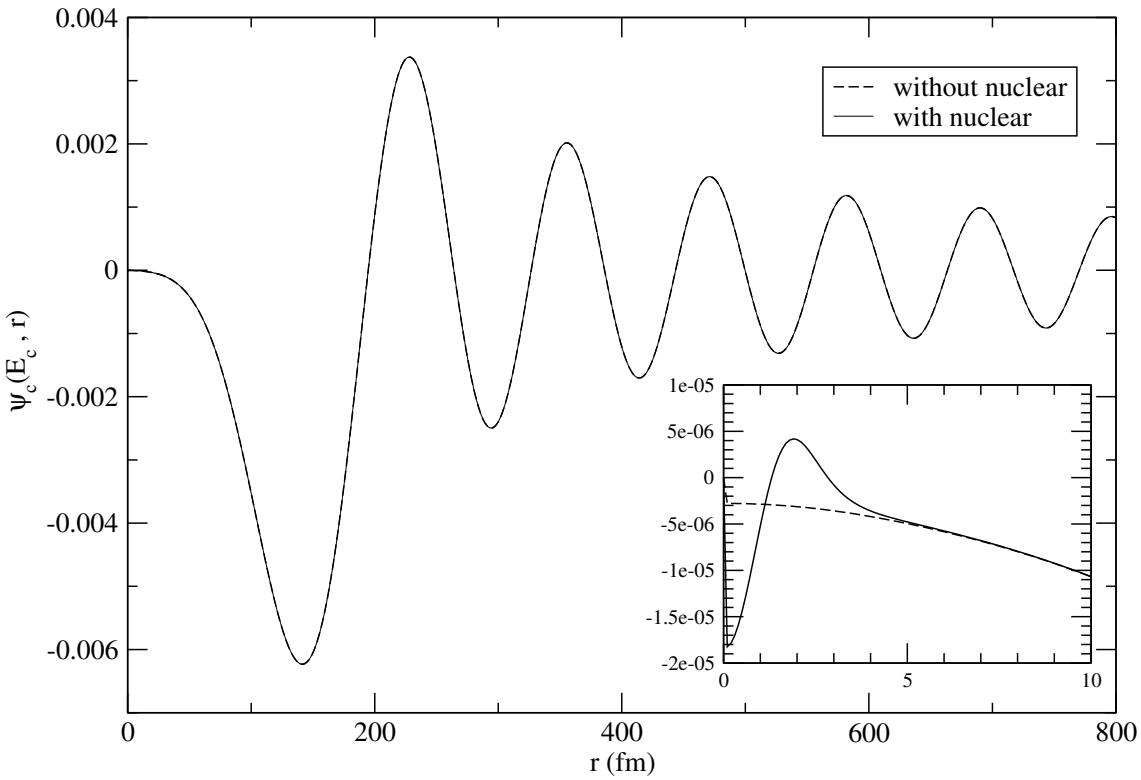

Figure 3.2: A comparison between α+^{3}He system wave functions for $E_c = 50$ keV is shown. The difference between the pure Coulomb wave-function and the actual one is important only in the interior region, where the nuclear potential is different from zero. However, in calculating matrix element, the interior region give most of the contribution, therefore this small overall difference plays an important role in a proper evaluation of electromagnetic response.

where the summation runs over all particles and, by using the definition of the spherical harmonic and by splitting the sum over the total nucleon number into two sums over the nucleons of each cluster, we obtain two relationships that contain the intrinsic quadrupole moments of each cluster and a term expressing the quadrupole operator for the relative motion, namely:

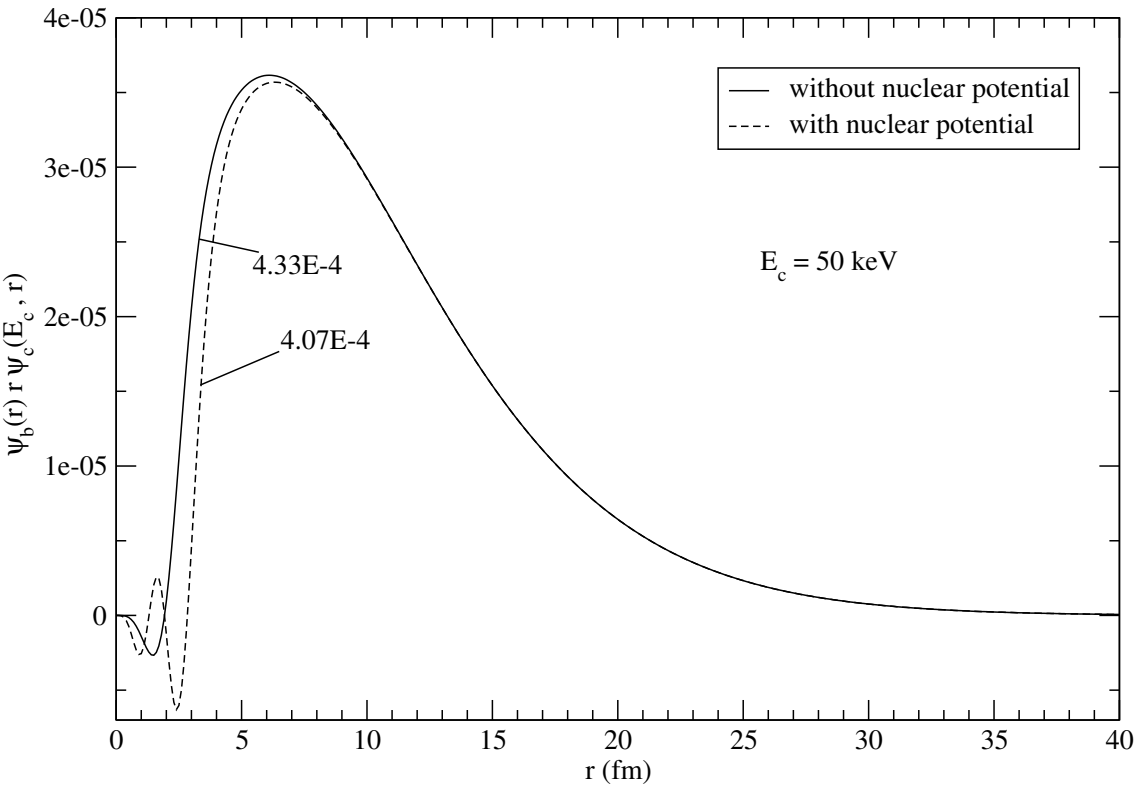

Figure 3.3: In this figure the shape of the integrand $\psi_b(r)r\psi_c(E_c, r)$ is shown. With respect to continuum wave-functions of figure (3.2) the difference between including or not the nuclear potential is not negligible, as shown by comparing the integrated values $4.33 \cdot 10^{-4}$ and $4.07 \cdot 10^{-4}$.

$$\begin{aligned} Q^{mat} &= Q_A^{mat} + Q_B^{mat} + \frac{AB^2 + BA^2}{(A+B)^2} R^2 Y_{20}(\Theta, \Phi) \\ Q^{ch} &= Q_{A_1}^{ch} + Q_B^{ch} + \frac{Z_A B^2 + Z_B A^2}{(A+B)^2} R^2 Y_{20}(\Theta, \Phi) \ . \end{aligned} \tag{3.4}$$

With these operators one can calculate the quadrupole moments by evaluating the expectation value in the ground state with the maximally aligned magnetic substate:

$$Q^{mo} = \sqrt{\frac{16\pi}{5}} \langle L, M = L \mid Q \mid L, M = L \rangle \ , \tag{3.5}$$

where Q is either the charge or the matter operator. For example in the case of the matter quadrupole moment one has:

$$\begin{aligned} Q^{mat.mo} &= Q_A^{mat.mo} + Q_B^{mat.mo} + \frac{AB^2 + BA^2}{(A+B)^2} \langle R^2 \rangle \cdot \\ &\cdot \quad 2(2L+1)(-1)^L \begin{pmatrix} L & 2 & L \\ -L & 0 & L \end{pmatrix} \begin{pmatrix} L & 2 & L \\ 0 & 0 & 0 \end{pmatrix} \ , \end{aligned} \tag{3.6}$$

where L is the angular momentum of the relative motion state. In the case of the two mirror isobars lithium and beryllium we have $L = 1$ and therefore the above formula reduces to

$$Q^{mat.mo} = Q_A^{mat.mo} + Q_B^{mat.mo} - \frac{2}{5} \frac{AB^2 + BA^2}{(A+B)^2} \langle R^2 \rangle \ . \tag{3.7}$$

Analogous expressions may be derived for the charge quadrupole moments that differ only in the coefficient depending linearly on charges rather than masses. Notice also that, while the coefficient of the relative motion contribution for the charge quadrupole moment is different for lithium and beryllium, the one for the matter quadrupole moment is the same. Another difference comes from the average square radius of the relative motion wave function, which is not identical for the two nuclei, due to the different charges of the lighter clusters.

3.3.1 Response to the continuum

We are interested in the electromagnetic response for the transitions from the ground state to the first excited state and to continuum states, via E1 and E2 interactions. In a subsequent section we will deal with the magnetic dipole response. In this model all the features of the transitions are due to modifications of the wave-function describing the relative motion between the two clusters. These clusters are considered frozen, therefore

Quantity	this work	experiments
$\langle r^2\rangle^{ch}_{A+B}$(fm)	2.44	$2.55\pm0.07^{(71)}$
		$2.39\pm0.03^{(71)}$
		$2.43\pm0.03^{(63)}$
$\langle r^2\rangle_{A+B}$ (fm)	2.48	$2.5\pm0.03^{(63)}$
Q^{charge} (fm^2)	- 3.77	$-3.8 \pm 1.1^{(71)}$
		$-3.4 \pm 0.6^{(71)}$
		$-3.70\pm 0.08^{(71)}$
$B(E2, 3/2^- \rightarrow 1/2^-)$ (e^{2}fm^4)	7.55	$8.3\pm0.6^{(71)}$
		$8.3\pm0.5^{(71)}$
		$7.59\pm0.12^{(70)}$
		$7.27\pm0.12^{(70)}$
$\Gamma(7/2^-)$ (keV)	~ 110	$93 \pm 8^{(66)}$
		$69^{(32)}$
$\Gamma(5/2^-)$ (MeV)	~ 0.93	$0.918^{(32)}$

Table 3.2: Comparison of calculated and experimental quantities of ^{7}Li. The second column shows our results, while in the third there are the corresponding experimental data. The superscripts in brackets indicate the references.

there is no any contribution to the strength arising from their intrinsic modification. Following the formalism delineated in chapter 17 of Ref. (23) the strength distribution for the transition form an initial state with wave-function $\psi_{n_i l_i}(r)$, with quantum number n_i, l_i, j_i to a final state in the continuum $\psi_{n_f l_f}(r, E_c)$ with quantum numbers n_f, l_f, j_f is written as (27):

Quantity	this work	experiments
$\langle r^2 \rangle^{ch}_{A+B}$ (fm)	2.52	$2.52 \pm 0.03^{(63)}$
$\langle r^2 \rangle_{A+B}$ (fm)	2.48	$2.48 \pm 0.03^{(63)}$
Q^{charge} (fm^2)	- 4.79	-
$B(E2, 3/2^- \rightarrow 1/2^-)$ $(e^2 fm^4)$	18.3	-
$\Gamma(7/2^-)$ (keV)	~ 90	$175 \pm 7^{(32)}$
$\Gamma(5/2^-)$ (MeV)	~ 0.8	$1.2^{(32)}$

Table 3.3: Comparison of calculated and experimental quantities of ^{7}Be. The second column shows our results, while in the third we report experimental data. The superscripts in brackets indicate the references.

$$\frac{dB(E\lambda}{dE_c} = e^2_\lambda \frac{(2j_f+1)(2l_f+1)(2l_i+1)(2\lambda+1)}{4\pi} \begin{pmatrix} l_f & \lambda & l_i \\ 0 & 0 & 0 \end{pmatrix}^2 \cdot \cdot \begin{Bmatrix} l_f & j_f & j_{cl} \\ j_i & l_i & \lambda \end{Bmatrix}^2 \cdot \left(\int_0^\infty \psi_{n_f l_f}(r, E_c) r^{\lambda+2} \psi_{n_i l_i}(r) \right)^2 , \tag{3.8}$$

where e^2_λ is the effective charge defined in eq. (2.16), l_i, j_i are the initial orbital and total angular momenta, l_f, j_f are the final orbital and total angular momenta, λ is the multi-polarity of the transition, $j_{cl} = 1/2$ refers to the spin of ^{3}H for ^{7}Li and of ^{3}He for ^{7}Be. Figure (3.4) and (3.5) show the response for $E1$ and $E2$ transitions for ^{7}Li. We refer to (27) for a more detailed treatment of electric response for ^{7}Li, while in this work, with regards to electric response, we focus on its mirror ^{7}Be.

Figure (3.6) shows differential $dB(E1)/dE_c$ for continuum states allowed by E1 interactions for ^{7}Be. Also in this case there are not any resonances in the low-lying continuum and the visible peaks have a non-resonant nature (19). Dot-dashed line refers to continuum $s_{1/2}$ state, dashed line and long-dashed refers to $d_{3/2}$ and $d_{5/2}$ states respectively. The solid line gives the sum of all contributions. The total integrated non-energy

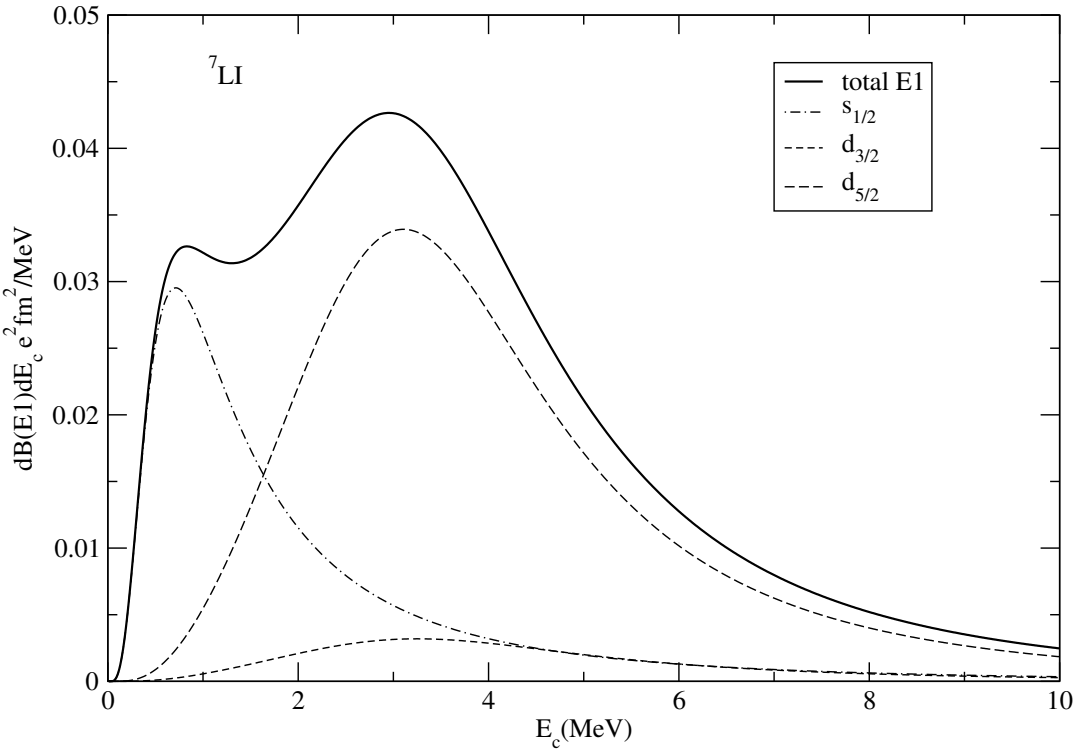

Figure 3.4: Differential dB(E1)/dE$_c$ in e^{2}fm^2/MeV of ^{7}Li for transitions from the ground-state to the continuum. Energies are in MeV, referred to the threshold for breaking into the $\alpha-^3$H channel. Separated contributions are indicated in the legend. Solid line shows the sum of all the electric dipole contributions. See also (27) for a more detailed description.

weighted B(E1) is 0.226 e^{2}fm^2. Figure (3.7) shows differential $dB(E2)/dE_c$ for continuum states allowed by an E2 interaction. Long-dashed and dashed lines refer to $f_{7/2}$ and $f_{5/2}$ states respectively, while dotted and dot-dashed lines refer to $p_{3/2}$ and $p_{1/2}$ states respectively. The f states take contributions both from the resonances and from the non-resonant part of the continuum, while the peaks of the p states arise purely from non-resonant transitions. We show also in the inset the full $f_{7/2}$ resonance on a different scale because it reaches a maximum of about 150 e^{2}fm^4/MeV. Finally solid line gives the

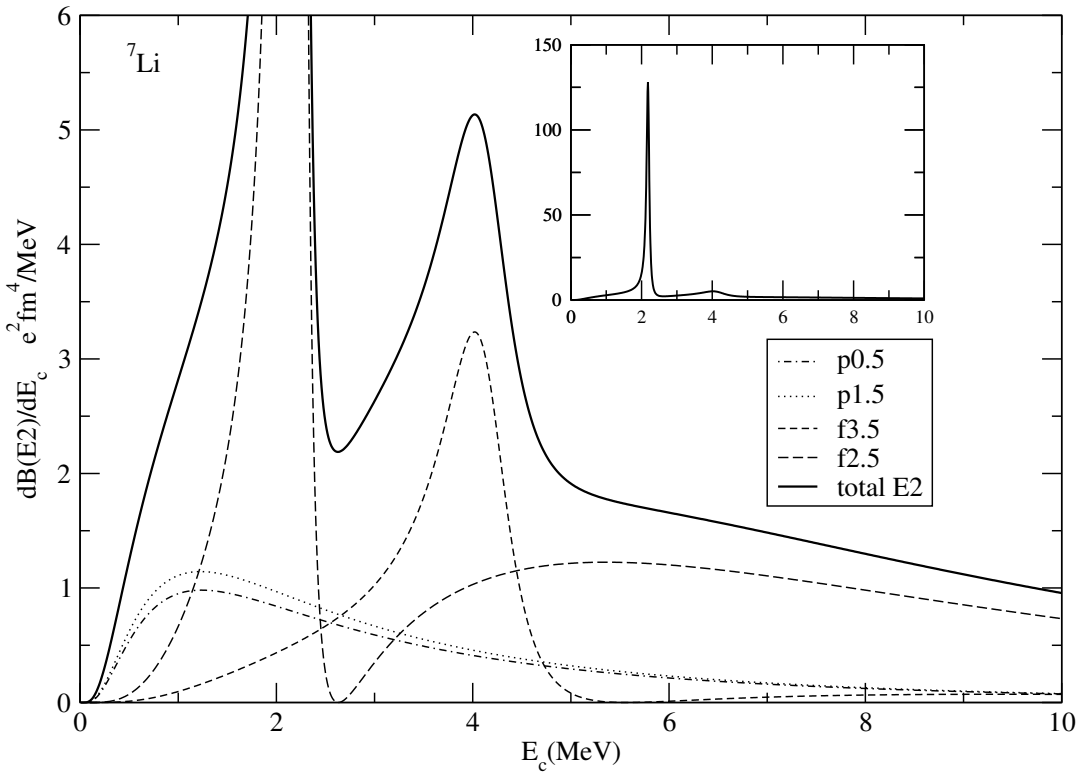

Figure 3.5: Differential dB(E2)/E_c in e^2fm^4/MeV of ^{7}Li for transitions from the ground-state to the continuum. Energies are in MeV, referred to the threshold for breaking into the $\alpha-^3$H channel. Separated contributions are indicated in the legend. Solid line shows the sum of all the electric quadrupole contributions. See also (27) for a more detailed description.

sum of all contributions. The total integrated non-energy weighted B(E2) is 113.5 e^2fm^4 to be compared with the B(E2) between the two bound state reaching 18.3 e^2fm^4. Non resonant continuum states $p_{1/2}$ and $p_{3/2}$ are dominant at very low continuum energy, while they become negligible at higher energies around and beyond the $f_{5/2}$ peak.

In addition to electric excitations we also consider magnetic ones. Magnetic dipole interactions give normally contributions to the transition probabilities that are almost comparable with electric quadrupole and smaller than electric dipole. It appears however,

already in old calculations (13), for the photo-disintegration of the deuteron (the smallest dicluster nucleus), that they are relevant at astrophysical energies (say below 200 keV) where they even turn out to dominate over the electric dipole. For this reason we will investigate this theme further in this chapter, see section 3.5 to better understand the role they might play in low-energy nuclear reactions involving dicluster systems.

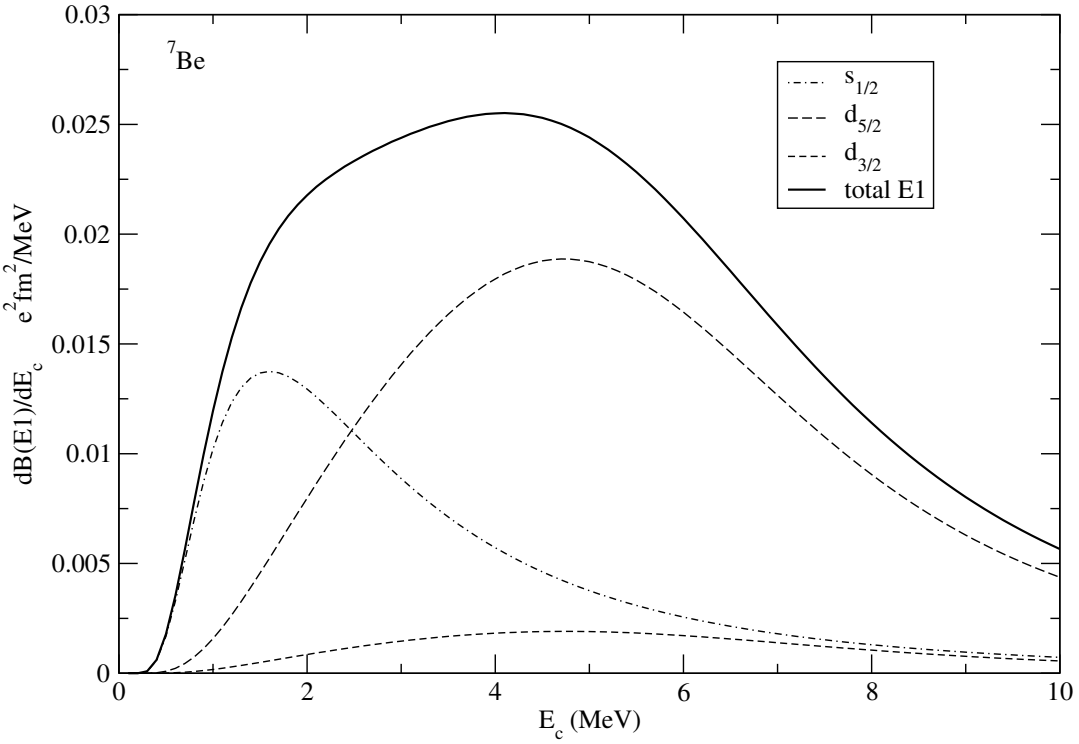

Figure 3.6: Differential dB(E1)/dE$_c$ in e^{2}fm^2/MeV of ^{7}Be for transitions from the ground-state to the continuum. Energies are in MeV, referred to the threshold for breaking into the $\alpha-^3$He channel. Separated contributions are indicated in the legend. Solid line shows the sum of all the electric dipole contributions.

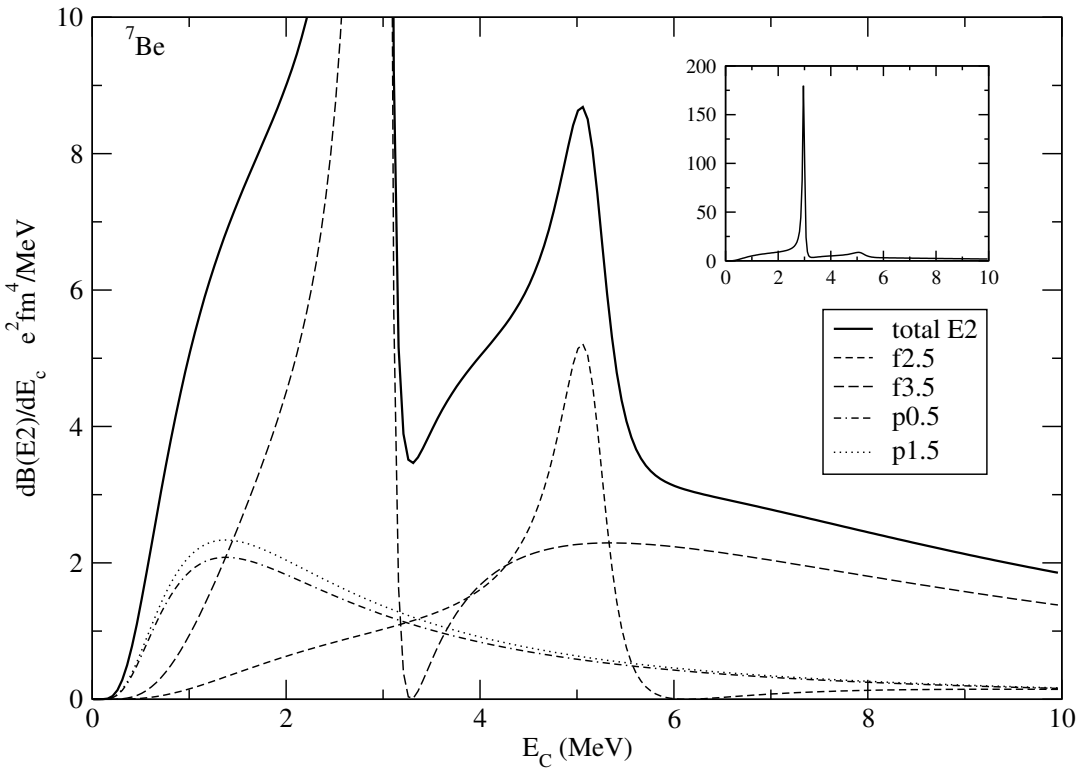

Figure 3.7: Differential dB(E2)/E_c in e^2fm^4/MeV of ^{7}Be for transitions from the ground-state to the continuum. Energies are in MeV, referred to the threshold for breaking into the $\alpha-^3$He channel. Separated contributions are indicated in the legend. Solid line shows the sum of all the electric quadrupole contributions.

3.4 Molecular sum rules

Dealing with the analysis of the nuclear spectra, it is often useful, in order to check calculations, to use general relations between transition operators that follow from basic algebraic relations, (i.e. the sum of the possible transition probabilities from a certain state is equal to one). These relations often can be expressed like sum rules (3; 12; 14; 44). In general, labeling with F a transition operator, with $|0\rangle$ the ground state and with $|a\rangle$

the complete set of states reachable from $|0\rangle$ this general relations holds (14):

$$S(F) \equiv \sum_a (E_a - E_0) \left|\langle a|F|0\rangle\right|^2 = \frac{1}{2}\langle 0 \left|[F,[H,F]]\right| 0\rangle \ , \tag{3.9}$$

where E_a is the energy of state $|a\rangle$ and H is the Hamiltonian of the system. The proof of eq. (3.9) is straightforward starting from the double commutator form: $[F,[H,F]] = 2FHF - FFH - HFF$ and, by inserting the completeness relation $\sum_a |a\rangle\langle a| = 1$ between every pair of operators, eq. (3.9) follows. If F is a one-particle moment, which does depend only on spatial coordinates,

$$F = \sum_k F(\vec{r}_k), \tag{3.10}$$

where the sum is on the nucleons coordinates, the only non vanishing contribution in the commutator with the Hamiltonian arises from the kinetic energy and in particular equation (3.9) yields (14) :

$$S(F) = \langle 0| \sum_k \frac{\hbar^2}{2M_k} \left(\nabla_k F(\vec{r}_k)\right)^2 |0\rangle \ , \tag{3.11}$$

Many common operators have the structure of eq. (3.10), as the multipole field operators,

$$F_{\lambda\mu} = f(r) Y_{\lambda\mu}(\theta,\phi) \ . \tag{3.12}$$

By using the general rules for the gradient of spherical harmonics, we have the general result (14):

$$\begin{aligned} S(F_\lambda) &\equiv \langle 0| \frac{\hbar^2}{2M} \sum_{\mu,k} |\nabla_k F_{\lambda\mu}(\vec{r}_k)|^2 |0\rangle \\ &= \frac{2\lambda+1}{4\pi} \frac{\hbar^2}{2M} A \langle \left(\frac{df}{dr}\right)^2 + \lambda(\lambda+1)\left(\frac{f}{r}\right)^2 \rangle \ . \end{aligned} \tag{3.13}$$

In particular when we consider the electric multipole moment for a system of nucleons in the center of mass frame (see eq. (2.19)), namely,

$$\mathcal{M}(E\lambda,\mu) = e\left(\sum_p \frac{N}{A} r^\lambda Y_{\lambda\mu} - \sum_n \frac{Z}{A} r^\lambda Y_{\lambda\mu}\right) \ , \tag{3.14}$$

by inserting this equation in (3.13) we obtain the well known results:

$$\begin{aligned} S(E1) &= \frac{9}{4\pi}\frac{\hbar^2}{2M}\frac{NZ}{A}e^2 \quad \text{TRK} \\ S(E2) &= \frac{50}{4\pi}\frac{\hbar^2}{2M}Ze^2\langle r^2\rangle^{ch}\,. \end{aligned} \tag{3.15}$$

where M is the nucleon mass and $\langle r^2\rangle^{ch}$ is the mean square charge radius. These results hold if nucleons can be considered elementary particles, hence there is not contribution from inner degrees of freedom (14). In addition there is also an opposite situation, when the transitions do not originate because of all nucleons, as if there would be frozen degrees of freedom, i.e. frozen sub-systems as α and ^{3}H in ^{7}Li and α and ^{3}Be in ^{7}Be. Our calculations show that the EWSR (3.15) are clearly not exhausted by considering only the transitions which imply changes in the relative motion (see table (3.6)). We assume that the suitable sum rules in this case are the energy weighted molecular sum rules (EWMSR) that can be obtained by removing the contributions of the individual clusters (3). If a nucleus with mass and charge (A+B, Z) is split into two clusters (A, Z_A) and (B, Z_B) then the EWMSR is in general defined as

$$S_{mol}(E\lambda, A+B) = S(E\lambda, A+B) - S(E\lambda, A) - S(E\lambda, B)\,. \tag{3.16}$$

For electric dipole (3) one obtains:

$$S_{mol}(E1, A+B) = \frac{9}{4\pi}\frac{(Z_A B - Z_B A)^2}{(A+B)AB}\frac{\hbar^2 e^2}{2M}\,. \tag{3.17}$$

This formula can be set in an equivalent form by extracting the dipole effective charge for a dicluster system, see eq. (2.16)

$$S_{mol}(E1, A+B) = \frac{9}{4\pi}\frac{\hbar^2 e^2}{2M}\left(Z_A\frac{B}{A+B} - Z_B\frac{A}{A+B}\right)\left(\frac{Z_A}{A} - \frac{Z_B}{B}\right)\,. \tag{3.18}$$

This form is useful in order to show the proportionality of the electric dipole EWMSR with respect to the effective charge and in order to see clearly that, for a di-cluster nucleus, like ^{6}Li, where the ratio between charge and mass of the two clusters is the

same, the molecular dipole energy-weighted sum rule vanishes. The derivation of the EWMSR for quadrupole interaction is straightforward just by inserting the di-cluster charge radius given in eq. (2.10) into eq. (3.15) and by subtracting the single cluster contributions:

$$S_{mol}(E2, A+B) = \frac{25}{4\pi}\frac{\hbar^2 e^2}{M}\left(Z_A\left(\frac{B}{A+B}\right)^2 + Z_B\left(\frac{A}{A+B}\right)^2\right)\langle R^2\rangle \tag{3.19}$$

With respect to the correspondent equation given in (3) eq. (3.19) shows directly the proportionality to the quadrupole effective charge.Here the sum rule exhibits a direct dependence on $\langle R^2\rangle$ rather than on a phenomenological intercluster separation distance, say S_0 in (3), that was introduced artificially.

3.4.1 The Wildermuth's rule

In order to properly calculate all the contributions to the EWSM it is necessary to include also the virtual states: these states are not physical ones and they lie in energy below the ground-state. They are not populated because of the Pauli exclusion principle and they yield a negative contribution to the EWSR. In particular their contribution is essential in order to compare theoretical predictions with numerical calculations. In dealing with E1 transitions, their negative contribution in modulus amounts up to 50% of the positive contribution arising form transitions to the continuum. In dealing with E2 contributions they are not particularly important because most of the strength goes to the continuum f-resonances. We have calculated all the contributions of E1 and E2 transitions, including also the contribution of "virtual" states, or states that are not allowed by the Wildermuth's rule, ($0s_{1/2}, 1s_{1/2}, 0d_{5/2}, 0d_{3/2}$ for electric dipole and $0p_{3/2}, 0p_{1/2}$ for quadrupole) which takes into account the Pauli principle. Virtual states for ^{7}Li and ^{7}Be are sketched in figure (3.8). The order of the states is the same for these nuclei and the position in energy is approximately correct.

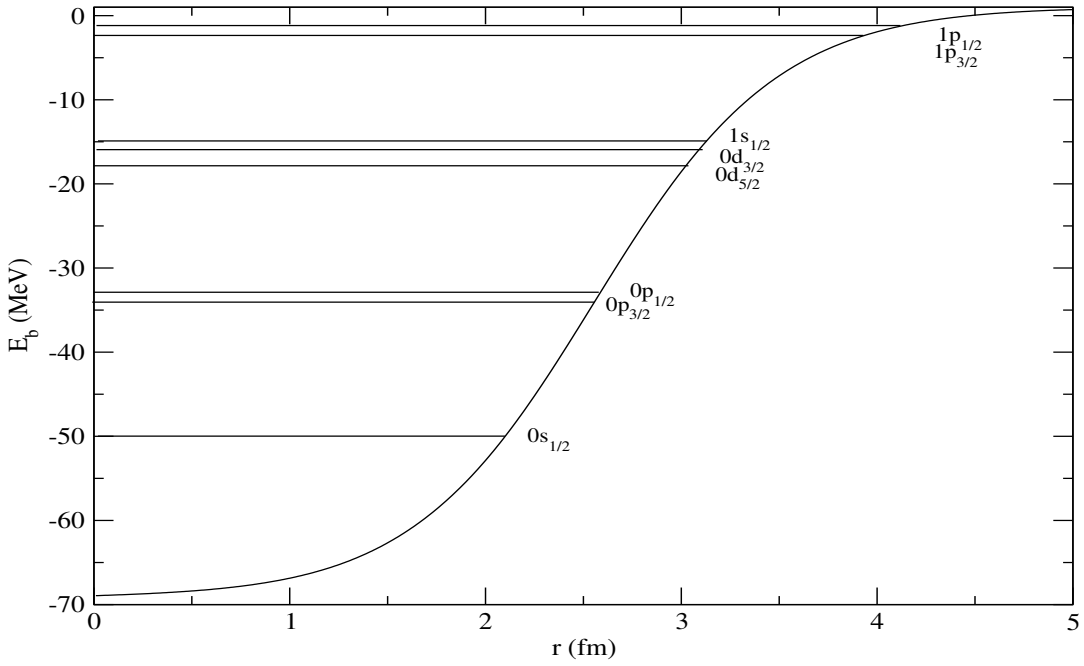

Figure 3.8: Virtual states, in addiction to the two bound states $1p_{3/2}$ and $1p_{1/2}$, are shown. The quantum numbers and the order of these states are the same for the two nuclei. The position in energy is approximately correct.

We can infer the quantum numbers of the ^{7}Be and ^{7}Li bound and resonance states by applying the Wildermuth's rule (73): by inspecting the plots of figure (3.9) it's clear that, by combining two zero-phonon nuclei (α and ^{3}H for ^{7}Li, α and ^{3}He for ^{7}Be) we obtain a three-phonon nucleus. By counting the principal quantum numbers n starting from 0, by labeling with l the angular momentum quantum number and with N the number of phonons this general rule holds:

$$N = 2n + l \ . \tag{3.20}$$

In our case $N = 3$, hence there are two different combinations of n and l that satisfied this: $n = 1,\ l = 1$, which represents the bound p-doublet, and $n = 0,\ l = 3$, which represents the two f-resonances in the continuum. We consider the p-states as bound

and the f-states as resonances according to the "penetrating orbit argument", asserting that states with larger angular momentum are higher in energy with respect to states with lower angular momentum. Moreover within a multiplet the spin-orbit interactions reduces the energy of the state with maximum j, therefore the ground state of ^{7}Li and ^{7}Be is a $3/2^-$ one and the $f_{7/2}$ resonances is lower in energy than the $f_{5/2}$ one. According to this rule also the parity can be explained: the parity of ^{7}Li and ^{7}Be is the product of the parity of their clusters and of the relative motion: α has spin-parity 0^+, ^{3}H and ^{3}He have spin-parity $1/2^+$ and hence ^{7}Li and ^{7}Be have spin-parity $3/2^-$. In order to make this scheme consistent, the relative motion has to carry a negative parity, in particular its spin-parity has to be 1^-.

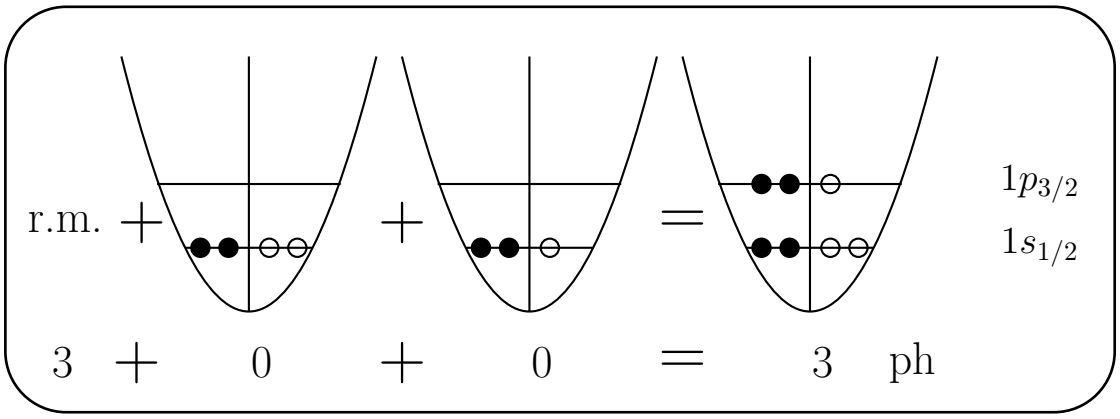

Figure 3.9: Sketch of the Wildermuth's rule: for ^{7}Li black circles are neutrons and empty circles are protons, hence from left to right we have α-particle, ^{3}H and ^{7}Li. For ^{7}Be, ^{7}Li mirror nucleus, black circles are protons and empty circles are neutrons, hence we have α-particle, ^{3}He and ^{7}Be. The numbers of phonons, namely the number of particles in the excited levels according to the Pauli principle, arising from the relative motion and from the single clusters are also shown. For the relation between the numbers of phonons and the quantum numbers see equation (3.20).

3.5 Magnetic properties

In this section we present a detailed treatment of magnetic properties of di-cluster nuclei: we start by pointing out the drawbacks of a standard shell-model picture in evaluating the static magnetic dipole moment for nuclei like ^{7}Li and ^{7}Be, by underlining the strong improvement given by a cluster picture. After this, we consider dipole magnetic response for transitions from the ground state to the first excited state and from the ground state to the continuum. Finally we derive a simple magnetic dipole energy weighted sum rule in order to check our numerical calculations. Usually dipole magnetic response is much weaker than electric dipole response and comparable with electric quadrupole one. It appears however, already in old calculations (13) for the photo-disintegration of the deuteron (the smallest dicluster nucleus), that they are relevant at astrophysical energies (say below 200 keV) where they even turn out to dominate over the electric dipole. For this reason we decided to investigate this theme to better understand the role they might play in low-energy nuclear reactions involving dicluster systems.

3.5.1 Dipole magnetic moment

In general the dipole magnetic moment of a nucleus depends on the currents of protons and neutrons, i.e. the orbital part of the magnetic moment, and on the intrinsic magnetic moments of nucleons. A nucleon with orbital angular momentum $\vec{l}$ and spin $\vec{s}$ carries a dipole magnetic moment (26)

$$\vec{\mu}_l = g^{(l)} \frac{e\hbar}{2Mc} \vec{l} + g^{(s)} \frac{e\hbar}{2Mc} \vec{s}, \tag{3.21}$$

where $g^{(l)}$ is 1 for protons and 0 for neutrons, $g^{(s)}$ is 5.586 for protons and -3.823 for neutrons. The combination $\frac{e\hbar}{2Mc}$, with e and M to indicate the charge and mass of the proton is the nuclear magneton μ_N. Hence, in units of μ_N, for a nucleus with A nucleons we have

$$\vec{\mu} = \sum_{i=1}^{A} g_i^{(l)} \vec{l}_i + g_i^{(s)} \vec{s}_i \ . \tag{3.22}$$

It can be useful, in particular cases, to split the magnetic moment in a iso-scalar and in a iso-vectorial part, by means of isospin formalism, therefore eq. (3.22) can be rewritten in the following way:

$$\begin{aligned}
\vec{\mu} &= \sum_{i=1}^{A} \frac{1+\tau_{i3}}{2} \vec{l}_i + \left(\frac{1+\tau_{i3}}{2} g_p^{(s)} + \frac{1-\tau_{i3}}{2} g_n^{(s)} \right) \vec{s}_i \\
&= \frac{1}{2} \sum_{i=1}^{A} \left(\vec{l}_i + \vec{s}_i \right) + \frac{1}{2} \left(g_p^{(s)} + g_n^{(s)} - 1 \right) \sum_{i=1}^{A} \vec{s}_i \\
&+ \frac{1}{2} \sum_{i=1}^{A} \tau_{i3} \left(\vec{l}_i + (g_p^{(s)} - g_n^{(s)}) \vec{s}_i \right) \\
&= \underbrace{\frac{\vec{J}}{2} + k_s \sum_{i=1}^{A} \vec{s}_i}_{iso-scalar} + \underbrace{\frac{1}{2} \sum_{i=1}^{A} \tau_{i3} \left(\vec{l}_i + k_i \vec{s}_i \right)}_{iso-vectorial} ,
\end{aligned} \tag{3.23}$$

where $\tau_3^{(p)} = 1$, $\tau_3^{(n)} = -1$, $\vec{J}$ is the total angular momentum of the nucleus, $k_s = g_p^{(s)} + g_n^{(s)} - 1 \simeq 0.38$ and $k_i = g_p^{(s)} - g_n^{(s)} \simeq 9.41$. From an experimental point of view the measurement of the magnetic dipole of a nucleus is the expectation value of the z-component of the operator $\vec{\mu}$ in a state of maximal alignment, i.e. $\Psi(J, M = J)$:

$$\mu = \langle J, M = J | \mu_z | J, M = J \rangle \ . \tag{3.24}$$

The theoretical evaluation of this expectation value is quite simple for nuclei with odd mass number A, because they have all the nucleons, expect one, coupled to zero total angular momentum, therefore the magnetic moment arises from the unpaired nucleon. If $\vec{l}$ and $\vec{s}$ are the quantum numbers of such a nucleon, eq. (3.24) becomes

$$\mu = \langle J, M = J | g^{(l)} l_z + g^{(s)} s_z | J, M = J \rangle \ . \tag{3.25}$$

In order to evaluate this expectation value we expand the state $|ljm\rangle$ in term of the states $|lm_l 1/2 m_s\rangle$:

$$|ljm\rangle = \sum_{m_l m_s} |lm_l 1/2 m_s\rangle\langle lm_l 1/2 m_s|ljm\rangle \ . \tag{3.26}$$

By using the eigenvalue equations

$$\begin{aligned} s_z|lm_l 1/2 m_s\rangle &= m_s|lm_l 1/2 m_s\rangle \\ l_z|lm_l 1/2 m_s\rangle &= m_l|lm_l 1/2 m_s\rangle \ , \end{aligned}$$

and by inserting (3.26) in (3.25) we obtain

$$\mu = \sum_{m_l,\, m_s} |\langle|lm_l 1/2 m_s|ljm\rangle|^2 (g^{(l)} m_l + g^{(s)} m_s) \ . \tag{3.27}$$

By considering the values of m_s we have $j = l \pm 1/2$. For the case $j = l + 1/2$, $\langle lm_l 1/2 m_s|lj, m = j\rangle = 1$ if $m_l = l$ and $m_s = 1/2$ and it is 0 in all other cases. Therefore eq. (3.27) becomes:

$$\mu = l g^{(l)} + \frac{g^{(s)}}{2} \ . \tag{3.28}$$

For the case $j = l - 1/2$ we have two non-vanishing Clebsch-Gordan coefficients:

$$\langle l\, m_l\, 1/2\, m_s|l\ j, m = j\rangle = \begin{cases} -\frac{1}{\sqrt{2j+2}} & m_l = l-1, m_s = \frac{1}{2} \\ \sqrt{\frac{2j+1}{2j+2}} & m_l = l, m_s = -\frac{1}{2} \end{cases} \ . \tag{3.29}$$

The corresponding magnetic moment is

$$\begin{aligned} \mu &= \frac{1}{2j+2}\left((l-1)g^{(l)} + \frac{1}{2}g^{(s)}\right) + \frac{2j+1}{2j+2}\left(l g^{(l)} - \frac{g^{(s)}}{2}\right) \\ &= \frac{j}{j+1}\left((l+1)g^{(l)} - \frac{g^{(s)}}{2}\right) \ . \end{aligned} \tag{3.30}$$

Now we can compare the predictions of this approach with simple odd-A nuclei, in order to see its limitations. Let's start with $A = 3$ nuclei, i.e. ^{3}H and ^{3}He. In ^{3}H there

is a pair of neutrons and an unpaired proton in the $1s_{1/2}$ shell, so we can evaluate μ by inserting $l = 0$ and $g^{(s)} = 5.587$ in (3.28) obtaining $\mu(^3\mathrm{H}) = \mu(^1\mathrm{H}) = 2.793$ while the experimental value is 2.979. Now consider ^{3}He, the mirror nucleus of ^{3}H, by following the same steps we expect $\mu(^3\mathrm{He}) = \mu_{(n)} = -1.913$ while the experimental value is -2.128. The errors are about 6% and 10% hence, by using the free-nucleons gyromagnetic factors, for these $A = 3$ nuclei results are not bad. Now we deal with $A = 7$ nuclei ^{7}Li and ^{7}Be. According to the nuclear Shell Model ^{7}Li has an unpaired proton in the $\mathrm{p}_{3/2}$ shell. We insert $l = 1$ and $g = 5.587$ in (3.28) obtaining $\mu = 3.793$, while the experimental value is 3.256. Its mirror-nucleus ^{7}Be has an unpaired neutron in the shell $p_{3/2}$ hence eq. (3.28) give $\mu = -1.913$ while the experimental value is -1.398. With respect to the former cases the errors made are quite large (almost 40% for ^{7}Be). We conclude that the simple approach stating that the whole magnetic moment of a nucleus is given by an unpaired nucleon, although it gives useful results in many cases, for example for one particle outside closed shells in heavier nuclei, is not as suited for these $A = 7$ systems. As we will show later, in order to give a reliable calculation of the magnetic moment of these nuclei we have to explicitly include their di-cluster structure.

Dipole magnetic moment for di-cluster nuclei

We calculate the dipole magnetic moment of a di-cluster nucleus. The interesting result is the dependence of this moment not only on the intrinsic magnetic moments of the clusters, but also on the *relative* angular momentum. We start from the definition:

$$\vec{\mu} = \sum_{i=1}^{A+B} \mu_i = \sum_{i=1}^{A+B} \left(g_i^l \vec{l}_i + g_i^s \vec{s}_i \right) \tag{3.31}$$

where we have the following identifications:

- A,B are the mass numbers of the clusters with atomic number Z_A, Z_B.
- g_i^l and g_i^s are the gyromagnetic ratios of the nucleons. In particular $g^l = 1$ for a proton and $g^l = 0$ for a neutron, whilst $g^s = 5.587$ for a proton and $g^s = -3.826$

for a neutron.

- $\vec{l_i}$ and $\vec{s_i}$ are the orbital angular momentum and spin of a nucleon with respect to the total center of mass.

- We define $\vec{r_i^*}$ ($\vec{r_j^*}$) as the position of a nucleon with respect to the center of mass of cluster $A(B)$. We have the following coordinate transformation between coordinates with respect to the whole nucleus center of mass (un-starred) and coordinates with respect to the single cluster center of mass (starred):

$$\begin{aligned} \vec{r_i} &= \vec{r_i^*} + \vec{R}_A \\ \vec{r_j} &= \vec{r_j^*} + \vec{R}_B \\ \vec{p_i} &= \vec{p_i^*} + \vec{P}_A \\ \vec{p_j} &= \vec{p_j^*} + \vec{P}_B \ . \end{aligned}$$

- $\vec{l_i} = \vec{r_i} \times \vec{p_i}$ is the angular momentum of a nucleon with respect to the center of mass, while $\vec{l_i^*} = \vec{r_i^*} \times \vec{p_i^*}$ is the same quantity with respect to the appropriate cluster center of mass.

The vectors $\vec{R}_A$ and $\vec{R}_B$ are related to a common vector

$$\begin{aligned} \vec{R}_A &= -\frac{B}{A+B}\vec{R} \\ \vec{R}_B &= \frac{A}{A+B}\vec{R} \ , \end{aligned} \tag{3.32}$$

with $\vec{R}$ being the vector connecting the centers of mass of the two fragments.
We can rewrite equation (3.31) in term of starred coordinates obtaining:

$$\begin{aligned}\vec{\mu} &= \sum_{i=1}^{A}\left(g_i^l(\vec{r}_i^{\,*}+\vec{R}_A)\times(\vec{p}_i^{\,*}+\vec{P}_A)+g_i^s\vec{s}_i\right)\\ &+ \sum_{j=1}^{B}\left(g_j^l(\vec{r}_j^{\,*}+\vec{R}_B)\times(\vec{p}_j^{\,*}+\vec{P}_B)+g_j^s\vec{s}_j\right)\ . \end{aligned} \tag{3.33}$$

Equation (3.33) can be rewritten extracting the first term of the vector products:

$$\begin{aligned}\vec{\mu} &= \overbrace{\sum_{i=1}^{A}(g_i^l\underbrace{(\vec{r}_i^{\,*}\times\vec{p}^{\,*}_i)}_{l_i^*}+g_i^s\vec{s}_i)}^{\mu_A}+\sum_{i=1}^{A}g_i^l\left[\vec{r}_i^{\,*}\times\vec{P}_A+\vec{R}_A\times(\vec{p}_i^{\,*}+\vec{P}_A)\right]\\ &+ \overbrace{\sum_{j=1}^{B}(g_j^l\underbrace{(\vec{r}_j^{\,*}\times\vec{p}_j^{\,*})}_{l_j^*}+g_j^s\vec{s}_i)}^{\mu_B}+\sum_{i=1}^{B}g_j^l\left[\vec{r^*}_j\times\vec{P}_B+\vec{R}_B\times(\vec{p}_j^{\,*}+\vec{P}_B)\right]\ . \end{aligned} \tag{3.34}$$

By recognizing the definitions of the intrinsic magnetic moments of the two clusters, and by using the appropriate values for g^l we are left with a simpler expression:

$$\begin{aligned}\vec{\mu} &= \vec{\mu}_A+\vec{\mu}_B+\underbrace{(\sum_{i=1}^{Z_A}\vec{r}_i^{\,*})}_{0}\times\vec{P}_A+\sum_{i=1}^{Z_A}(\vec{R}_A\times\vec{p}_i)\\ &+ \underbrace{(\sum_{j=1}^{Z_B}\vec{r}_j^{\,*})}_{0}\times\vec{p}_j+\sum_{j=1}^{Z_B}(\vec{R}_B\times\vec{P}_B)\ , \end{aligned} \tag{3.35}$$

where the under-braced sums are zero because of the definition of the center of mass of single clusters. Now we use the fact that the nucleus is at rest in the center of mass system:

$$\vec{P}=\vec{P}_A+\vec{P}_B=\vec{0}\Rightarrow\vec{P}_B=-\vec{P}_A\ , \tag{3.36}$$

and moreover

$$\vec{R}_A \times \vec{P}_A + \vec{R}_B \times \vec{P}_B = \vec{L}\,, \tag{3.37}$$

from which we obtain

$$\left(\vec{R}_A - \vec{R}_B\right) \times \vec{P}_A = -\vec{R} \times \vec{P}_A = \vec{L}\,. \tag{3.38}$$

Therefore, using these expression within the definition of the mean value:

$$\sum_{i=1}^{Z_A} \vec{p_i} = Z_A \langle \vec{p_i} \rangle = Z_A \frac{\vec{P}_A}{A}\,, \tag{3.39}$$

with the same for $\vec{p_j}$, and by using (3.32) for $\vec{R}_A$ and $\vec{R}_B$ we finally have:

$$\begin{aligned} \vec{\mu} &= \vec{\mu}_A + \vec{\mu}_B + \frac{BZ_A}{(A+B)A} \underbrace{\left(-\vec{R} \times \vec{P}_A\right)}_{\vec{L}} + \frac{AZ_B}{(A+B)B} \underbrace{\left(\vec{R} \times \vec{P}_B\right)}_{\vec{L}} \\ &= \vec{\mu}_A + \vec{\mu}_B + \frac{Z_A B^2 + Z_B A^2}{(A+B)AB} \vec{L}\,, \end{aligned} \tag{3.40}$$

that is the expression of the dipole magnetic moment operator for dicluster nuclei. For ^{7}Li the orbital contribution is $17/42\mu_N$ (71), while for ^{7}Be is $25/42\mu_N$, giving respectively a dipole magnetic moment of $3.37\mu_N$ and $-1.53\mu_N$, in good agreement with experimental values, $3.256427(2)\mu_N$ and $-1.398(15)\mu_N$. This agreement is certainly better than the one obtained in the shell model. From this derivation it is clear that the magnetic dipole of a dicluster nucleus is not just the sum of the magnetic moments of its clusters: this is true only when the two clusters are in a relative s-wave as in $^6\mathrm{Li} = \alpha + d$. In all other cases care must be taken to include the effect of the relative motion on $\vec{\mu}$.

Although it is clear from the discussion of the Wildermuth's rule that the relative motion must possess a $l = 1$ character, we can also see that using the intrinsic magnetic moment, masses and charges of the two clusters in formula (3.40) for the total magnetic moment, one can see from Table (3.4) that the value that gives the best agreement is

clearly $\ell = 1$. Due to spin-orbit interaction the ground state has $j = 3/2^-$, while the first excited state has $j = 1/2^-$.

	s	p	d	exp.
^{7}Li	2.97	3.37	3.78	3.256427(2)
^{7}Be	-2.12	-1.53	-0.93	-1.398(15)

Table 3.4: Total magnetic moments (in μ_N) of ^{7}Be and ^{7}Li for different choices of relative angular momenta compared with experimental value (last column). It is clear that the best agreement is obtained in both cases by considering a relative p-wave.

3.5.2 Magnetic interaction

In order to evaluate the magnetic interaction between two states we consider the reduced matrix element

$$\langle l_f j_f s_f || \mathcal{M}(M\lambda) || l_i j_f s_i \rangle \ , \tag{3.41}$$

where the general structure of the magnetic operator is (cfr. Ref. (23), ch.17):

$$\mathcal{M}(M\lambda) = \sum_i \vec{\nabla}(r_i^\lambda Y^i_{\lambda\mu}(\theta_i\phi_i)) \cdot (a_i \vec{l_i} + b_i \vec{s_i}) \ . \tag{3.42}$$

We are interested in the magnetic dipole interaction ($\lambda = 1$) of ^{7}Li and ^{7}Be where the initial and the final spins are the same, so we can drop the spin quantum numbers s_i, s_f while defining the initial and final states.

We use the general formula

$$\vec{\nabla}(r_i^\lambda Y^i_{\lambda\mu}) \cdot \vec{v} = \sqrt{\lambda(2\lambda+1)} r_i^{\lambda-1} [\vec{Y}^i_{\lambda-1} \times \vec{v}]^\lambda_\mu \ , \tag{3.43}$$

therefore for $\lambda = 1$ we have

$$\vec{\nabla}(r_i Y^i_{1\mu}) \cdot \vec{v} = \sqrt{3}[\vec{Y}^i_0 \times \vec{v}]^1_\mu \ . \tag{3.44}$$

We showed in eq. (3.40) that for a di-cluster nucleus we can express the magnetic moment as a sum of intrinsic single cluster dipole moments plus an orbital contribution

$$\vec{\mu} = \vec{\mu_1} + \vec{\mu}_2 + \mu_N G\vec{L} \ , \tag{3.45}$$

where $\vec{\mu_1}, \vec{\mu}_2$ are the intrinsic single cluster dipole moments and G is a factor that depends on mass and charge numbers of the two clusters; L is the orbital angular momentum. For ^{7}Li and ^{7}Be one of the two clusters is the alpha particle, so $\mu_1 = 0$ and $\vec{\mu}_2 = g\vec{s}$, where $g = 2\mu$ is the gyro-magnetic factor of ^{3}H for ^{7}Li and ^{3}He for ^{7}Be. Using the relation $\vec{j} = \vec{l} + \vec{s}$ we can write

$$\mathcal{M}(M1) = \sqrt{3}\vec{Y_0} \times (k\vec{j} + (2\mu - k)\vec{s}) \ . \tag{3.46}$$

Hence the next step is the evaluation of the following matrix element:

$$\begin{aligned} \langle l_f j_f || \mathcal{M}(M1) || l_i j_i \rangle &= k \langle l_f j_f || r^0 [\vec{Y_0} \times \vec{j}]^1 || l_i j_i \rangle + \\ &+ (2\mu - k) \langle l_f j_f || r^0 [\vec{Y_0} \times \vec{s}]^1 || l_i j_i \rangle \ , \end{aligned} \tag{3.47}$$

where we have put in evidence the overlap between the radial functions of initial and final states with the operator r^0. We use the general formalism developed in the book of De-Shalit and Talmi (23) in order to further simplify eq. (3.47), namely

$$\begin{aligned} \langle l_f j_f || r^0 [\vec{Y_0} \times \vec{J}]^\lambda || l_i j_i \rangle &= \langle r^0 \rangle \langle l_f j_f || \vec{Y_0} || l_i j_i \rangle \langle l_f j_f || \vec{J} || l_i j_i \rangle \cdot \\ &\cdot \sqrt{2\lambda + 1}(-1)^{j_f + f_i + \lambda} \left\{ \begin{array}{ccc} j_f & \lambda & j_i \\ 1 & j_i & \lambda - 1 \end{array} \right\} \ . \end{aligned} \tag{3.48}$$

In the last equation we expand $\langle l_f j_f || \vec{Y_0} || l_i j_i \rangle$ as

$$\begin{aligned}\langle l_f j_f||\vec{Y}_0||l_i j_i\rangle &= (-1)^{l_f+s_f+j_i+\lambda-1}\langle l_f||\vec{Y}_0||l_i\rangle \cdot \\ &\cdot \sqrt{(2j_i+1)(2j_f+1)}\left\{\begin{array}{ccc} l_f & j_f & s_f \\ j_i & l_i & \lambda-1\end{array}\right\}. \end{aligned} \tag{3.49}$$

Now we consider the second term in eq. (3.47):

$$\begin{aligned}\langle l_f j_f||r^0[\vec{Y}_0\times\vec{s}]^1||l_i j_i\rangle &= \sqrt{(2j_i+1)(2\lambda+1)(2j_f+1)}\cdot\langle r^0\rangle \\ &\cdot \langle l_f||\vec{Y}_0||l_i\rangle\langle s_f||\vec{s}||s_i\rangle\left\{\begin{array}{ccc} l_f & s_f & j_f \\ l_i & s_i & j_i \\ \lambda-1 & 1 & \lambda\end{array}\right\}\end{aligned} \tag{3.50}$$

In both terms there is the reduced matrix element $\langle l_f||\vec{Y}_0||l_i\rangle$ that can be evaluated using the general result

$$\langle l_f||\vec{Y}_\mu||l_i\rangle = \sqrt{\frac{2\mu+1}{4\pi}}(-1)^{l_f}\sqrt{(2l_f+1)(2l_i+1)}\left(\begin{array}{ccc} l_f & \mu & l_i \\ 0 & 0 & 0\end{array}\right), \tag{3.51}$$

from which we have the particular case, for $\mu=0$,

$$\langle l_f||\vec{Y}_0||l_i\rangle = (-1)^{l_f}\sqrt{\frac{(2l_f+1)(2l_i+1)}{4\pi}}\underbrace{\left(\begin{array}{ccc} l_f & 0 & l_i \\ 0 & 0 & 0\end{array}\right)}_{\frac{(-1)^{l_f}}{\sqrt{2l_f+1}}} = \sqrt{\frac{2l_i+1}{4\pi}}. \tag{3.52}$$

We remember also that (in our case $s_f=s_i$)

$$\langle s_i||\vec{s}||s_i\rangle = \sqrt{s_i(s_i+1)(2s_i+1)}, \tag{3.53}$$

therefore, by collecting all the terms and by noting that, in the transition between two states following with $|j_f-j_i|=\lambda$, the two Racah-6j vanish, we have only the contribution proportional to $(2\mu-k)$:

$$\begin{aligned}\langle l_f j_f s_f||\mathcal{M}(M\lambda)||l_i j_f s_i\rangle &= \sqrt{3}(2\mu-k)\langle\psi_f|\psi_i\rangle\sqrt{s_i(s_i+1)(2s_i+1)}\cdot \\ &\cdot \sqrt{(2j_f+1)(2\lambda+1)(2j_i+1)}\cdot \\ &\cdot \sqrt{\frac{2l_i+1}{4\pi}}\begin{Bmatrix} l_f & s_f & j_f \\ l_i & s_i & j_i \\ \lambda-1 & 1 & \lambda \end{Bmatrix}\end{aligned} \tag{3.54}$$

From this matrix element we have finally the reduced transition probability

$$B(M1, l_i, s_i, j_i \to l_f s_f j_f) = \frac{1}{2j_i+1}\left|\langle l_f j_f s_f||\mathcal{M}(M1)||l_i j_f s_i\rangle\right|^2 . \tag{3.55}$$

Starting from the $3/2^-$ ground state of ^{7}Li and ^{7}Be, by a M1 transition we can only reach the other bound state $1/2^-$ or the continuum states $1/2^-$. By inserting the specific quantum numbers in eq. (3.55), namely $s_i = s_f = 1/2,\ \lambda = 1,\ l_i = l_f = 1,\ j_i = 3/2,\ j_f = 1/2$ we obtain

$$B(M1, 3/2^- \to 1/2^-) = \frac{1}{4\pi}(2\mu-k)^2\left|\langle\psi_f|\psi_i\rangle\right|^2 . \tag{3.56}$$

that coincides to the formula given in Refs. (17; 71). In table (3.5.2) a comparison between static magnetic properties of ^{7}Li and ^{7}Be, namely the dipole magnetic moment and the $B(M1)$ from the ground state to the first excited state is shown. The agreement with experimental data is good.

From eq. (3.56) it is outstanding that the only difference in the magnetic dipole response between the transition from ground state to first excited state and from ground state to continuum states arises only in the radial overlap of initial and final wave-functions. As shown in figure (3.10) for ^{7}Li and in figure (3.11) for ^{7}Be the overlap between the bound wave functions of this nuclei is almost equal to one because these states shares the same p-character and are quite near in energy. When we consider the transition to the continuum the angular contribution of eq. (3.54) is the same: starting from a $p_{3/2}$ states, by means of a magnetic dipole interactions we can only reach $p_{1/2}$

Quantity	this work	experiments
$\mu(\mu_N)$ of ^{7}Li	3.37	3.256427(2)[67]
$\mu(\mu_N)$ of ^{7}Be	-1.53	-1.398(15)[67]
B(M1,3/2$^-$ $\rightarrow$ 1/2$^-$) (e^{2}fm^2) of ^{7}Li	2.45	2.49$\pm$0.12 [72]
B(M1,3/2$^-$ $\rightarrow$ 1/2$^-$)(e^{2}fm^2) of ^{7}Be	1.86	1.87$\pm$ 0.25[72]

Table 3.5: Static magnetic properties of ^{7}Li and ^{7}Be are shown. Calculations are compared with experimental data.

and $p_{3/2}$ states, but the overlap between $p_{3/2}$ bound state and $p_{3/2}$ continuum state is zero because of orthogonality of different eigenstates of the same Hamiltonian (42). This is not true for transitions from the $p_{3/2}$ bound state to $p_{1/2}$ bound o continuum states because the different spin-orbit interactions makes false the statement above. Therefore the weakness of the magnetic dipole continuum response is only due to the much weaker overlap between bound and continuum wave-functions.

As an example we show in figure (3.14) an hypothetical transition from ^{7}Li ground state to $p_{3/2}$ continuum: numerically the orthogonality of these wave-functions means that the response for this transition is many orders of magnitude smaller than the response for $p_{1/2}$ continuum states, as shown in figure (3.13).

The calculation of the $B(M1; 3/2 \rightarrow 1/2)$ to the bound state (that is within the two isospin partner levels) gives an excellent agreement with experimental measurements as seen from table (3.5.2). Figure (3.12) shows continuum states excited in M1 transitions for ^{7}Be. Only transitions to the $p_{1/2}$ states are allowed because of orthogonality between the ground-state $p_{3/2}$ and continuum $p_{3/2}$. We note that ^{7}Li and ^{7}Be have the same qualitative behavior because of their similar internal structure.

^{7}Li and ^{7}Be have also the same qualitative behavior with respect to transitions to the continuum: compare plots in figures (3.4) and (3.5) with figures (3.6) and (3.7) and compare figure (3.12) with figure (3.13). In particular the last one shows the magnetic dipole transition strength for transitions between the ground-state and the continuum. The re-

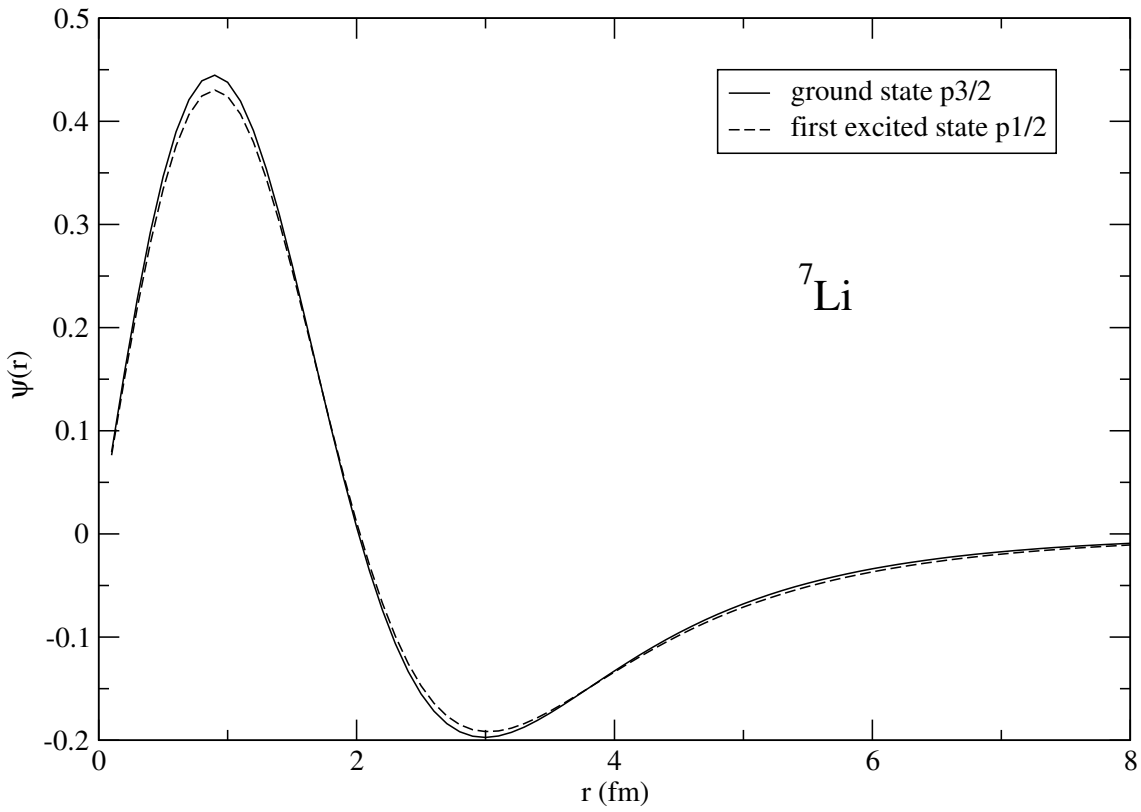

Figure 3.10: Reduced radial wave-functions of the bound states of ^{7}Li. By inspecting the figure it is clear that the overlap of these two wave-functions is almost one.

sults are the following: for ^{7}Be the total non-energy weighted B(M1) to the continuum states, integrated up to 50 MeV, is about 0.00408 μ_N^2, much smaller than the magnetic dipole strength to the first bound state, while for ^{7}Li the total integrated $B(M1)$ strength amounts to $0.0029\mu_N^2$ again much smaller than the B(M1) to the first excited bound state. The magnetic dipole contribution is, in both nuclides, not as important as for the deuteron.

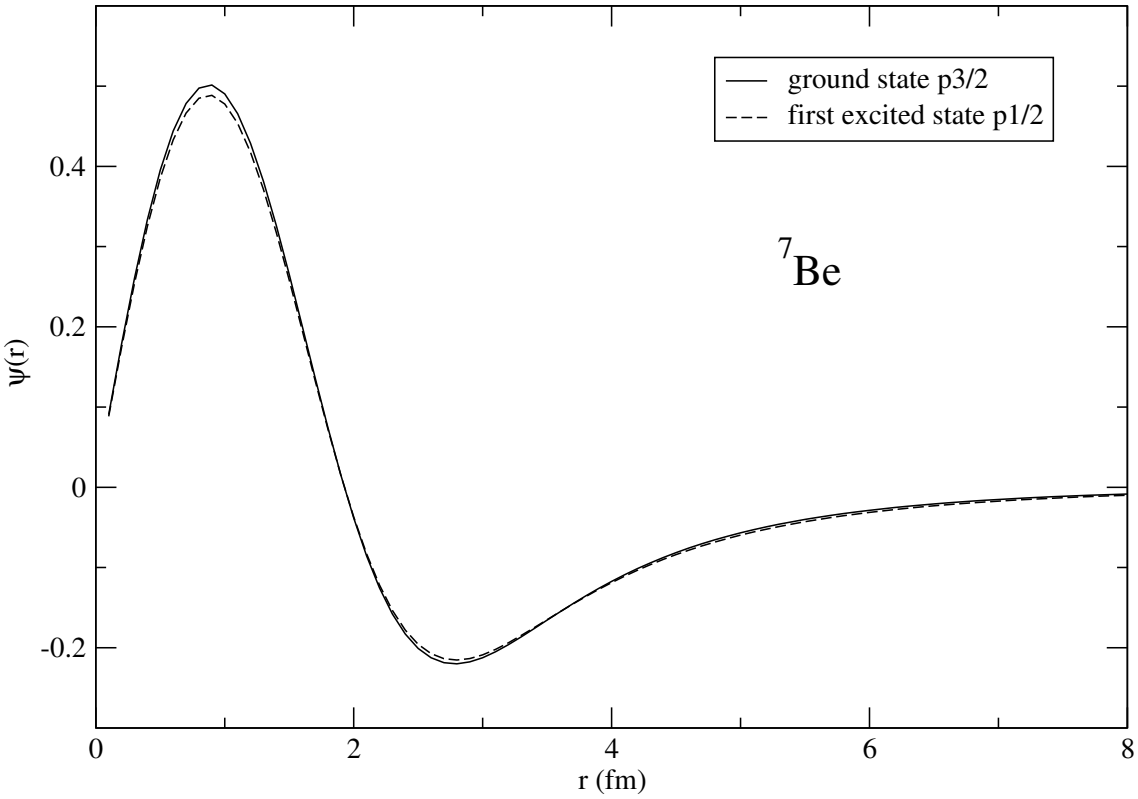

Figure 3.11: Reduced radial wave-functions of the bound states of ^{7}Be. By inspecting the figure it is clear that the overlap of these two wave-functions is almost one.

3.5.3 Magnetic energy weighted sum rule

Energy weighted sum rules for magnetic dipole (43) and higher multi-polarities (69) have been evaluated in a pure single-particle scheme with a shell model Hamiltonian containing a spin-orbit part. The magnitude of the spin-orbit splitting is directly proportional to the total energy-weighted strength. In our cluster picture, one can follow a similar idea in order to evaluate the Energy Weighted Molecular Sum Rule for the magnetic dipole interaction. Consider a generic two-body nuclear system Hamiltonian with a kinetic operator, spherical symmetric potentials (Wood-Saxon and Coulomb) and a spin-orbit

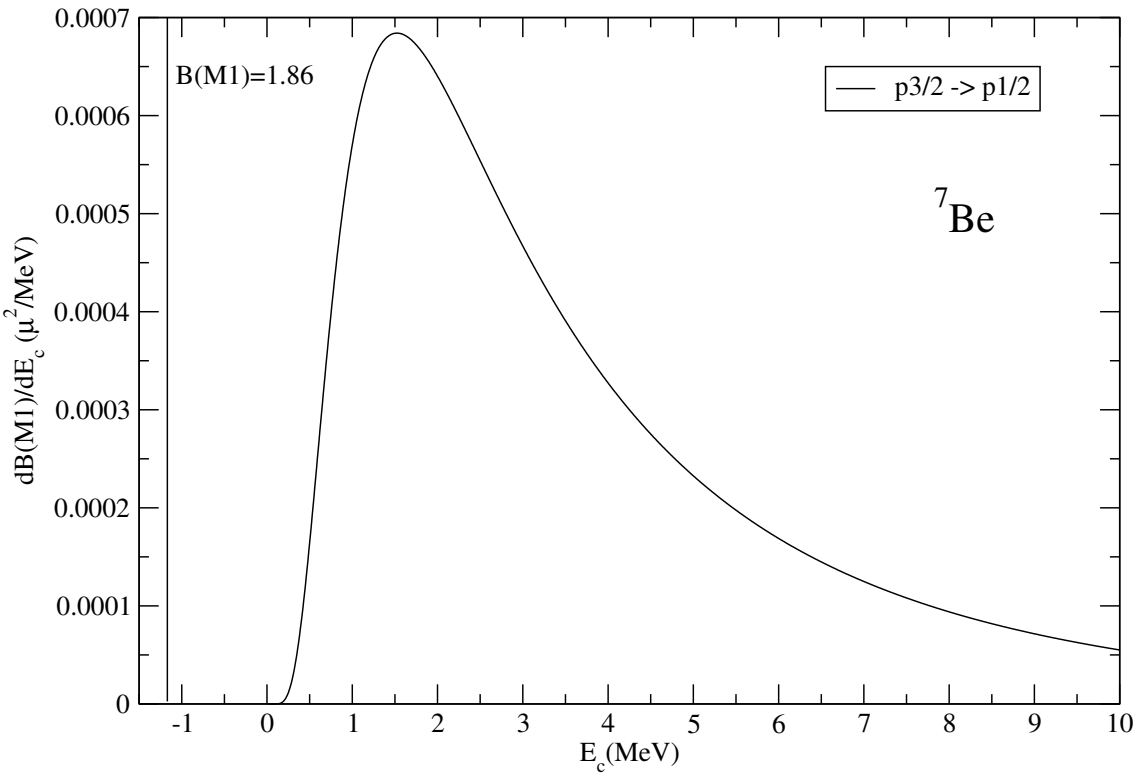

Figure 3.12: Differential dB(M1)/dE$_c$in μ_N^2/MeV for transitions from ground-state to the continuum for ^{7}Be. Energies are in MeV, referred to the threshold for breaking into the $\alpha-^3$He channel. The B(M1) between the two bound states is also indicated.

contribution:

$$H = \underbrace{\frac{P^2}{2\mu} + V(R)}_{H_0} + V_{so}(R)\,\vec{l}\cdot\vec{s}\,. \tag{3.57}$$

We showed that the magnetic dipole moment of a di-cluster nucleus can be expressed as a sum of intrinsic single cluster magnetic dipole moments plus an orbital term depending on the relative orbital angular momentum:

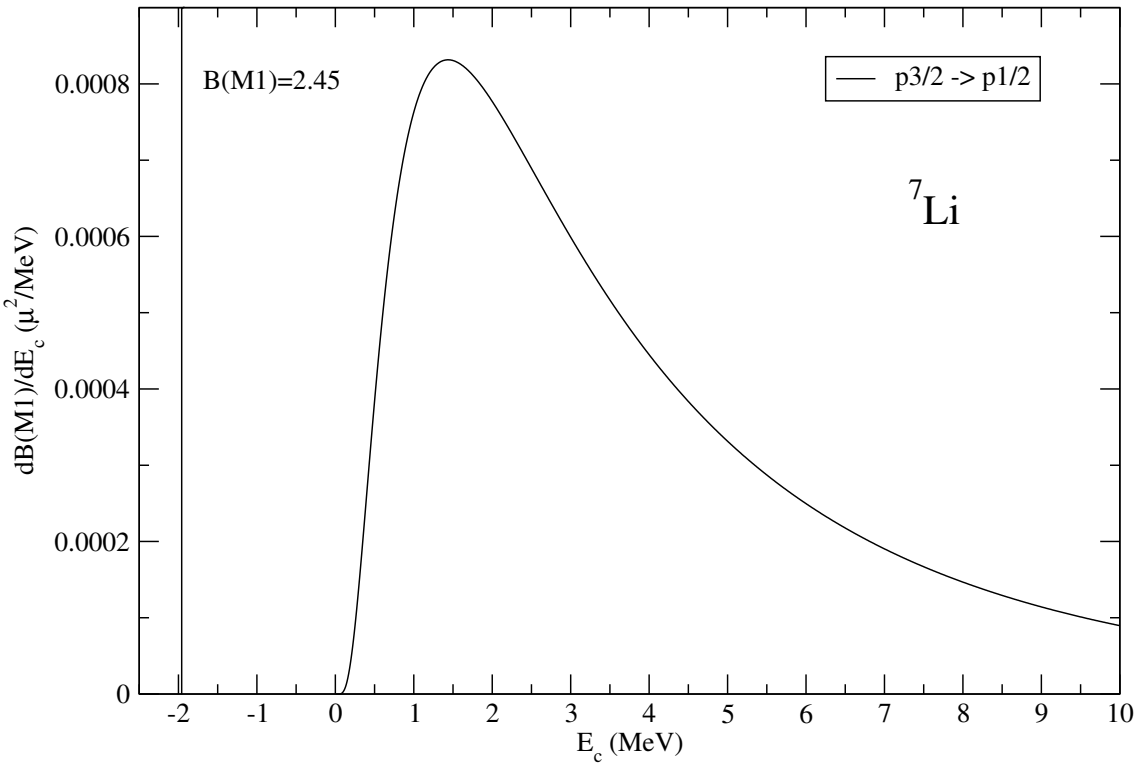

Figure 3.13: Differential dB(M1)/dE$_c$ in μ_N^2/MeV for transitions from ground-state to continuum^{7}Li . Energies are in MeV, referred to the threshold for breaking into the $\alpha - t$ channel. The B(M1) between the two bound states is also indicated.

$$\vec{\mu} = \vec{\mu}_1 + \vec{\mu}_2 + \frac{Z_A B^2 + Z_B A^2}{(A+B)AB}\mu_N \vec{L}\,, \tag{3.58}$$

where the last term of the previous equation is the relative motion dipole magnetic moment. In order to simplify the notation we define

$$\vec{\mu}_{mol} = \frac{Z_A B^2 + Z_B A^2}{(A+B)AB}\mu_N \vec{L} = k \cdot \vec{L}\,, \tag{3.59}$$

where A, Z_A are the mass and atomic numbers of cluster A and B, Z_B are the same for cluster B. In both ^{7}Li and ^{7}Be there is the α particle, hence $\mu_A = 0$ and $\mu_B \equiv \mu$.

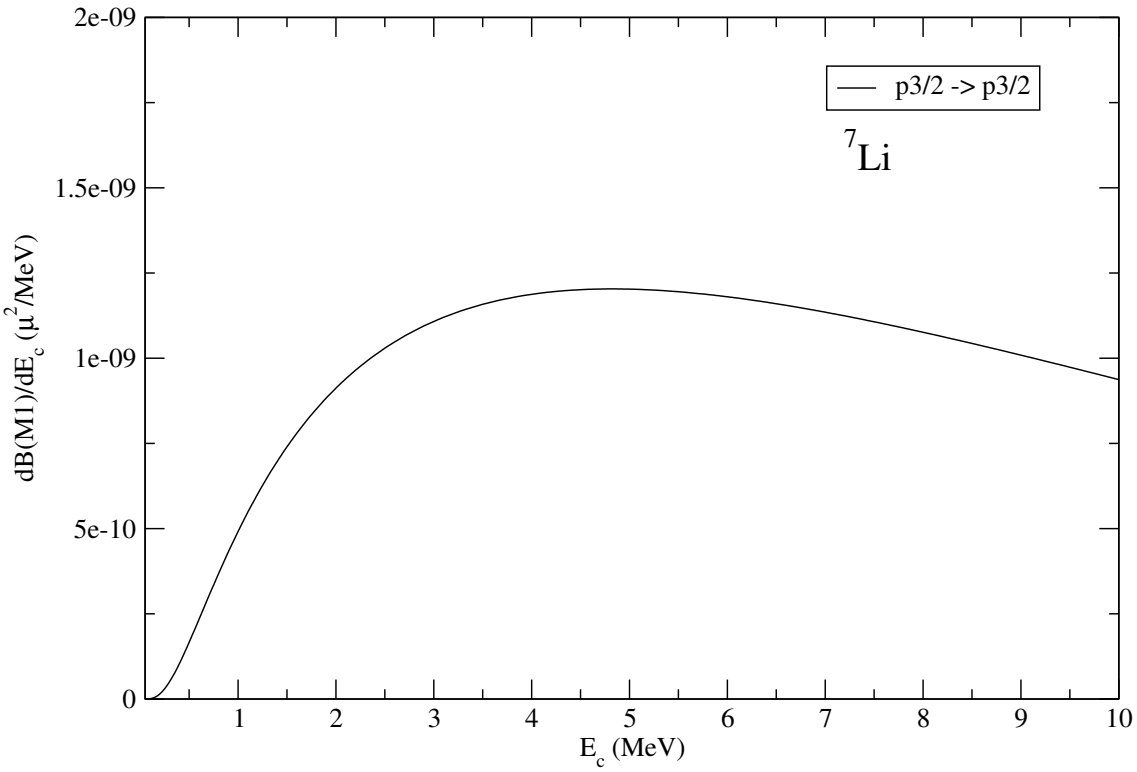

Figure 3.14: Differential dB(M1)/dE$_c$ in μ_N^2/MeV for transitions from ground-state to continuum for ^{7}Li. From a theoretical point of view this matrix element is equal to zero because of the orthogonality of initial and final states. We have check this orthogonality with a direct calculation, obtaining a good result. Energies are in MeV, referred to the threshold for breaking into the $\alpha - t$ channel. Compare this response with figure (3.13)

We consider the z-component of this operator (if we imagine the system in a magnetic field along z-axis, the x and y components of $\vec{\mu}$ average to zero because of the precession around z-axis) that amounts to $kl_z + gs_z$,where g is the gyromagnetic factor, $g = 2\mu$. Then our task is to evaluate the following double commutator:

$$\frac{1}{2}\langle 0|[kl_z + \mu s_z, [H, kl_z + gs_z]]|0\rangle \ . \tag{3.60}$$

In equation (3.57) H_0, because it depends only on R commutes with the angular momentum. As a consequence we have only to evaluate the double commutator in (3.60) with the spin-orbit term:

$$\langle 0|[kl_z + gs_z, [H, kl_+ gs_z]]|0\rangle = \langle 0|[kl_z + gs_z, [V_{so}(R)\vec{l}\cdot\vec{s}, kl_z + gs_z]]|0\rangle \ . \tag{3.61}$$

By expanding the scalar product we have

$$\langle 0|[kl_z + gs_z, V_{so}(R)[l_x s_x + l_y s_y + l_z s_z, kl_z + gs_z]]|0\rangle \tag{3.62}$$

and, by remembering the usual commutation rules between the components of the angular momentum operator and the spin, namely:

$$[l_i, l_j] = i\epsilon_{ijk} l_k \quad [s_i, s_j] = i\epsilon_{ijk} s_k \quad [l_i, s_j] = 0 \tag{3.63}$$

we find

$$\begin{aligned} [kl_z + gs_z, V_{so}(R)[l_x s_x + l_y s_y + l_z s_z, kl_z + gs_z]] &= \\ V_{so}(R)[k^2(-l_x s_x - l_y s_y) + 2kg(l_x s_x + l_y s_y) + g^2(-l_x s_x - l_y s_y)] &= \\ -V_{so}(R)(k^2 - 2gk + g^2)(\vec{l}\cdot\vec{s} - l_z s_z) & \end{aligned} \tag{3.64}$$

Because of symmetry, when we evaluate $l_z s_z$ on the ground state we obtain zero, hence we finally obtain:

$$\frac{1}{2}\langle 0|[kl_z + gs_z, [V_{so}(R)\vec{l}\cdot\vec{s}, kl_z + gs_z]]|0\rangle = -\frac{(k-g)^2}{2}\langle 0|V_{so}(R)\vec{l}\cdot\vec{s}|0\rangle \tag{3.65}$$

We have calculated all the contributions of M1 transitions, including also the contribution of "virtual" states, or states that are not allowed by the Wildermuth's rule. For magnetic dipole interaction we have to consider the virtual state $0p_{1/2}$, the first excited state $1p_{1/2}$ and the continuum $p_{1/2}$, but we do not need to consider the virtual state $0p_{3/2}$,

for the same reason explained by commenting the response to the continuum. In table (3.6) we compare EWSR and EWMSR with the values obtained in our model. We find that the low-lying dipole strength exhausts almost entirely the EWMSM, but represents only a small fraction of the EWSR.

In the same way the quadrupole strength coming from changes in the relative motion of dicluster configurations exhausts a large fraction of the EWMSR, but only a small part of the standard EWSR, as discussed previously.

The table (3.6) resumes all the discussion about energy weighted sum rule, for E1, E2 and M1 transitions.

	^{7}Li			^{7}Be		
EMλ	EWMSR	EWSR	ours	EWMSR	EWSR	ours
E1	1.02	36.7	1.01	1.02	36.7	1.00
E2	1120	2105	481.6	1424	3018	639
M1	1.36	-	1.20	0.87	-	0.82

Table 3.6: Comparison between EWSR, EWMSR and our calculations for ^{7}Li and ^{7}Be. Values are in MeV^{2}fm^3 for E1, MeV^{2}fm^5 for E2 and μ_N^2MeV for M1.

The energy weighted molecular sum rule for magnetic dipole transitions is fulfilled quite well by our calculations: 88% in the case of lithium and 94% in the case of beryllium. Practically all the contribution comes from the excitation to the first excited bound state, as we could expect by considering the great overlap of the two bound wave-functions with respect to the overlap with the continuum wave-functions.

3.6 Cross-sections and S-factors

The knowledge of the electromagnetic response to continuum is a basic ingredient to describe break-up processes. In fact, in kinematic conditions where the process is dominated by the Coulomb interaction (for example at very forward angles), the break-up

probabilities become directly proportional to the $B(E\lambda)$ values. Independently from kinematic conditions this is also the case for two other processes of fundamental importance for astrophysics that can be studied within the present model: the photo-dissociation and its inverse process, the radiative capture. These reactions are of well-known importance both in stellar cores and in their related neutrinos flux, than in the primordial nucleo-synthesis (22). For these reasons in the rest of this chapter we discuss about photo-dissociation and radiative capture of ^{7}Li and ^{7}Be, respectively:

$$\begin{array}{ll} {}^7\mathrm{Li} + \gamma \rightarrow \alpha + \mathrm{t} & {}^7\mathrm{Be} + \gamma \rightarrow \alpha + {}^3\mathrm{He} \\ \alpha + \mathrm{t} \rightarrow {}^7\mathrm{Li} + \gamma & \alpha + {}^3\mathrm{He} \rightarrow {}^7\mathrm{Be} + \gamma \end{array} \tag{3.66}$$

The electric and magnetic response functions obtained so far can be used to calculate the cross sections for these two processes. The radiative capture cross-section for type π (π = Electric or Magnetic) and multipolarity λ, can be expressed (68) as

$$\sigma_{capt}(\pi\lambda, E_C) = \frac{2(2j+1)}{(2j_\alpha+1)(2j_{cl}+1)} \left(\frac{k_\gamma}{k_{\alpha-cl}}\right)^2 \sigma_{ph.dis}(\pi\lambda, E_c) \tag{3.67}$$

where $k_{\alpha-cl}$ is the wave-number for the relative motion of the two clusters (one is always an α particle in the present case) and $\frac{2(2j+1)}{(2j_\alpha+1)(2j_{cl}+1)}$ is a spin factor from the detailed balance principle: a glimpse at eq. (3.66) shows that photo-dissociation and radiative capture are time-reversal processes. This expression relies on the knowledge of the photo-dissociation cross-section that may be expressed as follows (68):

$$\sigma_{ph.dis}(\pi\lambda, E_C) = (2\pi)^3 \frac{(\lambda+1)}{[\lambda(2\lambda+1)!!]^2} k_\gamma^{2\lambda-1} \frac{dB(\pi\lambda, E_c)}{dE_C} \tag{3.68}$$

where $\frac{dB(\pi\lambda,E_c)}{dE}$ is the reduced transition probability previously discussed, k_γ is the photon wave-number, λ is the multipolarity of the transition, $E_c = \hbar^2 k_{\alpha-cl}^2/2\mu_r$ is the relative energy of the two clusters in the continuum and $E_\gamma = E_c + E_b$ is the photon energy. Here we have used the notation μ_r for the reduced mass and E_b for the binding energy.

To evaluate the total photo-dissociation cross-section, starting from a given bound state, one has to sum over all possible angular momentum transfers and over possible allowed spins of the final states in the continuum. In the calculation of the total capture cross-section, in addition, one has to include all the bound states. In figure (3.15) and (3.16) the actual cross sections are shown, while in figure (3.17) we show separately the contributions to the radiative-capture cross section due to the ground state to the first excited state. With a good approximation the difference in these response depends strongly on the different spin factor, as one can see form eq. (3.67).There is also a weak dependence on the different energies of the ground state and first excited state. The dependence on the actual shape of the wave-functions is negligible because of their large overlap, as discussed dealing with magnetic interaction, see section (3.5) and in particular figures (3.10) and (3.11) . They are very similar at a qualitative level, but the different binding energies of the ground states of ^{7}Li and ^{7}Be (mostly due to the different charge) makes up for changes in the position of the resonances and in the intensity of the transition to the low-lying continuum. This is evident from the comparison of fig. (3.6) of the present paper and fig. 1 of older work on ^{7}Li (27). The $B(E1)$ to low-lying continuum states has slightly different contribution from the s and d states that explains the differences in the cross-section at small energies. Indeed it is known that the shape and position of the maxima in the response are affected by binding energy, initial and final angular momenta and Coulomb barrier height (47; 68).

By inspecting figure (3.15) and one sees that electric dipole clearly dominates the cross-section, although the electric quadrupole response shows peaks due to the presence of two low-lying resonances. The quadrupole contribution is not important at all at a variance with the case of nuclear break-up processes (27). The magnetic dipole is nevertheless negligibly small in comparison with E1 contributions, but it overcomes the E2 contribution except round about the f7/2 resonance in ^{7}Li and the two resonances in ^{7}Be. The photo-dissociation cross-section is shown only from the ground state, but the radiative capture can go directly to the ground state or proceed through the first excited bound state, see figure (3.16). In the latter case, due to the small energy difference,

the cross sections to the $p_{1/2}$ and $p_{3/2}$ are practically proportional, see figure (3.17) and the proportionality is fixed by the phase space factor depending on the total spin j, as previously discussed.

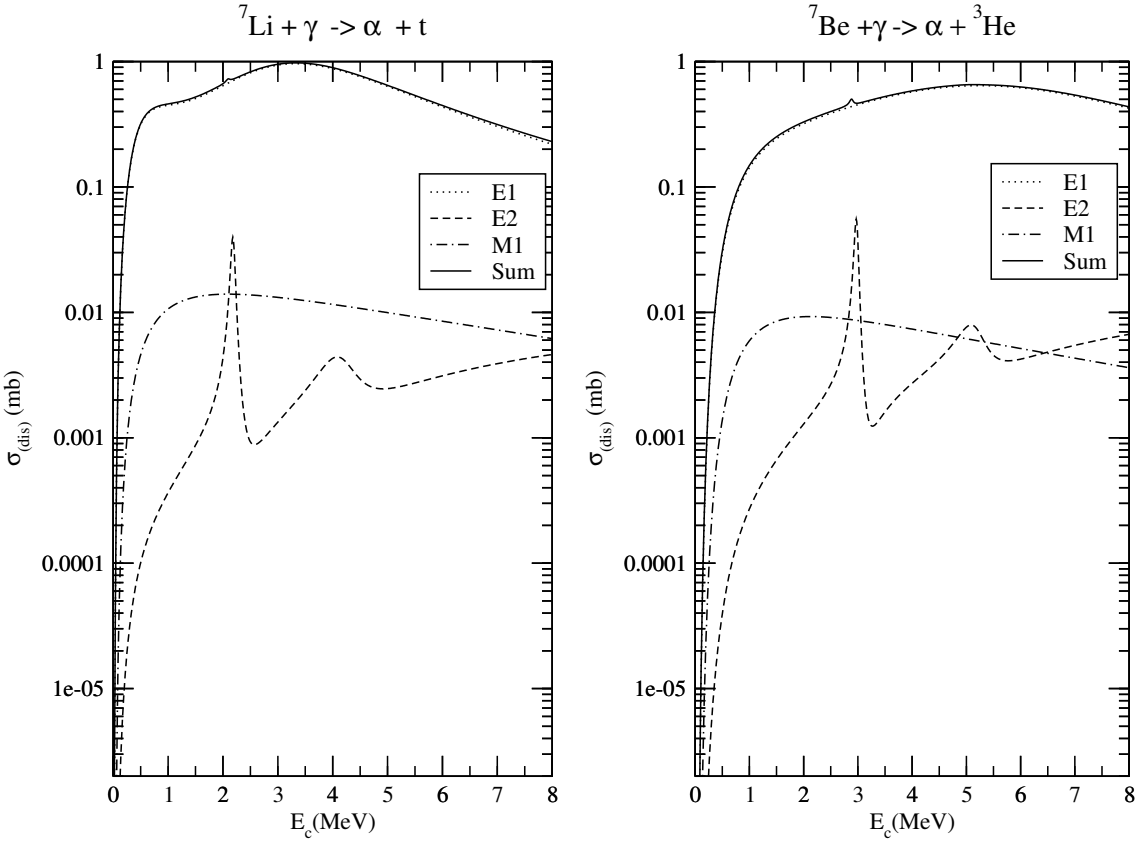

Figure 3.15: Photo-dissociation cross-sections plotted against the continuum energy for reactions involving ^{7}Li and ^{7}Be. The E1, E2 and M1 contributions are shown separately and the total practically coincides with the electric dipole contribution. The E2 resonances are seen in each picture.

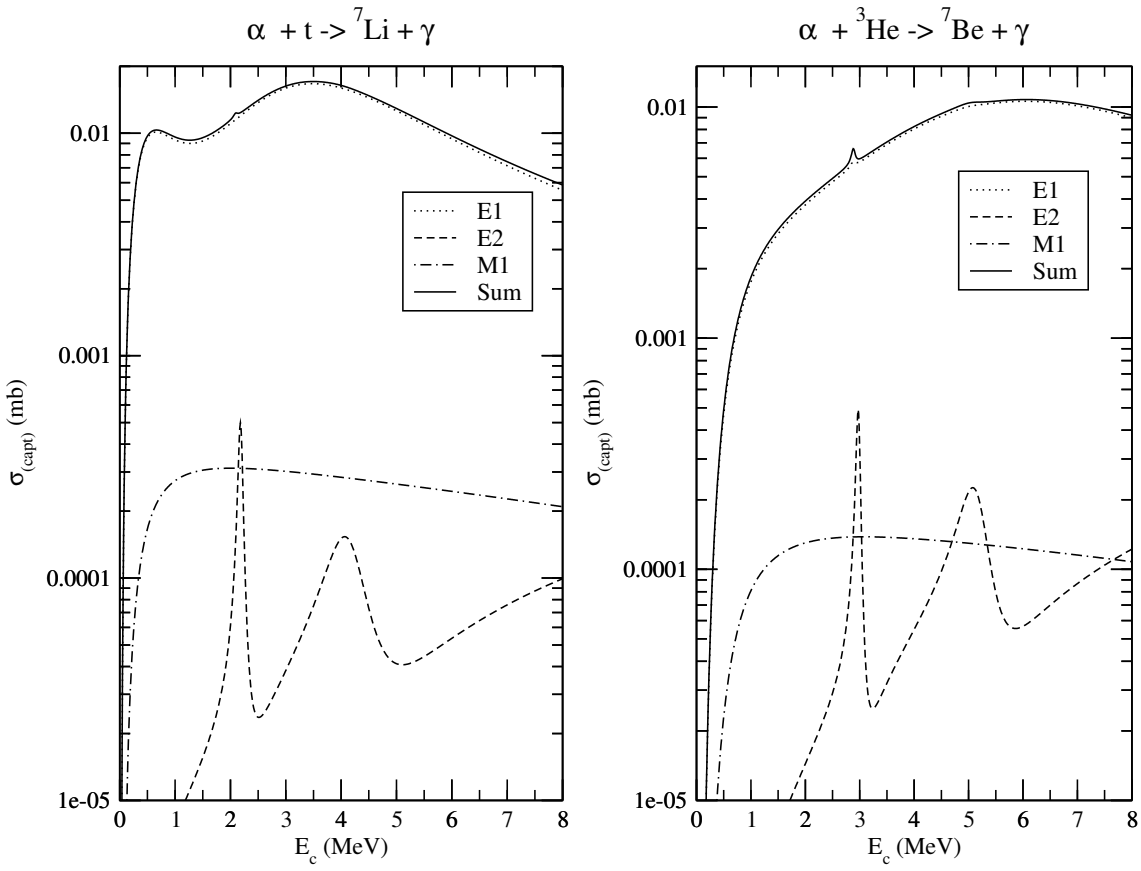

Figure 3.16: Radiative capture cross-section plotted against the continuum energy for reactions involving ^{7}Li and ^{7}Be. The E1,E2 and M1 contributions are shown separately and the total practically coincides with the electric dipole contribution. The E2 resonances are seen in each picture.

3.6.1 Astrophysical S-factor

In the stellar environment the occurrence of high temperatures and the large density of light isotopes makes the $\alpha-$capture a very likely process. Tritium and ^{3}He participate in (α, γ) reactions forming mass $A = 7$ isobars, which are one possible getaway toward heavier nuclei. It is therefore important to understand well these processes and to have

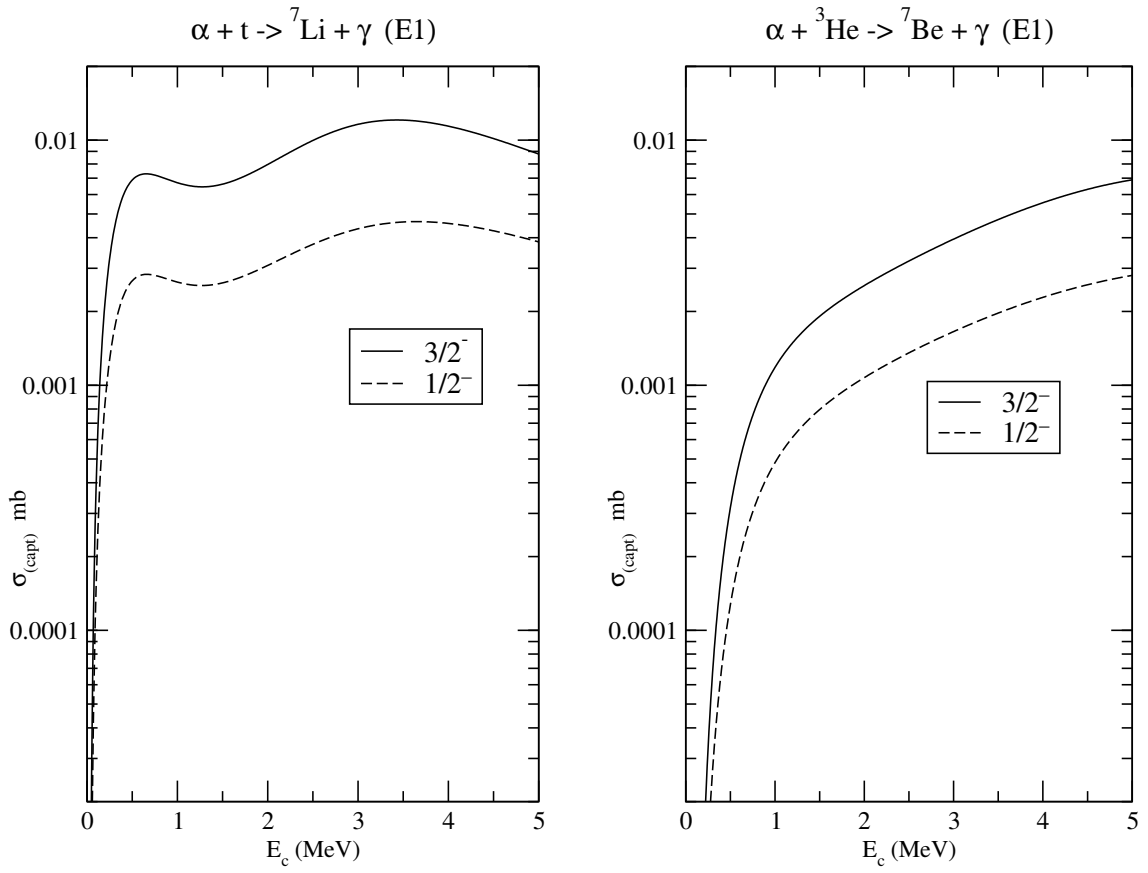

Figure 3.17: Separated contributions for the radiative capture cross-section plotted against the continuum energy for reactions involving ^{7}Li and ^{7}Be. With a good approximation the difference is due first to the different spin factor of ground state and first bound excited state, and second to the different energies of these two states. The dependence due to the different shape of these two wave-function is negligible, as thoroughly discussed in section (3.5)

.

simple models to treat the reactions. Once again the dicluster picture qualitatively and quantitatively entails the correct physics ingredients: indeed the astrophysical S-factor,

a reparametrization of the cross-section, defined by:

$$S = e_{rel}\sigma_{capt}(e_{rel})e^{2\pi\eta} \ ,$$

where η is the Sommerfeld parameter, for the reaction ^{3}He$(\alpha,\gamma)^7$Be is very well reproduced as can be seen in figures (3.18). Good results are also obtained for the partner reaction, ^{3}H$(\alpha,\gamma)^7$Li, as shown in (3.19). Each curve has both a positive and a negative aspect: while the result for ^{7}Be has a good magnitude, but a non-optimal slope, the result for ^{7}Li has a good shape, but it overestimates the data. Our results do not contain any rescaling of the S-factor or, in other words, we assume a spectroscopic factor for the α+cluster configuration equal to one. This might be the reason for the observed deviation in the case of ^{7}Li, where the ^{6}Li+n component may affect the total magnitude although possibly not the overall shape. The reason for the flat shape of the ^{7}Be curve might also reside in the prescription we have used to treat the dicluster system. Perhaps it is an indication that other components are affecting the properties at low energies although the results in table II were very satisfactory. The various sets of experimental measurements that are reported in these figures together with the calculated values, are taken from the NACRE database (46), where an extensive list of references can be found. Moreover a very recent analysis of the existing data about the ^{3}He$(\alpha,\gamma)^7$Be S-factor can be found in (22). A simple parabolic fit of the model curves give a S(0) of 0.42 and 0.13 keV-barn for beryllium and lithium respectively.

Other more refined approaches, like the R-matrix calculations (see discussion in Ref. ((34)), or the Multichannel Algebraic Scattering approach (18) have been applied with success to the same reaction. Although our model is much simpler than the cited approaches, it has a comparable predictive power. Of course this might still not be enough for elaborated nucleo-synthesis models that must consider a network of nuclear reactions with very precise fits. In that case a more precise determination of the S-factor might be necessary and one must go beyond the simple cluster picture.

In order to point out the importance of properly including the intercluster nuclear potential, although it affects only a small part of the initial and final state wave-functions,

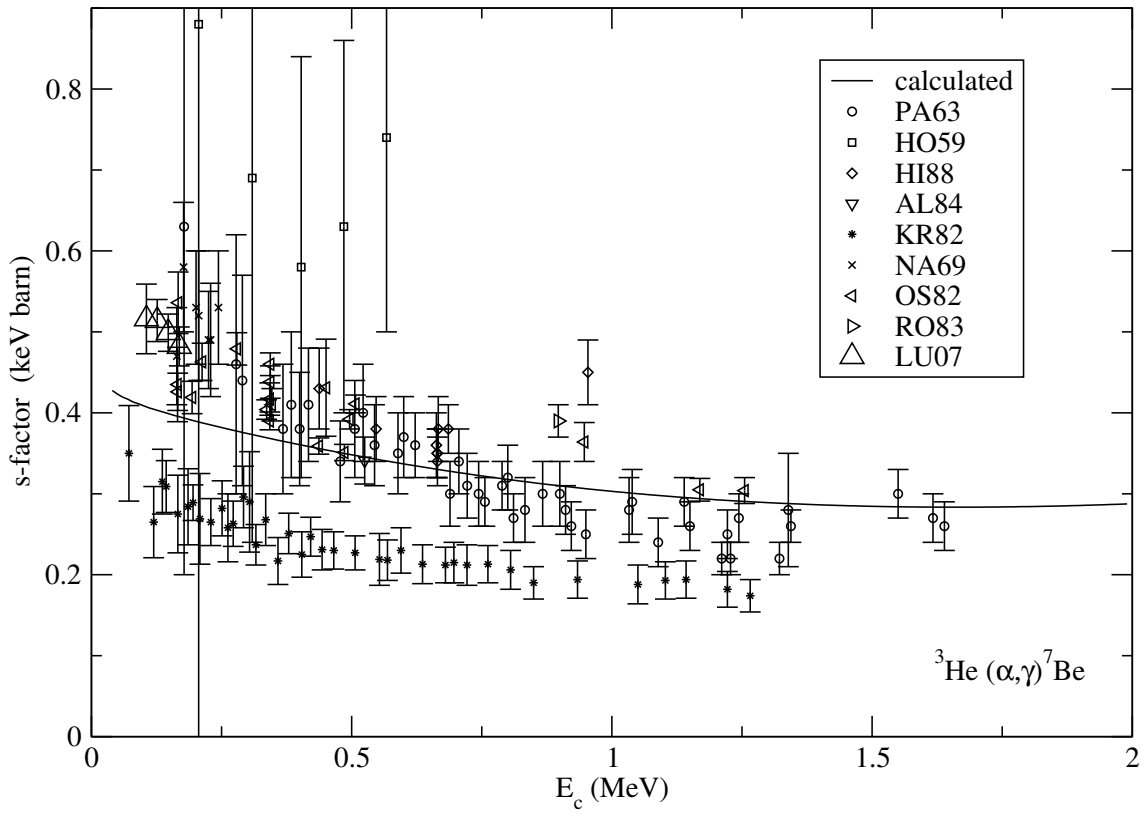

Figure 3.18: S-factor for the $^3\mathrm{He}(\alpha,\gamma)^7\mathrm{Be}$ reaction.

we show in figure (3.20 the integrand (same of figure (3.3)) and the corresponding S-factor with and without the inclusion of the nuclear potential. We have selected the $s_{1/2} \rightarrow p_{3/2}$ transition in ^{7}Be for the sake of simplicity. Clearly the nuclear potential does not affect the tail of the wavefunction, that matches a pure Coulomb wavefunction at large distances, but at distances smaller than the position of the Coulomb barrier, the presence of the nuclear potential affect the continuum wavefunctions and therefore the response in the continuum. The S-factor, in the low-energy regime, is displayed in the lower panel. The nuclear potential is seen to lower the S-factor significantly and cannot be excluded from calculations, as already found by several authors.

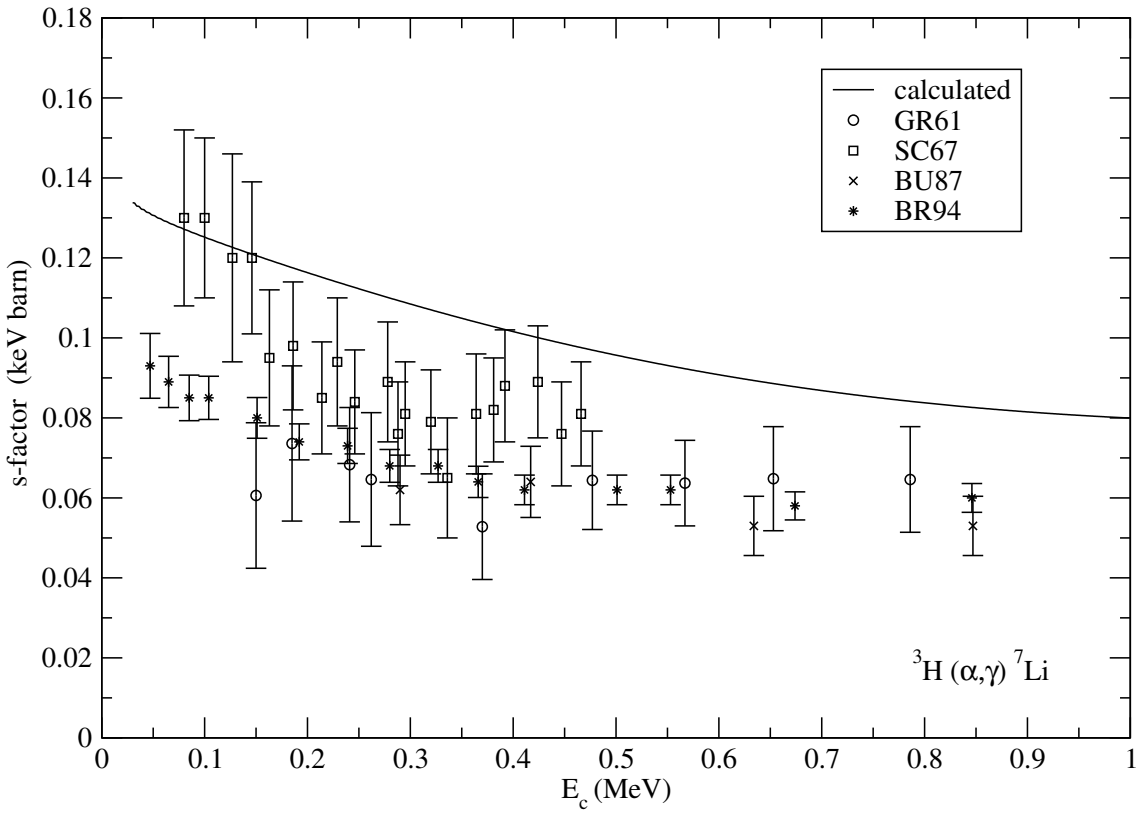

Figure 3.19: S-factor for the $^3\mathrm{H}(\alpha,\gamma)^7\mathrm{Li}$ reaction.

3.7 Conclusion

An elementary dicluster model is found to provide an effective description of static as well as dynamic properties of some light nuclei and can be used with confidence in reaction models. Although *ab initio* many-body models are expected to provide better results in the general case, we have shown that, for example, the astrophysical S-factor, which is a crucial quantity for interdisciplinary applications of nuclear physics, is reasonably well reproduced by the dicluster model. In particular in this work we have investigated the magnetic properties of $A = 7$ isobars, introducing a new molecular magnetic dipole sum rule, that has a close analogy with the single particle magnetic sum rule (69), and

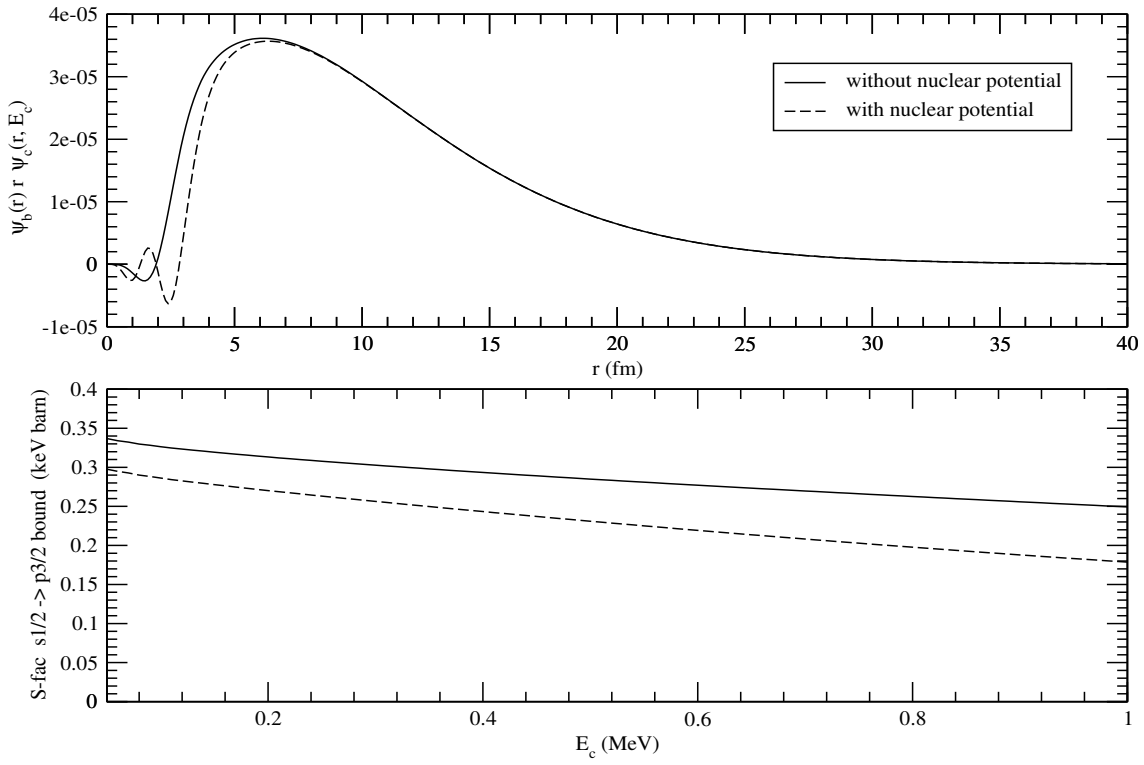

Figure 3.20: Partial S-factor for the $^3\mathrm{He}(\alpha,\gamma)^7\mathrm{Be}$ reaction with and without including the nuclear potential in evaluating the continuum wave-functions. For clearness the respective integrand of B(E1) in shown.

finding that (as expected) the contribution to photo-dissociation and radiative capture processes is rather small. This is in contrast with the strong M1 photo-dissociation peak at low energies in the case of deuteron, that has motivated our investigation.

Summary, epilogue and perspectives

Unfortunately nuclear physics has not profited as much from analogy as the atomic physics. The reason seems to be that the nucleus is the domain of new and unfamiliar forces for which men have not yet developed an intuitive feeling.

V. L. Telegdi

Notwithstanding the truth hidden in the quote just above physics has achieved a good understanding of nuclei, in their structure as well as in their reactions. Nuclear phenomena are so numerous and various that a unique model is not able to encompass them, hence several models have been carried out in order to reduce wide classes of phenomena in a unique framework.

In this work a comprehensive discussion about two-cluster nuclei has been presented. We started by briefly surveying some standard nuclear models and important themes, such as the nuclear shell model and the spin-orbit interaction, in order to set the language used and in order to emphasize the limitations of these models in many cases of interest.

Next we have considered a few selected topics in the field of halo nuclei, focusing in the two-body halo nuclei, pointing out the connections with two-body cluster nuclei. Indeed many standard formulas, i.e. regarding charge and matter radii, effective charges, static

electromagnetic moments, are broadly used in both these cases. For sake of completeness we have derived these formulas for general two-body nuclei, considering two-body halo nuclei as peculiar cluster nuclei. Some of these formulas are well-known, but often they are used without any comment, (see for example the discussion about the effective charge for two-body nuclei), thus we think that a formal derivation can be useful in order not to mislead their meaning or their range of pertinence.

Dealing with halo nuclei we have also presented some reaction models, such as the coupled channel approach and a few related remarkable models, i.e. the coupled discretised continuum channel (CDCC) and its high-energy approximation, namely the sudden or adiabatic model. The discussion is not exhaustive, because in our calculations we do not use a fully quantum-mechanical approach, such as the CDCC, but a semi-classical one. Moreover, for the interested reader, there exist many reviews about them.

In the third chapter ^{7}Li and ^{7}Be have been described in the framework of Di-cluster nuclei. The first step has been the description of the model used, discussing the Hamiltonian of the system and the actual optical parameters for bound and continuum states. Then we have computed several static and dynamic properties of these nuclei, by means of numerical integration.

Our calculations for E1 and E2 transitions has been checked by comparison with energy weighted sum rules (EWSM) and energy weighted molecular sum rules (EWMSM). These theoretical tools turn out to be in agreement with the basic assumptions of our model, namely that we can describe ^{7}Be and ^{7}Li as formed by two inert clusters in which all the electromagnetic strength arises from excitation of the relative motion. Indeed the EWSM overstimates the electromagnetic strength whilst the EWMSR well reproduces the calculations.

A similar discussion has been presented dealing with dipole magnetic interaction. In detail we have discussed the limitations of the shell model picture in computing the static dipole magnetic moment, in spite of the fact that we can consider ^{7}Be and ^{7}Li as nuclei with a single hole in the 1p3/2 shell. We have shown that, by including the di-cluster structure, the calculated static dipole moment improves the agreement with the

experimental results. Then we have developed the calculations for the reduced matrix elements for M1 interaction, for transitions to continuum and between the two bound states. Finally we have derived a simple, yet powerful, EWMSR for M1 transitions in order to check our calculations. The agreement is fairly good.

After computing the reduced matrix elements for E1, E2 and M1 transitions we have calculated the cross-section for photo-dissociation and radiative capture processes, because of their astrophysical interest. Then we have compared our results with experimental measurements of the S-factor. The agreement that we have found in quite good, as discussed in the text.

Finally we have pointed out two aspects related to these calculations: the M1 contribution is comparable with the E2 contribution in the radiative capture and in the photo-dissociation cross-section, but they are much smaller thean the E1 contribution. In this way we have a situation that is rather different from the deuteron case. Indeed the photo-dissociation of the deuteron is known to have an appreciable component of M1 strength at very low continuum energies. The other remark is the importance of properly including the nuclear potential in evaluating the continuum wave-functions, because it affects the response in a non negligible way.

We can resume our work, by affirming that in spite of its simplicity, from a physical point of view and from a computational point of view, our model is able to encompass the basic features of di-cluster nuclei, and it is enough flexible to permit other calculations, such as break-up processes of ^{7}Be on ^{208}Pb, that actually are in progress, as we briefly discuss in the following section.

Work in progress

We are interested in the cross-section for break-up of ^{7}Be into α+^{3}He in the electrostatic field of ^{208}Pb. A similar work has been performed in (27) for the Break-up of ^{7}Li in $\alpha + t$ in the field of ^{208}Pb. Hence we refer to (27) for a more detailed description of the adopted formalism.

We have considered a classical trajectory, while the excitations to the continuum (break-up) are treated with a coupled channel formalism with quantal excitations. We have computed all the partial cross-section for E1 and E2 transitions for various incident energies of ^{7}Be, i.e. $36, 40, 44, 48$ MeV in the laboratory frame. Our preliminary results indicate that the E2 contribution is not negligible with respect to the E1 contribution, as in radiative capture and photo-dissociation cross sections. Indeed the ratio $\sigma_{bu}(E2)/\sigma_{bu}(E1) \sim 0.45$, indicates a roughly similar behavior with respect to the ^{7}Li break-up.

The choice of these incident energies is related to an incoming experiment in the INFN Laboratories of Legnaro (LNL) aimed at measuring the ^{7}Be break-up cross-section in the field of ^{208}Pb at energies around and below the Coulomb Barrier, that is approximately 40 MeV.

The preliminary estimated total break-up cross-section is shown in fig. (3.21), where we have also reported the contribution from electric dipole and quadrupole. Other multipolarties (E3, M1) have been neglected. The incident energies are in the center of mass frame, namely $34.8, 38.7, 42.6, 46.4$ MeV.

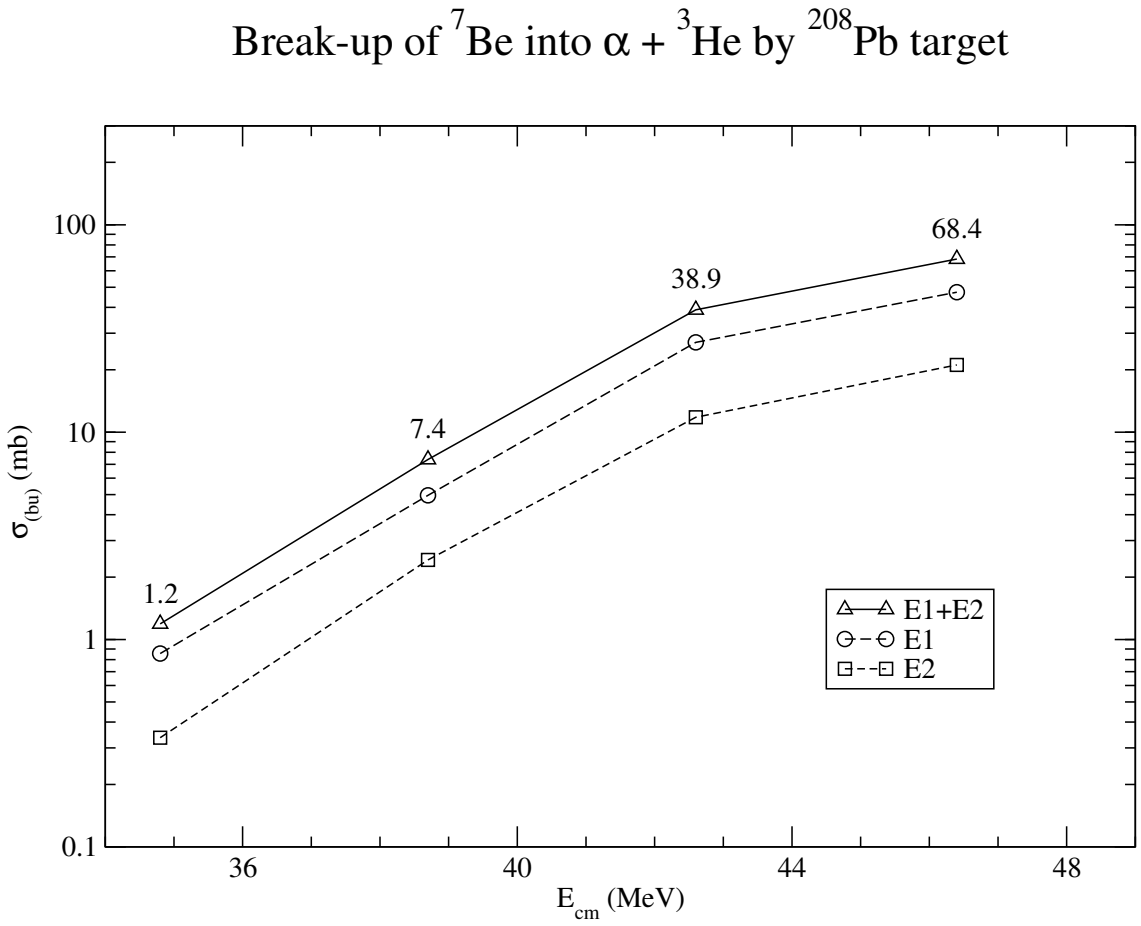

Figure 3.21: Preliminary calculations of Break-up cross-section ^{7}Be into α+^{3}He by ^{208}Pb target. The energies on the x-asis refer to the ^{7}Be incident energy in the center of mass frame. Partial cross-sections for E1, E2 transitions are shown, in addition to the total one. The E2 contribution is not negligible, as for radiative capture and photo-dissociation cross-sections, but amounts up to ~ 0.45 of the E1 contribution. This behavior is similar to the breakup of ^{7}Li by ^{208}Pb target, as discussed in (27). Other multipolarities have been neglected in the calculations. The Coulomb barrier between beam and target is approximately 40 MeV.

Bibliography

[1] M. Abramowitz and I.A. Stegun, *Handbook of Mathematical Functions with Formulas, Graphs, and Mathematical Tables*, (Dover 1964).

[2] F. Ajzenberg-Selove, Nucl. Phys. A **413**, 1 (1984).

[3] Y. Alhassid, M. Gai, G.F. Bertsch, Phys. Rev. Lett. **49**, 1482 (1982).

[4] J.S. Al-Khalili "An introduction to Halo nuclei", In J.S. Al-Khalili, E. Roeckl, (Eds.) *The Euroschool lectures on physics with exotic beams Vol. 1*, L.N.P. **651** (Springer, 2004) pp. 77-112.

[5] J.S. Al-Khalili, F. Nunes, J. Phys. G **29**, R89 (2003).

[6] J.S. Al-Khalili, T.A. Tostevin, *Scattering*, ed P. Sabatier, E.R.Pike (London Academic, 2001).

[7] T.Altmeyer, Z. Phys. A **330**, 277 (1988).

[8] H.J. Assenbaum, K. Langanke, A. Weiguny, Phys. Rev. C **35**, 755 (1987).

[9] N. Austern *et al.*, Phys. Rep. **154**, 125 (1987).

[10] J.L. Basdevant, J. Rich, M. Shiro, *Fundamentals in Nuclear Physics: From Nuclear Structure to Cosmology*, (Springer, 2005).

[11] C. Bernardini, G. Guaraldo, *Fisica del nucleo* (Editori Riuniti, 1982).

[12] C.A. Bertulani, A.Sustich, Phys. Rev. C **46**, 2340.

[13] J.M. Blatt and V.F. Weisskopf, *Theoretical Nuclear Physics* (John Wiley and Sons, Inc. 1952).

[14] A. Bohr, B.R. Mottelson, *Nuclear Structure* (W.A. Benjamin, Inc, New York, Amsterdam, 1969).

[15] M. Born, *Fisica atomica*, (Bollati Boringhieri, 1976).

[16] C.R.Brune, arXiv:0502588v1[astro-ph].

[17] B.Buck, R.A. Baldock and J. Alberto-Rubio, J.Phys.G: Nucl. Phys. **11** (1985), L11-L16.

[18] L. Canton, L.C. Levchuk, arXiv:0805.2667v2[nucl-th].

[19] F.Catara, C.H. Dasso and A. Vitturi, Nucl. Phys. A **602**,181 (1996).

[20] A. Csótó, K. Langanke, arXiv:nucl-th/9906053v2.

[21] A. Csótó, K. Langanke, Nucl. Phys. A **688** 511c-513c (2001).

[22] R.H. Cyburt, B. Davis, arXiv:0809.3240v1[nucl-th].

[23] A. DeShalit and I. Talmi, *Nuclear Shell Theory* (Academic Press, New York and London, 1963).

[24] A. DeShalit, H, Feshbach, *Theoretical Nuclear Physics, Nuclear Structure* (Wiley, New York, 1974) Vol.I, p.706-709.

[25] D.V. Fedorov, A.S. Jensen and K. Riisager, Phys. Rev. C **49**, 201 (1994).

[26] H.Feshbach, *Theoretical Nuclear Physics: Nuclear Reactions* (Wiley, 1993).

[27] L. Fortunato, A. Vitturi, Eur. J. Phys. A **26**, 33 (2005).

[28] R.J. Glauber, in *Lectures in Theoretical Physics* ed W.E. Brittin (Interscience, N.Y.,1959) Vol. 1, 315.

[29] H. Grawe, "Shell Model from a Practitioner's point of view", In J.S. Al-Khalili, E. Roeckl, (Eds.) *The Euroschool lectures on physics with exotic beams Vol. 1*, L.N.P. **651** (Springer, 2004) pp. 33-75.

[30] P.G. Hansen, A.S.Jensen, B. Jonson, Ann. Rev. Nucl. Part. Sci **45**, 591 (1995).

[31] P.G. Hansen, B. Jonson, Europhys. Lett. **4**, 409 (1987)

[32] D.R. Tilley *et al.*, Nucl. Phys. A **708**, 3 (2002) and corrections in D.R. Tilley *et al.* TUNL manuscript.

[33] F. Iachello, *Lie algebras and applications*, L.N.P. **708**, (Springer, 2006).

[34] Gy. Gyürky *et al.*, Phys. Rev. C **75**, 035805 (2007); F.Confortola *et al.*, Phys. Rev. C **75**, 065803 (2007); Gy.Gyürky *et al.* J. Phys. G: Nucl. Part. **35**, 014002 (2008).

[35] A.S. Jensen, K. Riisager, D.V. Ferodov, E. Garrido, Rev. Mod. Phys. **76**, 215 (2004).

[36] B. Jonson, Phys. Rep. **389**, 1 (2004).

[37] T. Kajimo, T. Matsure, A. Arima, Nucl. Phys. A **413**, 323 (1984).

[38] T. Kajino, A. Arima, Phys. Rev. Lett. **52**, 739 (1984).

[39] T. Kajino, Nucl. Phys. A **460**, 559 (1986).

[40] T. Kajino *et al.*, Phys. Rev. C **37**, 512 (1988).

[41] N. Keeley, K.W. Kemper, K. Rudek, Phys. Rev. C **66**, 044605 (2002).

[42] D. Krolle *et al.*, Z. Phys. A **328**, 291 (1987).

[43] D. Kurath, Phys. Rev. **130**, 1525 (1963).

[44] K. Langanke, Nucl. Phys. A **457**, 351 (1986).

[45] D.J. Millener, J.W. Olness, E.K. Warburton, S.S. Hanna, Phys. Rev. C **28**, 497 (1983).

[46] NACRE database `http://pntpm.ulb.ac.be/Nacre/nacre_d.htm`.

[47] M.A. Nagarajan, S.M. Lenzi, A. Vitturi, Eur. J. Phys. A **24**, 63 (2005).

[48] G.Neyens, Rep. Prog. Phys. **66**, 633 (2003).

[49] R.Noigart, G.Neyens, "Nuclear moments", in J.S. Al-Khalili, E. Roeckl, (Eds.) *The Euroschool lectures on physics with exotic beams Vol. 2*, L.N.P. **700** (Springer, 2006) pp. 135-191.

[50] K. Nollett, Phys. Rev. C **63**, 054002 (2001).

[51] F.M. Nunes *et al.*, Nucl. Phys A **736**, 255 (2004).

[52] A. Ozawa, T. Suzuki, I. Tanihata, Nucl. Phys. A **693**, 32 (2001).

[53] S. kappertz *et al*, Proc.Conf on Exotic Nuclei and Atomic Masses, Bellaire, Michigan, June 23-27, 1998, p.110 (1998); AIP Conf.Proc. 455 (1998).

[54] A. Mason, R. Chatterjee, L. Fortunato and A. Vitturi, Proc. Conf. on "State of the Art in Nuclear Cluster Physics", Strasbourg, France, May 13-16, 2008, on IJMPE **17**, 2310 (2008); A. Mason, R. Chatterjee, L. Fortunato and A. Vitturi, The Eur. Phys. J. A **39**, 107 (2009)

[55] K. Riisager, Rev. Mod. Phys. **66**, 1105 (1994).

[56] K. Riisager, "Nuclear halos and experiments to probe them", in J.S. Al-Khalili, E. Roeckl, (Eds.) *The Euroschool lectures on physics with exotic beams Vol. 2*, L.N.P. **700** (Springer, 2006) pp. 1-36.

[57] K. Riisager, A.S. Jensen, P. Møller, Nucl. Phys. A **548**, 393 (1992).

[58] P. Ring and P. Schuck, *The Nuclear Many-Body Problem*, (Springer-Verlag, New York, 1980).

[59] C. Rolfs, Nucl. Phys. A **217**, 29 (1973).

[60] C.E. Rolfs and W.S. Rodney, *Cauldrons in the Cosmos*, (Univ. Chicago Press, 1988).

[61] N.C. Summers, J.S. Al-Khalili and R.C. Johnson, Phys, Rev. C **66**, 014614 (2002).

[62] N.C. Summers, F.M. Nunes, Phys. Rev. C **70**, 011602(R) (2004).

[63] I.Tanihata *et al.*, Phys. Rev. Lett. **55**, 2676 (1985).

[64] I.Tanihata *et al.*, Phys. Lett. B **160**, 380 (1985).

[65] I.Tanihata, Prog. Nucl. Phys. **35**, 505 (1995).

[66] Y. Tokimoto *et al.*, Phys. Rev. C **63**, 035801 (2001).

[67] TUNL database `http://www.tunl.duke.edu/nucldata/index.shtml`

[68] S. Typel and G. Baur, Nucl. Phys. A **759**, 247 (2005); G. Baur and S. Typel, Prog. Part. Nucl. Phys. **59**, 122 (2007).

[69] M. Traini, Phys. Rev. Lett. **41**, 1535 (1978).

[70] H.G. Voelk, D. Fick, Nucl. Phys. A **530**, 475 (1991).

[71] H. Walliser, T. Fliessbach, Phys. Rev. C **31**, 2242 (1985).

[72] H. Walliser, Q.K.K. Liu, Y.C. Tang, Phys. Rev. C **28**, 57 (1983).

[73] K. Wildermuth and Y.C. Tang, *A Unified Theory of the Nucleus* (Academic Press, New York, 1977).

[74] M.V.Zhukov *et al.*, Phys. Rep. **231**, 151 (1993).